M 2022

U.PORTO
FEUP FACULDADE DE ENGENHARIA
UNIVERSIDADE DO PORTO

THERMO-HYDRAULIC MODELING OF EXTERNAL COOLING SYSTEMS OF POWER TRANSFORMERS: RADIATORS

GABRIEL SILVA E SILVA
MASTER THESIS IN CHEMICAL ENGINEERING
PRESENTED TO THE FACULTY OF ENGINEERING
OF THE UNIVERSITY OF PORTO

Master in Chemical Engineering

Thermo-Hydraulic Modeling of External Cooling Systems of Power Transformers: Radiators

Master dissertation

of

Gabriel Silva e Silva

Developed within the course of dissertation

held in

Efacec Energia, Máquinas e Equipamentos Elétricos, S.A.
R&D Department of Transformers Unit



Supervisor at FEUP: **Dr.ª Erica Doutel Costa**

Joint supervisor(s) at FEUP: **Dr.ª Joana Ferreira**

Coordinator at EFACEC: **Eng.ª Sandra Couto**

U.PORTO
FEUP FACULDADE DE ENGENHARIA UNIVERSIDADE DO PORTO

DEPARTAMENTO DE ENGENHARIA QUÍMICA

FCT Fundação para a Ciência e a Tecnologia
MINISTÉRIO DA CIÊNCIA, TECNOLOGIA E ENSINO SUPERIOR

REPÚBLICA PORTUGUESA

CLASSIFIED DOCUMENT. USE ONLY FOR EVALUATION PURPOSES *(delete this box in final version or if not applicable)*

September 2022

Acknowledgments

Firstly, my sincerest thanks to my supervisors, Erica Doutel, Joana Ferreira and Sandra Couto, for the knowledge they passed on, particularly regarding CFD and data processing. Their guidance and expertise have enabled me to complete this task and will be crucial to me for the rest of my career as an engineer. In addition, I would like to thank them for their tireless dedication, unyielding patience, and extreme attention to detail.

Secondly, I would also like to thank all the members of CEFT – Transport Phenomena Research Center, which was financially supported by LA/P/0045/2020 (ALiCE), UIDB/00532/2020 and UIDP/00532/2020 (CEFT) funded by national funds through FCT/MCTES (PIDDAC), for their advice, friendliness, and humorous disposition.

Then, I extend my gratitude to the Efacec Transformers R&D Thermal and Fluids team, for their warm welcome and lending me their resources. Within this group, I give special acknowledgment to Ricardo Lopes and Catarina Corte-Real, for sharing with me extensive knowledge regarding transformer design and CFD.

Additionally, I thank my working partner and friend, Diogo, with whom many moments of stress and hard work were spent.

Finally, it is with particular sentiment that I thank my close family, my mother Beatriz, my father Celestino and my sister Victória, who have stood beside me no matter the circumstance. I thank them deeply for their particular patience, readiness to help in whatever was required, concern, sacrifice, and for their faith in me.

Abstract

In this master's dissertation, the external cooling of power transformers was studied. Power transformers are an essential part of any energy distribution grid. They facilitate the transmission and distribution of electrical energy to places very distantly located from a central power station. Despite being remarkably efficient machines, power transformers still have energy losses, which manifest in the form of heat. This heat is unhealthy for the functioning of the transformer. As such, cooling systems must be used to maintain transformer temperature at an adequate level. These cooling systems have an internal and an external component, this work's focus was on the latter.

Summarily, the main objective of this work is to evaluate the influence of morphological aspects (such as plate height and number of plates) and convective settings (such as oil flow rate and external convective heat transfer coefficient) on the thermo hydraulic performance of transformer external cooling systems. In this project, multiple studies were carried out regarding many aspects regarding radiator thermo-hydraulic behavior of these cooling systems. The main elected tool to do so was CFD (more specifically using the ANSYS Suite). Geometries of one, seven, twelve and twenty radiator plates were studied, with varying heights of 0.8 m, 1.5 m and 3 m. In addition to these geometrical parameters, different flow rates and ventilation types were studied. Through these simulations, the following variables were studied: pressure drop, heat dissipation, outlet temperature, oil convective heat transfer coefficient and overall heat transfer coefficient. These values were then analyzed through graphs, contours and correlations. These analyses provided plenty of knowledge regarding the thermo-hydraulic behavior of power transformers' cooling systems.

Finally, this knowledge (in the form of data) was used to create a machine learning simulator, capable of predicting the output variables from a set of input variables, which will significantly aid engineers with the design of external cooling systems of power transformers.

Keywords: core type power transformers, CFD, machine learning, windings, external cooling, mineral oil, heat transfer, flow, convection, numerical simulation

Resumo

Nesta dissertação de mestrado, foi estudado o arrefecimento externo dos transformadores de potência. Os transformadores de potência são uma parte essencial de qualquer rede de distribuição de energia. Eles facilitam a transmissão e distribuição de energia para locais muito distantes de uma central eléctrica. Apesar de serem máquinas muito eficientes, os transformadores de potência ainda têm perdas de energia, que se manifestam sob a forma de calor. Este calor não é saudável para o funcionamento do transformador. Como tal, devem ser utilizados sistemas de arrefecimento para manter a temperatura do transformador a um nível adequado. Estes sistemas de arrefecimento têm uma componente interna e uma componente externa, o foco deste trabalho foi a segunda componente.

Em resumo, o principal objectivo deste trabalho é avaliar a influência de aspectos morfológicos (tais como a altura da placa e o número de placas) e parâmetros convectivos (tais como o caudal de óleo e o coeficiente de transferência de calor convectivo externo) no desempenho termo-hidráulico dos sistemas de arrefecimento externo de transformadores. Neste projecto, foram realizados múltiplos estudos sobre muitos aspectos relativos ao comportamento termo-hidráulico dos radiadores destes sistemas de arrefecimento. A principal ferramenta eleita para o fazer foi o CFD (mais especificamente utilizando a ANSYS Suite). Foram estudadas geometrias de uma, sete, doze e vinte placas de radiadores, com alturas variáveis de 0,8 m, 1,5 m e 3 m. Para além destes parâmetros geométricos, foram estudadas diferentes taxas de fluxo e tipos de ventilação. Através destas simulações, foram estudadas as seguintes variáveis: queda de pressão, dissipação de calor, temperatura de saída, coeficiente de transferência de calor por convecção de óleo e coeficiente global de transferência de calor. Estes valores foram depois analisados através de gráficos, contornos e correlações. Estas análises forneceram muitos conhecimentos sobre o comportamento termo-hidráulico dos sistemas de arrefecimento dos transformadores de potência.

Finalmente, este conhecimento (sob a forma de dados) foi utilizado para criar um simulador de "machine learning", capaz de prever as variáveis de saída a partir de um conjunto de variáveis de entrada, o que ajudará significativamente os engenheiros na construção de sistemas externos de arrefecimento de transformadores de potência.

Declaration

I hereby declare, under word of honour, that this work is original and that all non-original contributions is indicated and due reference is given to the author and source

26/09/2022

Index

Index i

List of Figures v

List of Tables xi

Notation and Glossary xiii

1 Introduction 15

1.1 Framing and presentation of the work 15

1.2 Presentation of the company 16

1.3 Author's Contribution 17

1.4 Organization of the dissertation 17

2 Context and State of the art 18

2.1 Background on Power Transformers 18

2.1.1 General overview of Power Transformers 18

2.1.2 Overview of the main components of a Power Transformer 18

2.2 Background on cooling systems of Power Transformers 20

2.2.1 Overview 20

2.2.2 External Cooling Media 22

2.2.3 Heat Dissipation surfaces for air-cooled transformers 22

2.2.4 Ventilation types for air-cooled transformers 23

2.2.5 Background on research regarding power transformer cooling systems 23

2.3 Background on Machine Learning 29

2.3.1 Machine Learning Algorithms 29

2.3.2 Performance Metrics for Machine Learning Algorithms 31

3 Computational Applications and their Usage 33

3.1 ANSYS Workbench 33

3.2 Python 34

3.2.1 Scikit-learn 34

3.2.2 NumPy 34

3.2.3 Pandas 34

3.2.4 Tkinter 34

4 Theory and modeling approach 35

4.1 Problem Description 35

4.2 Employed thermo-hydraulic models 35

4.2.1 Studies of Pressure Drop 35

4.2.2 Velocity Profiles 36

4.2.3 Heat Transfer Coefficients 37

4.2.4 Studies of Heat Dissipation and Temperature Distribution 38

4.2.5 Governing Fluid Flow Equations 39

4.3 CFD Thermo-hydraulic Simulations: Radiators 39

4.3.1 Geometry 40

4.3.2 Mesh 41

4.3.3 Simulation Settings 41

5 Results and discussion 43

5.1 CFD Simulations: Thermo-hydraulic studies of radiator design 43

5.1.1 Pressure Drop 43

5.1.2 Outlet Temperature and Dissipated Losses 44

5.2 Machine Learning: Simulator Performance and Results 47

5.2.1 Algorithm Evaluation 48

6 Conclusion 52

7 Assessment of the work done 53

7.1 Objectives Achieved 53

7.2 Other Work carried out 53

7.3 Future Work 53

7.4 Final Assessment 53

8 References 55

Appendix A - User Defined Functions 61

A.1. Density 61

A.2. Specific Heat 61
A.3. Thermal Conductivity 61
A.4. Dynamic Viscosity 61
A.5. Parabolic inlet velocity profile for laminar flow 63
A.5. Parabolic inlet velocity profile for turbulent flow 64
Appendix B - CFD Simulations: Hydraulic studies of a single radiator plate 65
B.1. Geometry 65
B.2. Mesh 67
B.3. Pressure Drop and Velocity Magnitude Distribution 68
B.4. Velocity Distribution 72
B.5. Pressure drop contour plots 77
Appendix C - Mesh full Settings and Numerical Settings 79
C.1. Single Plate Hydraulic Simulations 79
C.2. Radiator thermo-hydraulic simulations 85
Appendix D - CFD Simulator Code 92
Appendix E - Additional Pressure Drop Results obtained from thermo-hydraulic simulations 96
E.1. Correlations of pressure drop and mass flow rate 96
E.2. Correlations of pressure drop and plate height 97
Appendix F - Additional graphs regarding the effect of ventilation on oil convection (for radiators of 7 and 20 plates) 98
Appendix G - Radiator Flow Rate Graphs per plate (12 plate radiator) 100
G.1. Height of 0.8 m 100
G.2. Height of 1.5 m 102
G.3. Height of 3 m 105

List of Figures

Figure 1 – Examples of Power transformers produced by Efacec. Power transformers (a) and distribution transformers (b) 16

Figure 2 – Example of a power transformer [9] 18

Figure 3 – Tank of a Power Transformer [11] 19

Figure 4 – Comparison between Shell and Core type transformer cores and windings [15] 19

Figure 5 – Transformer general schematic [18] 20

Figure 6 – Structure of the Cooling Mode Nomenclature 21

Figure 7 - Example of a vertical plate radiator (a) and a figure depicting the oil flow within the cooling system (b) 22

Figure 8 – Types of tradiator ventilation. Radiators with bottom ventilation (a) [22] and radiators with side ventilation (b) [27] 23

Figure 9 - Geometry of the simulated ONAN model [31] 24

Figure 10 – a) 3D radiator CFD model; b) Side view of radiator CFD model; c) Cross-sectional view of middle of the radiator (oil domain in grey, wall domain in blue) [32] 24

Figure 11 - Oil flow velocity and direction (a) and air flow streamlines with temperature contours (b) [32] 25

Figure 12 - Power Transformer equipped with fans, to work in an AF regime [35] 26

Figure 13 - Comparison of measured and calculated radiator panel temperature over the radiator height both for ONAN as ONAF condition [36] 27

Figure 14 – Fan velocity streamlines (a). The overall temperature distribution of the radiator before and after the fan is turned off (b)[37] 27

Figure 15 – Obtained correlations between cooling capacity and number of plate pairs [22] 28

Figure 16 - Solid model and computational domain for (a) the vertical and (b) horizontal ventilation over the radiators [38] 28

Figure 17 – Comparison of the fitting of a linear model and polynomial model to a training dataset . 31

Figure 18 – Essential ANSYS CFD workflow. It is composed by three modules: the Geometry module (left), the Mesh module (center) and the Fluent Module (right) 33

Figure 19 – Types of fluid velocity profile. Uniform velocity profile (a), parabolic velocity profile (b), velocity profile based on a power law (c) 36

Figure 20 – Selection of inwards facing surfaces (a) and outwards facing surfaces (b) 37

Figure 21 – Example of a radiator geometry 40

Figure 22 - Correlations for pressure drop (ΔP) as a function of flow rate for three numbers of plates for a height of 1.5 m *43*

Figure 23 - Correlations for pressure drop (ΔP) as a function of flow rate for three numbers of plates for the flow rate Q2 ..... *44*

Figure 24 – Output temperature and energy dissipation rate as a function of plate height with varying external convective heat transfer coefficients for a radiator of 7 plates and Q2 ..... *45*

Figure 25 - Output temperature and energy dissipation rate as a function of plate height with varying external convective heat transfer coefficients for a radiator of 12 plates and Q2 ..... *45*

Figure 26 - Output temperature and energy dissipation rate as a function of plate height with varying external convective heat transfer coefficients for a radiator of 20 plates and Q2 ..... *45*

Figure 27 - Output temperature and energy dissipation rate as a function of plate height with varying external convective heat transfer coefficients for a radiator of 7 plates and a height of 0.8 m *46*

Figure 28 - Output temperature and energy dissipation rate as a function of plate height with varying external convective heat transfer coefficients for a radiator of 7 plates and a height of 1.5 m *46*

Figure 29 - Output temperature and energy dissipation rate as a function of plate height with varying external convective heat transfer coefficients for a radiator of 7 plates and a height of 3 m *47*

Figure 30 – Simulator GUI *50*

Figure 31 – Simulator operation *51*

Figure 32 – Plate geometry *65*

Figure 33 – Full plate geometrical specifications *66*

Figure 34 - Pressure drop (ΔP) in function of the flow rate (Q) in a single radiator plate for three different plate heights (h). The lines indicate second order polynomial regressions. *68*

Figure 35 - Pressure drop (ΔP) in function of plate height (h) in a single radiator plate for three different flow rates. The lines indicate linear regressions. *69*

Figure 36 – Contours plots of velocity magnitude normalized by each simulation's inlet velocity. Plate features a height of 0.8 m. *70*

Figure 37 – Contours plots of velocity magnitude normalized by each simulation's inlet velocity. Plate features a height of 1.5 m. *71*

Figure 38- Contours plots of velocity magnitude normalized by each simulation's inlet velocity. Plate features a height of 3 m. *71*

Figure 39 – Radiator plates with inclined distributor zones and curved corners [74] *72*

Figure 40 - Contours of velocity magnitude normalized by the maximum inlet velocity (0.213 ms^{-1}). Plate features a height of 800 mm *73*

Figure 41 - Contours of velocity magnitude normalized by the maximum inlet velocity (0.213 ms^{-1}). Plate features a height of 800 mm 73

Figure 42 - Contours of velocity magnitude normalized by the maximum inlet velocity (0.213 ms^{-1}). Plate features a height of 800 mm 74

Figure 43 – Volume flow rate distribution between plate ducts with an inlet flow rate of 0.048 dm3s-1 75

Figure 44 – Volume flow rate distribution between plate ducts between plate ducts with an inlet flow rate $Q2$ = 0.11 dm^3s^{-1} 75

Figure 45 – Volume flow rate distribution between plate ducts between plate ducts with an inlet flow rate $Q2$ = 0.376 dm^3s^{-1} 75

Figure 46 - Contours of static pressure obtained from hydraulic CFD simulations of a single radit. Plate features a height of 800 mm 77

Figure 47 – Contours of static pressure obtained from hydraulic CFD simulations of a single radiator plate. Plate features a height of 1.5 m. 77

Figure 48 – Contours of static pressure obtained from hydraulic CFD simulations of a single radiator plate. Plate features a height of 3 m. 78

Figure 49 – Plate geometry with mesh independence testing zones 79

Figure 50 – Duct Geometry 79

Figure 51 – Velocity profile Duct mesh Independence tests 80

Figure 52 – Velocity magnitude profiles obtained from the top distributor line in the hydraulic mesh tests 80

Figure 53 – Velocity magnitude profiled obtained from the bottom distributor line in the hydraulic mesh tests 81

Figure 54 – View of the right side of the hydraulic mesh distributor 81

Figure 55 – View of the left side of the hydraulic mesh distributor 82

Figure 56 – View of a corner of the distributor of the hydraulic mesh 82

Figure 57 – View of a detail of the hydraulic mesh 83

Figure 58 – View of the inlet of the hydraulic mesh 83

Figure 59 – Numerical settings of the single plate hydraulic simulations 84

Figure 60 – Thermo-hydraulic Duct Mesh independence tests 85

Figure 61 - Velocity magnitude profiled obtained from the bottom distributor line in thermo-hydraulic mesh tests 86

Figure 62 – Velocity magnitude profiles obtained from the top distributor line in thermo-hydraulic mesh tests 86

Figure 63 – Frontal view of the thermo-hydraulic plate mesh *87*

Figure 64 – Overall view of the thermo-hydraulic plate mesh *88*

Figure 65 – Top view of the radiator mesh with 7 plates and a height of 0.8 m *88*

Figure 66 – Front view of the radiator mesh with 7 plates and a height of 0.8 m *89*

Figure 67 - Numerical settings of thermo-hydraulic simulations *90*

Figure 68 – Correlations for pressure drop (ΔP) as a function of flow rate for three numbers of plates for a height of 0.8 m *96*

Figure 69 - Correlations for pressure drop (ΔP) as a function of flow rate for three numbers of plates for a height of 3 m *96*

Figure 70 - Correlations for pressure drop (ΔP) as a function of flow rate for three numbers of plates for the flow rate Q1 ..... *97*

Figure 71 - Correlations for pressure drop (ΔP) as a function of flow rate for three numbers of plates for the flow rate Q3 ..... *97*

Figure 72 – Output temperature and energy dissipation rate as a function of plate height with varying external convective heat transfer coefficients for a radiator of 7 plates and Q1 ..... *98*

Figure 73 – Output temperature and energy dissipation rate as a function of plate height with varying external convective heat transfer coefficients for a radiator of 7 plates and Q3 ..... *98*

Figure 74 - Output temperature and energy dissipation rate as a function of plate height with varying external convective heat transfer coefficients for a radiator of 12 plates and Q1 ..... *98*

Figure 75 - Output temperature and energy dissipation rate as a function of plate height with varying external convective heat transfer coefficients for a radiator of 12 plates and Q3 ..... *99*

Figure 76 - Output temperature and energy dissipation rate as a function of plate height with varying external convective heat transfer coefficients for a radiator of 20 plates and Q1 ..... *99*

Figure 77 - Output temperature and energy dissipation rate as a function of plate height with varying external convective heat transfer coefficients for a radiator of 20 plates and Q3 ..... *99*

Figure 78 – Flow rate proportion per plate for AN *100*

Figure 79 – Flow rate proportion per plate for AF1 ..... *100*

Figure 80 - Flow rate porportion per plate for AF2 ..... *101*

Figure 81 – Flow rate proportion per plate for Q1 ..... *101*

Figure 82 – Flow rate proportion per plate for Q2 ..... *101*

Figure 83 – Flow rate proportion per plate for Q3 ..... *102*

Figure 84 – Flow rate proportion per plate for AN *102*

Figure 85 – Flow rate proportion per plate for AF1 ..... *103*

Figure 86 – Flow rate proportion per plate for AF2 ..... *103*

Figure 87 - Flow rate proportion per plate for Q1 ..... *104*

Figure 88 - Flow rate proportion per plate for Q2 ..... *104*

Figure 89 - Flow rate proportion per plate for Q3 ..... *105*

Figure 90 – Flow rate proportion per plate for AN *105*

Figure 91 – Flow rate proportion per plate for AF1 ..... *106*

Figure 92 - Flow rate proportion per plate for AF2 ..... *106*

Figure 93 - Flow rate proportion per plate for Q1 ..... *107*

Figure 94 - Flow rate proportion per plate for Q2 ..... *107*

Figure 95 - Flow rate proportion per plate for Q3 ..... *108*

Figure 96 – Recirculation zone taking place at the bottom of the collector tube. (Radiator of 12 plates, height of 0.8 m and $Q1$) *109*

List of Tables

Table 1 - Cooling class designation description [19] 21

Table 2 – Values of $hairm$ for AF in W·m^{-2}·ºC^{-1} used for each radiator geometry 38

Table 3 - Values of $hairm$ for AF1 and AF2 in W·m^{-2}·ºC^{-1} 38

Table 4 – Simulated radiator heights 40

Table 5 – Simulated plate numbers 40

Table 6 – Characterization of the meshes used in the thermo-hydraulic simulation of a radiator with a height of 0.8 m 41

Table 7 – Characterization of the meshes used in the thermo-hydraulic simulation of a radiator with a height of 1.5 m 41

Table 8 – Characterization of the meshes used in the thermo-hydraulic simulation of a radiator with a height of 3 m 41

Table 9 – Flow rate values (Q) pertaining to each plate number. Underlined flow rates had Re > 4000 at the radiator inlet 42

Table 10 – Evaluation of Machine Learning regression algorithms for pressure drop (ΔP). 48

Table 11 – Evaluation of Machine Learning regression algorithms for Power output (Power). 48

Table 12 – Evaluation of Machine Learning regression algorithms for outlet temperature (To) 49

Table 13 – Evaluation of Machine Learning regression algorithms for oil convective heat transfer coefficient 49

Table 14 – Evaluation of Machine Learning algorithms for overall heat transfer coefficient 50

Table 15 – Mesh characteristics for simulated plate geometries 67

Table 16Table 16 – Oil physical properties at 60ºC 67

Table 17 – Inlet velocities for a single radiator plate 68

Table 18 – Mesh performance comparison for duct mesh independence tests 80

Notation and Glossary

C_p	Specific heat	J kg^{-1} K^{-1}
k	Thermal conductivity	W m^{-1} K^{-1}
h	Height	m
$\dot{m}$	Mass flow-rate	kg h^{-1}
P	Power	W
D_h	Hydraulic diameter	m
T	Temperature	ºC
v	Velocity	m s^{-1}
Re	Reynolds number	
r	Radius	m
h_{air}	Air convective heat transfer coefficient	W m^{-2} K^{-1}
h_{airm}	External convective heat transfer coefficient	W m^{-2} K^{-1}
h_{oil}	Oil convective heat transfer coefficient	W m^{-2} K^{-1}
U	Overall convective heat transfer coefficient	W m^{-2} K^{-1}
ΔTo	Temperature Drop	ºC
R	Total Radius	m

Greek Letters

ρ	kg m^{-3}
μ	Kg m^{-1} s^{-1}

List of Acronyms

CFD	Computational Fluid Dynamics
THNM	Thermal Hydraulic Network Model
PT	Power transformer
R&D	Research and Development
CFD	Computational Fluid Dynamics
ML	Machine Learning
ON	Oil with natural convection
OD	Oil with directed convection
PT	Power transformer
UDF	User defined function
AN	Air with natural convection
AF	Air with forced convection
WF	Water with forced convection
OF	Power transformer
WF	Water with forced convection

1 Introduction

1.1 Framing and presentation of the work

Power transformers are a vital part of any energy distribution grid. They facilitate the transmission and distribution of electrical energy to places very distantly located from a central power station. Consequently, their adequate maintenance is vital to the healthy functioning of any place where human activity is present, for without maintenance these machines lose efficiency and eventually malfunction. Furthermore, at time of writing, Humanity's rampant demand for energy collides with its current circumstances: the climate crisis, the surge of the world's population and the migration of people from rural to urban areas result in higher energy needs. As such, the adequate management of energy will play a crucial role in the coming times.

Although transformers are very efficient machines [1], heat is still generated by their active parts, mainly due to conductor resistivity and the presence of eddy currents. This results in the heating of the active components. This phenomenon presents a threat to a transformer's proper functioning since its temperature must be kept below a critical level. Moreover, the lifetime of this type of machines highly depends on the temperature inside them [2].

To ensure temperatures are maintained acceptable during transformer lifetime, a cooling circuit must be properly designed. Informed guidelines for the external cooling circuit design are of utmost importance – they grant minimization of material waste and, therefore, can result in more compact transformers while minimize production costs. It is particularly important to have compact power transformers when they are placed in city centers, where there is a lack of space to place them. Increasing the ration MVA/ton is a major challenge to be answered.

The main objective of the present work was to provide insights and guidelines on the external cooling circuit performance to provide an adequate design that will allow for a boost in power transformers' performance.

Indeed, in this project, through CFD and ML, much was learned regarding these topics, which presents a significant contribution to the aforementioned objectives. Although more data needs to be obtained and further research will lead to a more complete understanding of the thermo-hydraulic behavior of power transformers, the main goal was secured.

1.2 Presentation of the company

Founded in 1948 but with its origins in early 20th century, Efacec Power Solutions SGPS, S.A is a Portuguese corporation, with business activity in the electrotechnical field. Efacec supplies systems and provides both services and solutions in the areas of energy, environment, industry and mobility [3]. The company has, for instance, facilitated the supply and installation of two 165 MVA and 185 MVA 132/30 kV transformers, destined for a solar park that will benefit 50,000 families with clean energy. A project that represents another great contribution to the production of renewable energy, avoiding the emission of toxic gases and supporting the sustainable energy transition. Furthermore, Efacec is one of the largest manufacturers in the fast-charging infrastructure market for electric vehicles [4].

Among other endeavors (such as the development of automation technology and components used in electrical systems), Efacec manufactures power transformers. These can be classified as either power or distribution transformers. Examples of power and distribution transformers are displayed in Figure 1.



a) b)

Figure 1 – Examples of Power transformers produced by Efacec. Power transformers (a) and distribution transformers (b)

The produced power transformers can be classified according to differences in the way they are built, such as the winding type, the coils' shape, or the magnetic core arrangement (vertical or horizontal) as either Shell or Core types, with rated powers up to 1500 and 350 MVA, respectively. Distribution transformers can be either dry or oil immersed, ranging from 50 kVA to 20 MVA [3].

1.3 Author's Contribution

Transformers' cooling design and thermo-hydraulic behavior is a topic of great interest to the electrical industry. This subject is, at time of writing, being tackled by Efacec's Transformer R&D Thermal and Fluids team, to further optimize and obtain more knowledge regarding the thermo-hydraulic aspects of transformer cooling.

In this master's thesis, several cooling configurations and designs were studied, resorting to CFD simulations. In these simulations, relevant data was obtained. This data was then adequately processed and analyzed, which provided plenty of information on how to more efficiently cool transformers and the thermo-hydraulic phenomena that take place in their cooling systems. A key aspect of this work was the usage of machine learning algorithms to correlate input variables (number of plates in a radiator, plate height, flow rate, convection type) with the output variables (Power, output temperature, oil convective heat transfer coefficient, overall heat transfer coefficient and pressure drop). These correlations allow engineers to predict the output parameters that will come out of

1.4 Organization of the dissertation

This dissertation is divided in 7 main chapters and respective subchapters.

Chapter 1 is an introductory chapter, in which the theme and scope of the dissertation is presented, as well as the author's contribution to the field.

Chapter 2 provides a look into the functioning of transformers and their external cooling mechanisms. In addition, research, particularly CFD-related works, is presented in order to contextualize the reader and provide some insight into state-of-the-art of the thesis subject.

Chapter 3 enumerates the most relevant computational applications that were employed throughout the elaboration of this project.

Chapter 4 reveals the methodology inherent to the present work.

Chapter 5 presents all the results of the simulations and machine learning processes. In addition, here are written all the hypotheses, discussion and explanations that arose from their analysis.

Chapter 6 features the main, final conclusions that were drawn through the present work.

Chapter 7 focuses on the achievements made along the execution of the dissertation, as well as the future works that can be made, complementary to this study.

2 Context and State of the art

2.1 Background on Power Transformers

2.1.1 General overview of Power Transformers

Transformers are electrical devices essentially consisting of two or more coils of wire used to transfer electrical energy by means of a changing magnetic field [5]. There are numerous types of transformers, such as air core transformers, pulse transformers, power transformers, among others [6]. These can be used in various applications such as audio, radio, instrument, and power [7]. This work deals exclusively with power transformers. These play a vital role in the transmission and distribution of electrical energy. This is because power transformers enable the transmission of electricity to any location [8]. Below, in Figure 2, an example of these machines is depicted.



Figure 2 – Example of a power transformer [9]

Indeed, power transformers are extensively used by electric utility companies, power plants, and industrial plants [10]. This is due to their ability to minimize substantial energy losses in the transmission of large amounts of electrical power over long distances. This is done by converting the output current of a power plant into a high-voltage current and then stepping it down to a safer low-voltage current. This low-voltage current is more suitable for consumer usage such as domestical appliances.

2.1.2 Overview of the main components of a Power Transformer

The main components of power transformers are the following:



Figure 3 – Tank of a Power Transformer [11]

- Tank: As depicted in Figure 3, it provides external coverage to all components. It is usually made of steel. The core and windings are completely enclosed by the tank. Changes in oil volume due to changes in temperature must be taken into account, so a conservator tank must be used [12]. The bushings are placed on top of it (as seen in Figure 3) and they transmit electric power in and out of the tank. In addition, they work as insulators between the terminals and the tank [12].
- Magnetic Core and windings: This component offers a continuous path to the magnetic circuit flow as a means of strengthening the magnetic field [13]. It is made up of laminated steel sheets in order to reduce losses due to eddy current losses and losses by hysteresis [14]. Despite this countermeasure, it remains nonetheless one of the main heat sources in the transformer. The shape of this component varies with the type of the transformer (core type or shell type). Below, Figure 4 displays the core shapes relevant to this classification.

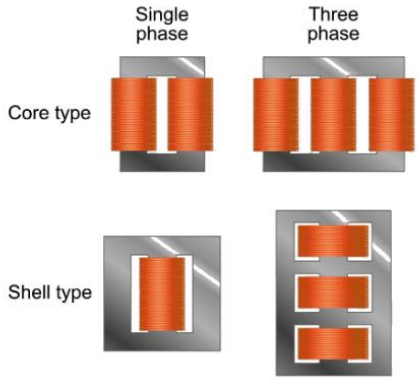


Figure 4 – Comparison between Shell and Core type transformer cores and windings [15]

- Cooling System: Power transformers feature both internal and external cooling mechanisms. Internal cooling refers to the cooling inside the tank performed with cooling fluids. For an oil-immersed transformer, internal cooling is promoted by the dielectric fluid [15]. External cooling, the main focus of this work, is made with radiators, fans or heat

exchangers (aerocoolers or hydrocoolers, e.g.). This part of the transformer will be detailed in the next section.

2.2 Background on cooling systems of Power Transformers

2.2.1 Overview

As mentioned before, a magnetic core is usually employed as a means of strengthening the magnetic field [13]. However, the magnetic flux created by the primary coil induces a current within the core. This phenomenon is described as an eddy current. Under the influence of this current, the magnetic core heats up [16]. This is undesirable, since this energy, if left unchecked, increases temperature to undesirable levels. Adding to this, conductor resistivity also generates heat when the electrical current circulates. As such, steps must be taken to ensure the stability of the equipment. The first countermeasure is to laminate the iron core, to break the current paths, thereby limiting eddy currents. This greatly reduces this effect's impact [17]. However, the main heat hazard that can negatively impact this machine's operation is the windings' own heating. Consequently, additional steps must be taken to deal with this matter.

In pursuance of an adequate heat management, mineral oil is used as a means of transferring heat to radiator modules that act as heat exchangers, which in turn, cool the hot oil. This cyclical procedure is shown below, in Figure 5.

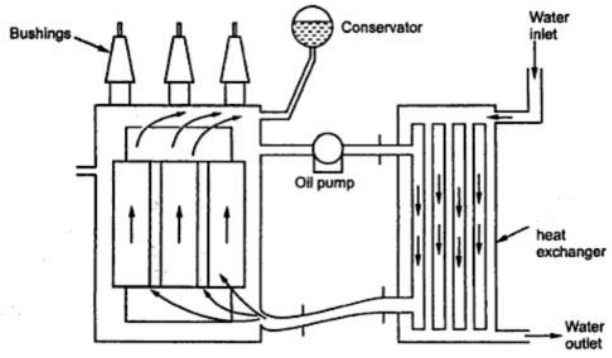


Figure 5 – Transformer general schematic [18]

In this representation, we can see that the oil is heated up near the windings' zone to be then cooled in the heat exchanger. It is worth noting that in this depiction, an oil pump facilitates the oil's circulation, and its cooling is aided by the flow of water within the heat exchanger.

A transformer can operate at different cooling modes. As such, it can have multiple designations according to the way it operates. This designation depends on the used cooling media and their flowing mechanisms. This designation is usually referred as a four-letter acronym. Below in

Figure 6 and Table 1, the structure of said acronym and the significance of each letter is explained.

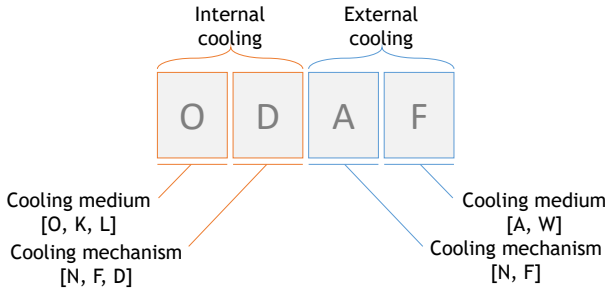


Figure 6 – Structure of the Cooling Mode Nomenclature

Table 1 - Cooling class designation description [19]

		Code Letter	Description
Internal	First letter (cooling medium)	O	Liquid with flash point less than or equal to 300 °C
		K	Liquid with flash point greater than 300 °C
		L	Liquid with no measurable flash point
	Second letter (cooling mechanism)	N	Natural convection through cooling equipment and windings
		F	Forced circulation through cooling equipment, natural convection in windings
		D	Forced circulation through cooling equipment, directed flow in main windings
External	Third Letter (Cooling medium)	A	Air
		W	Water
	Fourth letter (Cooling mechanism	N	Natural Convection
		F	Forced Convection

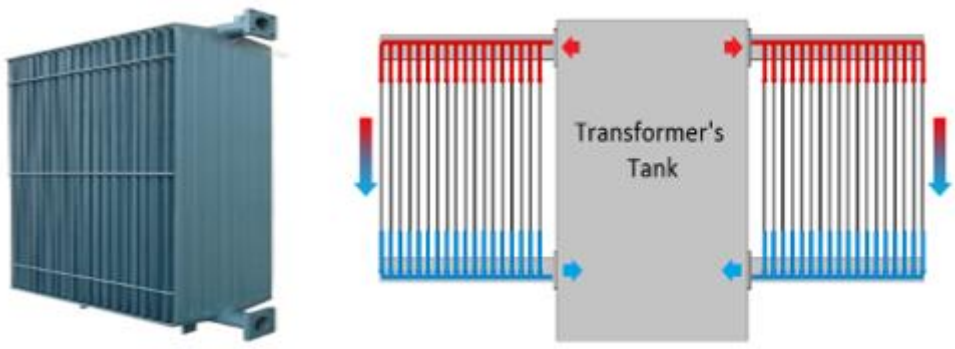
In this work, air natural and air forced cooling modes were studied. Regarding internal cooling, only oil-directed cooling systems were studied. Oil immersion is commonly used because this fluid features higher dielectric strength than air, which is fundamental to prevent electric breakdown or discharges at the coils and transformer core. It also acts as a cooling medium. The typical dielectric fluids used in transformers are mineral oils. Mineral oils provide efficient cooling and electrical insulation. On the other hand, they have low biodegradability [20]. As such, esters have been studied in recent times as a possible replacement [21].

2.2.2 External Cooling Media

In the matter of external cooling, the external cooling medium can be either air or water. In this work, only air-based systems were studied. Air is frequently chosen to be the external cooling medium since it does not have acquisition costs and its return to the environment does not require special attention. The same may not be true when using water [22]. However, the usage of water can be of use in some circumstances. Indeed, water features a higher specific heat capacity than air [23],[24]. This means that large amounts of energy can be carried away throughout long distances. In addition, it features a higher convective heat transfer coefficient. This means that water absorbs heat faster than air, and its temperature does not increase as much when doing so. Consequently, the heat transfer driving force of water reduces at a slower rate than air. Despite all these benefits, water cooling can only be used when the transformer is located near a large body of water, which limits their usage to activities like hydropower applications, where water it is available in large quantities at all times [25]. Another disadvantage is that in OFWF systems, is that there is a risk that the water may enter inside the transformer and any kind of leakage will contaminate the oil inside of it [26].

2.2.3 Heat Dissipation surfaces for air-cooled transformers

In external cooling systems, heat exchangers must be employed to transfer heat to an outer medium. The typical heat exchangers used in power transformers consists in thin vertical plate radiators. Figure 7 shows an example of this type of heat exchangers and a scheme of an oil circuit that can be implemented in it. There is great interest in using these radiators due to their construction simplicity, which makes them more economically sustainable [22].



(a) (b)

Figure 7 - Example of a vertical plate radiator (a) and a figure depicting the oil flow within the cooling system (b)

The oil, heated by the active part of the transformer, flows upwards, reaching the top of the tank (through natural or forced convection) and then enters the radiator plates. In the radiator plates, the oil is cooled (by natural or forced air convection) as it flows downward and enters

the tank at its bottom. The plates' cross section may vary. Different manufacturers may produce plates with different cross-sections.

2.2.4 Ventilation types for air-cooled transformers

As a means of enhancing the heat that is dissipated by the aforementioned heat transfer surfaces, forced convection is often enacted. This is done by ventilating the heat dissipation surfaces. To this effect, side and bottom ventilation can be implemented to increase cooling efficacy. Below in Figure 8 are depicted examples of these types of ventilation.



(a) (b)

Figure 8 – Types of tradiator ventilation. Radiators with bottom ventilation (a) [22] *and radiators with side ventilation (b)* [27]

Studies have been made to assess which the most adequate form of ventilation in each situation, these are analyzed in further detail in section 2.2.5.

2.2.5 Background on research regarding power transformer cooling systems

Concerning external cooling systems with air as cooling fluid, the transformer can be cooled by two different mechanisms: natural convection (AN) or forced convection (AF).

In the case of an AN cooling system, the cooling of the radiators is done by natural convection induced by the buoyancy force due to the temperature difference between the ambient air and the hot oil [28]. As a means of increasing heat transfer between the transformer and the outer medium, extra dissipating surfaces in the form of tubes or radiators connected to the transformer tank can be implemented [29].

The absence of fans in this type of system means that it has reduced mechanical vibration and noise [30], and its simplicity makes it economically interesting. In 2021, a thermal study of radiator-based cooling of transformers based on CFD simulations was conducted by Nogueira *et al*. [31] using the ANSYS CFX © software. This software uses the finite volume method to perform CFD simulations. In Figure 9, the geometry of the simulated ONAN model is represented.

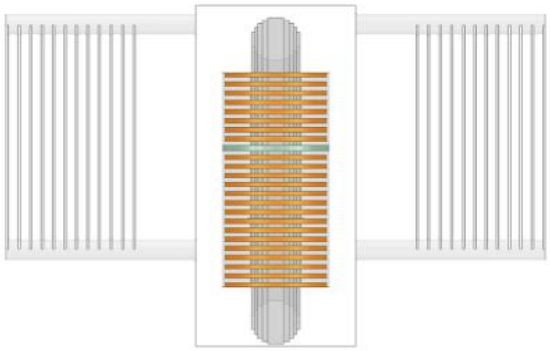


Figure 9 - Geometry of the simulated ONAN model [31]

In this work, it was concluded that ONAN has the worst cooling capacity of all cooling modes, resulting in a negative impact on the equipment's lifespan. Therefore, it was concluded that ONAN configuration is more suitable when dealing with power transformers of a lower scale, without the need of a greater heat dissipation. On this same topic, in order to facilitate the modelling of ONAN cooling, a reduced radiator CFD model was proposed in 2022 by Zhao *et al.* using an optimized air heat transfer coefficient equation to replace the air flow simulation [32]. This equation was comprehensively verified by using a full radiator CFD model including the air domain and a set of experiments under different operating conditions. To this effect, a CFD model detailing oil distribution and temperature profile within the plates was also produced. The radiator geometry consisted of top and bottom header pipes, as well as four 1-meter-high plates. The geometry of the transformer radiator model is shown below in Figure 10.

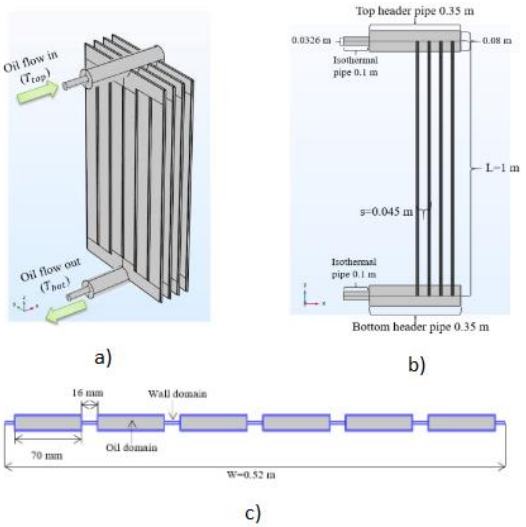
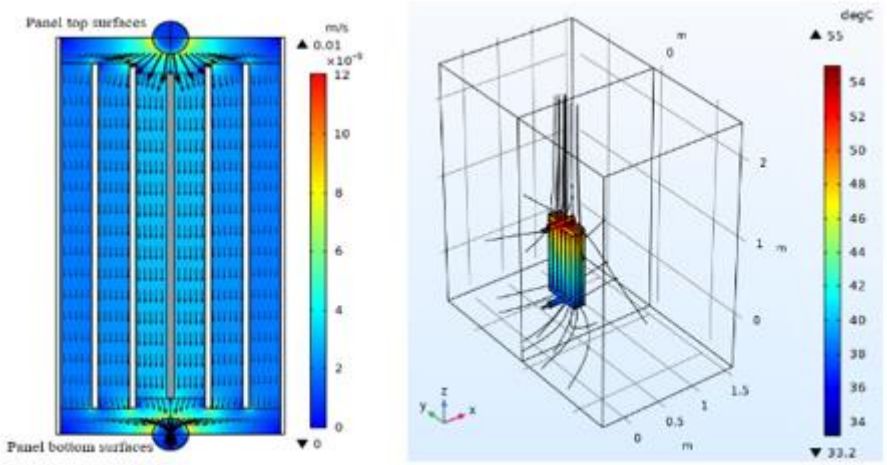


Figure 10 – a) 3D radiator CFD model; b) Side view of radiator CFD model; c) Cross-sectional view of middle of the radiator (oil domain in grey, wall domain in blue) [32]

The results produced by this model are shown below, in Figure 11:



(a) (b)

Figure 11 - Oil flow velocity and direction (a) and air flow streamlines with temperature contours (b) [32]

In (a) the oil's slight tendency to flow with increased velocity in the center of the plate can be seen. In (b), it is shown the temperature drop between the top and bottom of the radiator.

Additional work on this subject was done in 2017 by Córdoba *et al*. [33], where a 3D numerical modeling of an ONAN distribution transformer was presented. It is however worth noting that this was a model of a transformer with fins, and not radiators. It was found that the 3D problem of natural convection in this thermo-hydraulic device can be studied by a numerical model that represents a 3D slice of an ONAN distribution transformer. Also, in this work, the numerical temperature distribution was satisfactorily compared with thermographies presented in a heating test performed in an ONAN transformer provided by Tubos Trans Electric S.A. However, this cooling mode is not always adequate. Sometimes, a higher cooling performance or a more compact device is required. An alteration with some benefit [34] to this regard is the use of forced air, resulting in an ONAF cooling mode. As mentioned above, in AN, the heat exchange is induced by the buoyancy force due to the temperature difference between the ambient cooling air and the hot oil [28]. On the other hand, in an AF system, fans are installed on the sides or below the radiators, forcing air convection through them. A power transformer designed to operate in AF conditions is displayed below in Figure 12. In this example, we can see fans, which create conditions of forced air.

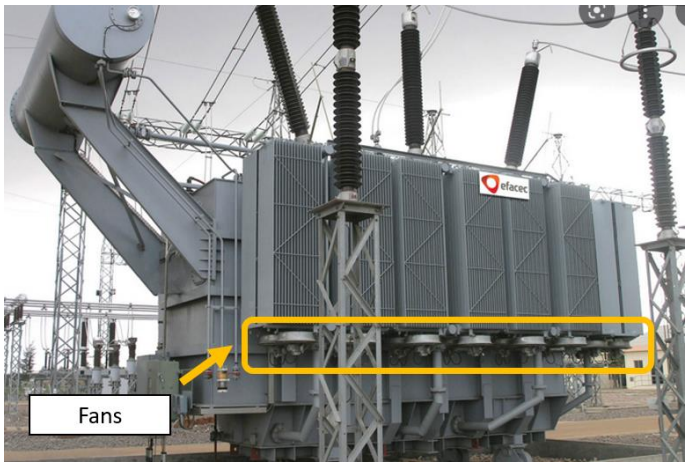


Figure 12 - Power Transformer equipped with fans, to work in an AF regime [35]

An increase in air velocity results in an increase in the dissipation capacity of the convection process. Furthermore, two characteristics of this regime are a reduction of the average temperature in the transformer and a reduction in the number of radiators to achieve the same efficiency of the AN [31].

Similar conclusions were drawn in Kim *et al.*'s numerical studies [28], in which it was concluded that the cooling performance of AF horizontal models is higher than that for the AN and AF vertical model in the studied radiator cooling system regardless of oil flow rate. In addition, it was inferred that the cooling performance of radiators in the AF cooling models strongly depends on the location of cooling fans along the bottom and right surface of radiators. Lastly, the cooling capacity obtained from the present computation using different turbulence model is compared with the measured data obtained from the present experiment, showing good agreement between them, especially when the standard $k - \varepsilon$ turbulence model is used.

Studies conducted by Van der Weken and Paramane in 2016 [36] further corroborate these results in the ONAF cooling mode. In this study, a thermo-hydraulic radiator model was developed. Numerical and experimental data highlight a more effective heat removal when using air forced systems. It is worth noting that this work's main goal was not to draw conclusions regarding thermo-hydraulic behavior of power transformers but to assess the performance of a transformer model that could later be used for that purpose. In Figure 13 are depicted graphs that show the performance of the model.

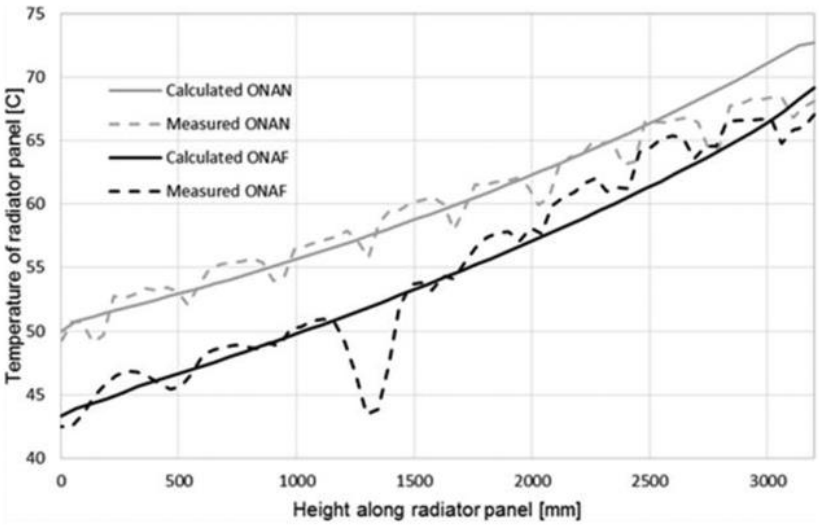
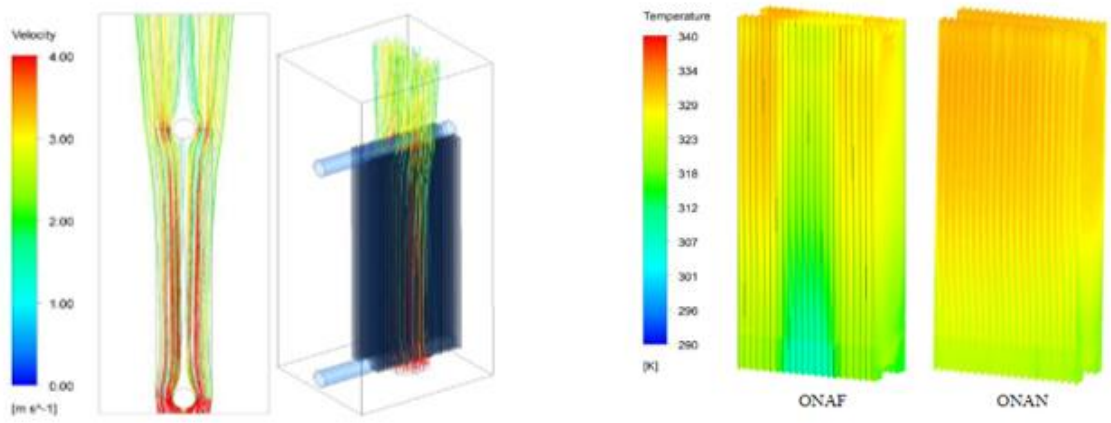


Figure 13 - Comparison of measured and calculated radiator panel temperature over the radiator height both for ONAN as ONAF condition [36]

As it can be seen, the calculated values follow the trend set by the measured ones, indicating a good degree of accuracy. Still with respect to ODAF cooling systems, CFD simulations of ODAF power transformers were carried out in 2021 by Wang *et al.* [37]. These offer further insight of the effect of upwards-facing forced cooling. The obtained results are depicted below in Figure 14.



(a) (b)

Figure 14 – Fan velocity streamlines (a). The overall temperature distribution of the radiator before and after the fan is turned off (b)[37]

In these graphs, the effects of forced convection are displayed. As shown in Figure 14, the stramlines of air, shown in the left graph, are in the same place as the colder zones displayed in the graph on the right. This means that the zones in which the air flows are cooled more effectively.

However, in addition to bottom ventilation, side ventilation can also be employed. Indeed, in 2014 Baltasar *et al.* [22] concluded that resorting to correlations obtained through numerical simulations, that choosing side or bottom ventilation depends on the number of radiators in series and the length of their plates.

The obtained results reveal that, if the number of plate pairs is increased by enough units, side ventilation becomes more efficient than bottom ventilation, as it can be seen in Figure 15.

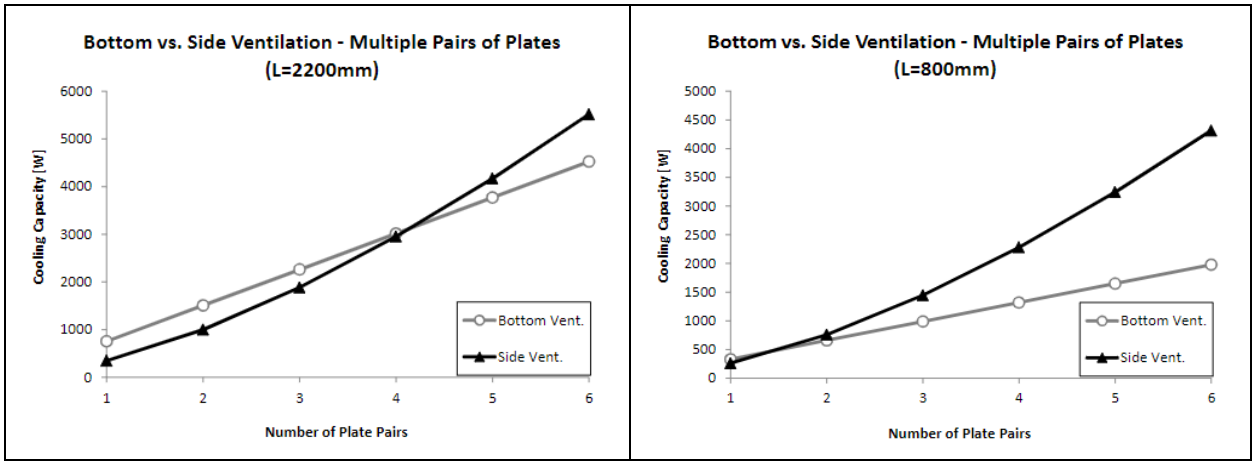


Figure 15 – Obtained correlations between cooling capacity and number of plate pairs [22]

This transition point seems to increase with the length of the plates. For a length of 2200 mm, at 5 plate pairs, side ventilation becomes more efficient than bottom ventilation, whilst for a plate length of 800 mm, 2 plate pairs are sufficient for this transition. Still regarding fan configuration, it was concluded in 2014 by Paramane *et al.* [38] that, for the geometry presented in Figure 16, side ventilation is more efficient. This is due to less sideways leakage of air.

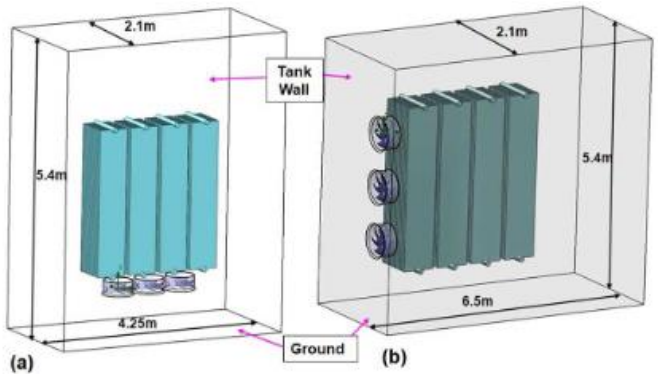


Figure 16 - Solid model and computational domain for (a) the vertical and (b) horizontal ventilation over the radiators [38]

To conclude this section, one can see that the design of cooling systems of power transformers can be a complex matter. There are multiple factors that influence their performance, such as

the type of air convection, the type of oil flow, the number of plates used, ventilation type, among others.

In addition, the performance of these configurations can be evaluated using multiple parameters, such as cooling capacity, equipment reliability, cost, and lifespan. As a means of studying all these factors, CFD, THNM and experimental work were used by researchers in the field. Knowledge obtained by experimental work can be quite desirable since there aren't any numerical approximations inherent to these studies. However, preparing a rigorous laboratorial setup with all desired conditions can be quite expensive. CFD presents a solution on that front since it comes with fewer material costs for researchers. Nonetheless, it is a numerical simulation, therefore its results are based on general equations and subject to numerical errors, these can arise from large convergence residuals or inaccurate numerical methods.

Lastly, THNM are quick in their application. However, the process of analytically describing the heat transfer and fluid mechanics phenomena can be quite difficult. This characteristic reduces this approach's feasibility, compared to CFD or experimental work. The election of the most adequate method is highly dependent on the situation at hand. The balance between the chosen method's swiftness and simplicity versus its accuracy must be carefully considered to achieve an optimum solution.

2.3 Background on Machine Learning

Machine learning is a field of study in which the goal is to enable systems to learn from data (that is, experience) and improve their performance without requiring explicit programming. That is, through the application of machine learning algorithms to datasets, models are produced and thus the knowledge acquired from the data is preserved and can be applied to new data.

2.3.1 Machine Learning Algorithms

In the present work, it was required the correlation of output variables with multiple input variables. To correlate multiple input variables with output variables through analytical means is quite difficult since multiple regressions need to be incorporated in one final equation. This constitutes an immensely complicated exercise, in which very large equation systems with multiple variable substitutions. As such, to this effect, machine learning algorithms present a good solution [39]. Since the goal of the present work is to formulate predictions from previously obtained data, this can also be referred as a supervised learning task [40].

The data that was dealt with was of a continuous nature, consequently, classification algorithms were deemed irrelevant and only regression algorithms were considered, which

includes: linear regression, ridge regression, polynomial regression, support vector machines and random forests.

Linear regression

This algorithm generates a model of linear nature. Its goal is to minimize the residual sum of squares between the observed targets in the dataset, and the targets predicted by a linear approximation [41].

Ridge regression

Ridge regression operates similarly to linear regression, however, it shrinks the regression coefficients by imposing a penalty on their size. This penalty introduces a reasonable amount of bias which considerably reduces variance. This penalty can alleviate the issue of multicollinearity often present in the linear regression algorithm, frequently due to models trained on large amounts of features [42]. It does so by adding the squared magnitude of the coefficients as penalty term to the loss function (also known as L2 regularization, or weight decay on neural networks) [43]. Generally speaking, this method provides increased efficiency in parameter estimation issues by avoiding the problem of overfitting [44].

Support Vector Machines

Support vector machines (SVM) is a family of algorithms suitable for both classification and regression tasks [45]. Their main advantages are their effectiveness in high dimensional spaces, their memory efficiency and their performance in cases in which the amount of dimensions surpasses the amount of samples [46].

Polynomial Regression

Polynomial regression generates a regression model in the form of a polynomial equation that predicts the value of a dependent numeric variable [47]. Compared to the two previous algorithms, this regressor is more suitable for fitting highly disperse data. However, this reduction in variance is followed by an increase is bias and the possibility of overfitting. Indeed, one must be cautious with the degree of the polynomial expression, since for p data points, a polynomial with a degree of (p-1) or higher will fit them with an error of zero, but an overfitted model will be the most likely outcome. This effect is shown in Figure 17, where the linear and polynomial regression algorithms (represented by the red and black lines, respectively) were applied to a training dataset created for demonstration purposes (represented by the blue dots).

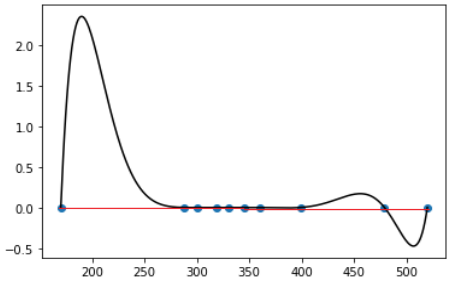


Figure 17 – Comparison of the fitting of a linear model and polynomial model to a training dataset

As the picture depicts, both the linear model and polynomial model are good at predicting training data, since both lines pass through the blue dots. However, the polynomial model deviates significantly from the general trend of the data in certain zones, namely near the values 200 and 450 of the x-axis.

Random Forests

Random forests are, in essence, a combination of tree predictors formed by sampling from the training data. This procedure consists in training the same tree multiple times and then averaging the result [48].

This algorithm is categorized as a form of ensemble learning. Methods featured in this category resort to multiple estimators in pursuance of obtaining a better predictive performance than any of those estimators alone. An ensemble of models is a set of models that combined their predictive capabilities in some way to improve the evaluation of new examples [49].

2.3.2 Performance Metrics for Machine Learning Algorithms

As stated above, multiple machine algorithms were studied and evaluated. In a regression problem, a model's performance assessment is generally made by analyzing the residuals, which represent the difference between predicted and observed [44]. In this work, five metrics based on this principle were used: the mean absolute error (MAE), the mean squared error (MSE), the root mean squared error (RMSE), the mean absolute percentage error (MAPE) and the coefficient of determination (R^2).

MAE, MSE, and RMSE are parameters that express average prediction error in the units of the variable at hand. MAPE produces the average prediction error in percentage, normalized by the observations. Consequently, the outcome value is based upon a true observation. These metrics can range from 0 to ∞, are negatively oriented and indifferent to the direction of errors. MAE assesses the magnitude of the error in a set of predictions by assuming equal weights of each residual. Having the same target units of the real values makes the metric very intuitive to interpret. RMSE and MSE square errors before they are averaged, which provided higher weights

to larger errors. This property makes these metrics particularly useful when significant errors are particularly undesirable. Generally, RMSE tends to be more used than MSE due to its superior interpretability in the target units. MAPE puts a more substantial penalty on negative errors than on positive ones and its usage is not advised if the target variable features zero-valued observations. Nevertheless, MAPE is useful for positive target value sets due to its particularly intuitive interpretation in terms of relative error. Lastly R^2 expresses the proportion of the variance in the dependent variable that is predictable from the independent variables. It ranges from 0 to 1 (0 to 100%), and it is positively oriented (that is, the higher the value, the better the model performance).

3 Computational Applications and their Usage

3.1 ANSYS Workbench

ANSYS Workbench is a multi-tool workspace, which allows for the usage of multiple simulation-related software and information transfer between them. Figure 18 depicts the essential CFD ANSYS workflow.

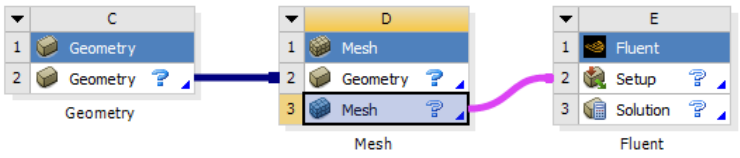


Figure 18 - Essential ANSYS CFD workflow. It is composed by three modules: the Geometry module (left), the Mesh module (center) and the Fluent Module (right)

This workflow is composed of three modules: the *Geometry* module, the *Mesh* module and the *Fluent* module.

The first module contains the geometry of the all domains to be meshed, and thus subjected to later CFD-related treatment. *Space Claim* was the selected software to draw all geometries relevant to this work.

The second module uses the previously generated geometry to produce a mesh. In CFD, the meshing process can be defined as the discretization of the domain of interest [50]. This domain is shaped by the *Geometry* module.

The meshing process is a crucial step to any CFD simulation for the spatial discretization of the governing equations. The momentum equations, the continuity equation and the energy equation must be applied in integral form. As such, spatial discretization is required when solving these equations between a set of boundaries [51]. This means that a more refined mesh allows for a less crude numerical resolution of these equations, which leads to superior results than those obtained using a mesh with less cells [52].

Lastly, the third module receives the project mesh as an input and solves the aforementioned equations with additional specifications that depend on the particular case that is being dealt with. This module uses ANSYS Fluent 2021 R2 for these proceedings. This software allows the user to specify the materials, boundary conditions and numerical methods that are more suitable to the case at hand.

3.2 Python

Python is an interpreted, intuitive, high-level programming language. Its high-level built-in data structures, combined with typing and binding dynamics make it very attractive for *Rapid Application Development*, as well as for use as a scripting or to connect existing components together. Python supports modules and packages, which encourages program modularity and code reuse [53]. This language was used to program the machine learning simulator. In addition, Python libraries, packages and modules that were of use in this work are presented below.

3.2.1 Scikit-learn

Scikit-learn is a free and open-source library that helps tackle supervised and unsupervised machine learning problems. This software is built entirely in Python and utilizes *NumPy*, an important Python library in this work and contains multiple useful algorithms (such as Support Vector Machines or Random Forests) used for machine learning [54]. The regression algorithms used to correlate output variables that will be described later on came from this library.

3.2.2 NumPy

NumPy is a very useful package for scientific computing in Python. It is a Python library that provides a multidimensional array object, derived objects (such as matrices and masked arrays), and a list of routines suitable for fast operations on arrays, including mathematical, logical, shape manipulation, sorting, selecting, input/output, discrete Fourier transforms, basic linear algebra, basic statistical operations, random simulation and much more [55]. This library was useful to convert input variables in order for them to be processed by the program.

3.2.3 Pandas

Pandas is a Python package providing fast, flexible, and expressive data structures designed to make working with multiple types of data simple. It aims to be the fundamental high-level building block for doing practical, real-world data analysis in Python [56]. This library facilitated the reading of the training datasets, written in an Excel file.

3.2.4 Tkinter

The *Tkinter* module allows for the creation of graphical interfaces that allow the user to interact with Python-coded applications [57]. The simulator GUI was created using this package.

4 Theory and modeling approach

4.1 Problem Description

Summarily, the main objective of this work was to evaluate the influence of morphological aspects (such as plate height and number of plates) and convective settings (such as oil flow rate and external convective heat transfer coefficient) on the thermo-hydraulic performance of transformer external cooling systems. Firstly, simulations of a single radiator plate were carried out, as preparation for the simulation of radiators. This section will deal with the settings and results of radiator simulations. The settings and results inherent to single plate are detailed in Appendix C.

4.2 Employed thermo-hydraulic models

4.2.1 Studies of Pressure Drop

Pressure drop is the difference in total pressure between two points in a fluid-carrying network. When a fluid enters one end of the system, and leaves the other, pressure drop, or pressure loss, will occur. The mathematical manipulation of Bernoulli's equation allows one to conclude that pressure drop (ΔP) is related to the system's volume flow rate (Q) by Equation (1)

$$\Delta P = a \cdot Q^2 + b \cdot Q \quad (1)$$

It is also known that the geometrical aspects of the system at hand, such as pipe length or the hydraulic diameter affect the flow pressure drop [58]. Another factor that influences the fluid pressure drop is the Reynolds number [59]. This dimensionless parameter can be described as the ratio between inertial forces and viscous forces [60]. The Reynolds number (Re) can be calculated by Equation (2).

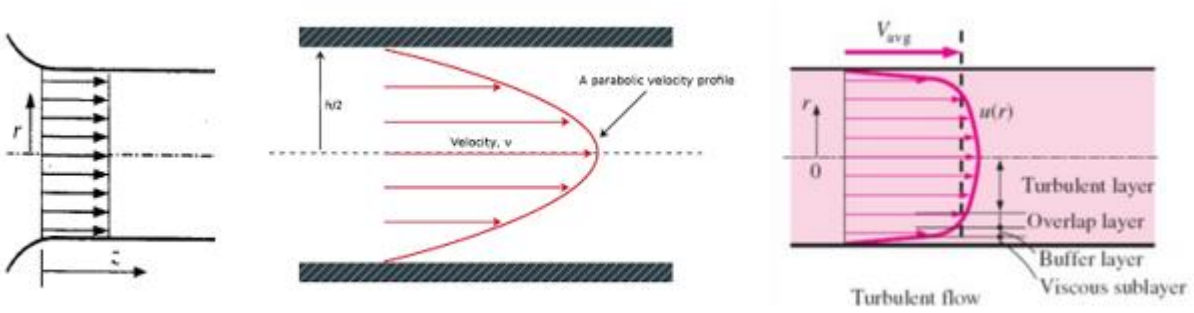
$$Re = \frac{\rho \cdot v \cdot D_h}{\mu} \quad (2)$$

where variable Re is the Reynolds Number, ρ is the density, v is the fluid velocity, D_h is the hydraulic diameter and μ is the dynamic viscosity. Both fluid density and viscosity decrease with the fluid's temperature [61], [62]. Hence, the effect of heat dissipation in the fluid pressure drop was also studied by introducing user-defined functions (UDFs) in which the oil properties (viscosity, density, specific heat and conductivity) were set as a function of temperature. These UDFs were then

interpreted by the program (Fluent) and the oil thermophysical properties were defined by them. For more details about the applied UDF, see Appendix X.

4.2.2 Velocity Profiles

When setting up all CFD simulations, an inlet velocity must be selected. However, there are velocity profiles depending on the inlet direction and flow type at hand.



(a) (b) (c)

Figure 19 – Types of fluid velocity profile. Uniform velocity profile (a), parabolic velocity profile (b), velocity profile based on a power law (c)

Firstly, there is the uniform velocity profile, possibly the simplest of them all. This profile is characterized by all flowing area having an equal velocity value and direction, as depicted in Figure 19. Secondly, there is the velocity profile present in fully developed laminar flow, which is the parabolic velocity profile. For a cylindrical pipe, it is characterized as described as follows in Equation (3):

$$v = vmax\left(1 - \left(\frac{r^2}{R}\right)\right) \tag{3}$$

In which v is the velocity at each point of the profile, $vmax$ is the maximum velocity within the profile, located in its center. R is the pipe maximum radius and r is the radius. The general aspect of the parabolic profile is depicted in Figure 19. Lastly, when the fluid reaches turbulent flow, it strays away from the parabolic profile and its velocity distribution flattens, as depicted above in Figure 19.The profile depicted in Figure 24 can be mathematically defined by a power law, as written in Equation (4):

$$\frac{v}{vmax} = \left(1 - \left(\frac{r}{R}\right)^m\right)^{\frac{1}{n}} \tag{4}$$

In which v is the velocity at each point of the profile, R is the pipe maximum radius and r is the radius at which the velocity is v. m and n are exponents that used to mold the profile, usually in order to fit to experimental data [63]. Unfortunately, the calculation of $vmax$ as a

function of the average velocity is quite difficult. However, it was found in [63] that when the values of m and n are 2 and 7, respectively, the following correlation can be used:

$$vavg = 0.875 \cdot vmax \quad (5)$$

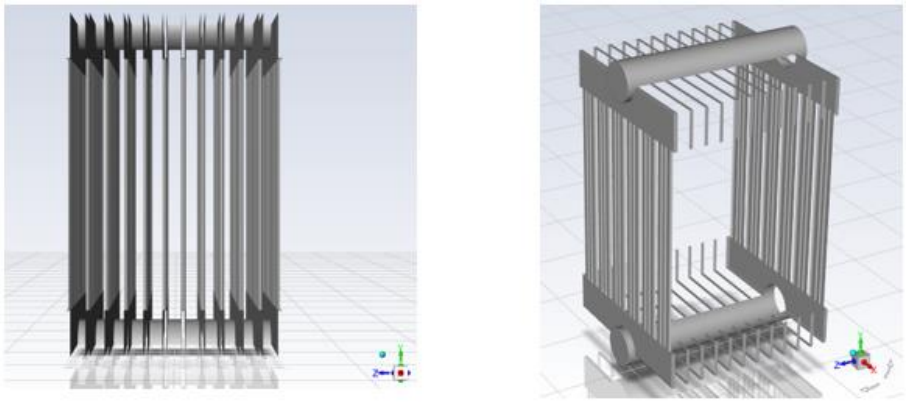
4.2.3 Heat Transfer Coefficients

One of purposes of the thermo-hydraulic simulations of this work was to assess the influence of different types of convection in the thermo-hydraulic behavior of the transformer cooling system. As such, to simulate and study this factor, a thermal boundary condition had to be specified on the radiator's plates wall. This condition required the air ambient temperature (which was set at 20ºC) and a convective heat transfer coefficient.

In order to calculate this parameter, Fourier's Law and Newton's Law of cooling were resorted to, resulting in Equation (6):

$$\frac{1}{hairm} = \frac{1}{hair} + \frac{l}{k} \quad (6)$$

Where $hairm$ is the external heat transfer coefficient, which combines the air and metal resistance, $hair$ is the air heat transfer coefficient, l is the plate thickness and k is the plate thermal conductivity. Three convection modes were studied: Air Natural (AN), Air Forced with moderate ventilation (AF1) and Air Forced with intense ventilation (AF2).For AN, the effects of the heat boundary layer are particularly relevant, since there is no ventilation to remove it. As such, two surface types were considered: inwards facing surfaces and outward facing surfaces. The selection of each is represented below in Figure 20.



(a) (b)

Figure 20 – Selection of inwards facing surfaces (a) and outwards facing surfaces (b)

Using this selection, the $hairm$ for AN was calculated through equation (7), as shown below:

$$hairm_{AN} = \frac{1}{\frac{1}{\frac{A_{inwards}}{A_{total}} \cdot 4.38 + \left(1 - \frac{A_{inwards}}{A_{total}}\right) \cdot 9.49} + \frac{l}{k}} \quad (7)$$

In this equation, $A_{inwards}$ is the inwards-facing area depicted in Figure 20, and A_{total} is the total radiator surface area (excluding the inlet and the outlet). In the denominator, there are two absolute values: 4.38 and 9.49 [32]. 4.38 is the air heat transfer coefficient for natural convection for inwards facing surfaces and 9.49 is the heat transfer coefficient for outwards-facing surfaces. This was done to include the effect of the boundary layer in the inwards facing surfaces. Since these cooling surfaces are often close to each other, their heat boundary layers affect each other's driving force. As such, for AN, $hairm$ acquired a different value for each height and number of plates. As such, it attained in total nine values, as shown in Table 2:

Table 2 – Values of $hairm$ for AF in W·m^{-2}·ºC^{-1} used for each radiator geometry

	N1 (7 plates)	**N2 (12 plates)**	**N3 (20 plates)**
H1 (0.8 m)	5.4	5.0	4.8
H2 (1.5 m)	5.2	5.0	4.7
H3 (3 m)	5.2	4.9	4.7

For air forced regimes, ventilation helps to dispel the thermal boundary layer. Consequently, the previously mentioned effect is not so intense. As such, the same coefficient was applied to all surfaces. These values are shown below, in Table 3.

Table 3 - Values of $hairm$ for AF1 and AF2 in W·m^{-2}·ºC^{-1}

	AF1	**AF2**
$\boldsymbol{hair}$ **/ W·m^{-2}·ºC^{-1}**	11.6	16.0
$\boldsymbol{hairm}$ **/ W·m^{-2}·ºC^{-1}**	11.6	16.0

As it can be seen, there is not much influence of the conductive resistance inherent to the steel wall since the values of $hair$ and $hairm$ values are essentially the same.

4.2.4 Studies of Heat Dissipation and Temperature Distribution

Temperature distribution is entirely calculated by Ansys Fluent (R). However, to assess the power that was dissipated in each case, the following equation was used:

$$P = \dot{m} \cdot C_p \cdot (T_{in} - T_{out}) \quad (8)$$

In equation (8), P is the dissipated power, $\dot{m}$ is the mass flow rate, T_{in} is the temperature of the inlet fluid and T_{out} is the temperature of the outlet fluid.

4.2.5 Governing Fluid Flow Equations

The Navier-Stokes equation, in fluid mechanics, a partial differential equation that describes the flow of incompressible fluids. The equation is a generalization of the equation devised by Swiss mathematician Leonhard Euler in the 18th century to describe the flow of incompressible and frictionless fluids [64]. These equations consist of a time-dependent continuity equation for conservation of mass, three time-dependent conservation of momentum equations and a time-dependent conservation of energy equation.

For a steady flow, incompressible and laminar and with a Newtonian behavior, the governing equations for fluid flow are as follows:

$$\rho\, \partial V\, \partial t \;+\; \rho(V \cdot \nabla)V \;=\; -\nabla P \;+\; \nabla \cdot \tau \qquad (9)$$

and the continuity equation:

$$\nabla \cdot V \;=\; 0 \qquad (10)$$

In which V represents the velocity vector, ρ the mean density, P the pressure, and $\boldsymbol{\tau}$ the stress tensor.

4.3 CFD Thermo-hydraulic Simulations: Radiators

The following thermo-hydraulic simulations are the backbone of this work. In addition to contributing to the better understanding of radiator cooling, this data was later processed using machine learning algorithms. The models generated by these algorithms were then used to build a tool capable of predicting the results, when giving the input of the number of plates in the radiator, the plate height, the flow rate and convection type.

4.3.1 Geometry

In these simulations, radiators were simulated. These are structures composed of plates connected by a collector tube. In these simulations their height acquired the values described in Table 4:

Table 4 – Simulated radiator heights

H1 (m)	H2 (m)	H3 (m)
0.8	1.5 m	3 m

However, in addition to this geometrical dimension, the number of plates was also a variable, which acquired the values described below in:

Table 5 – Simulated plate numbers

N1	N2	N3
7 plates	12 plates	20 plates

These values were taken from the company's internal bibliography,adiator was reviewed and selected. However, the maximum number of simulated plates was 20 due to the computational requirements of these simulations against the available computational resources.

Below it is depicted an example geometry of a radiator, of 7 plates and 0.8 m height.

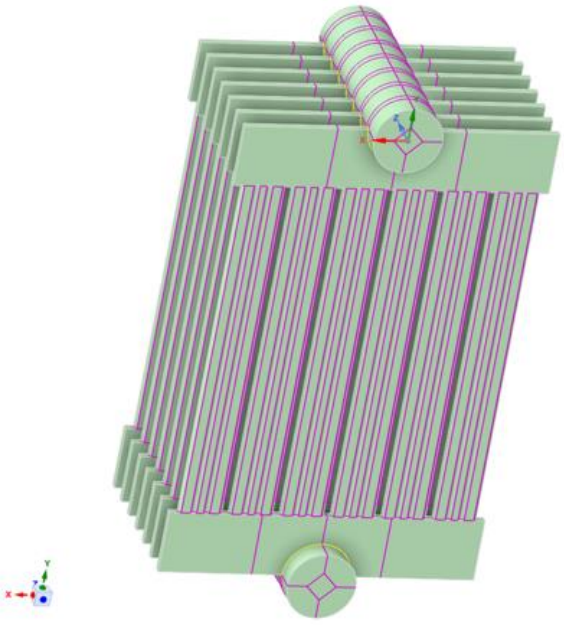


Figure 21 – Example of a radiator geometry

4.3.2 Mesh

For these simulations, new mesh independence tests were conducted. This was due to the computational requirements of the radiator simulations. Not only they factored in the energy equation and temperature-dependent thermophysical properties, but the geometry was also much larger and more complex.

These mesh tests resulted in the following meshes, as shown in Table 6, Table 7 and Table 8.

Table 6 – Characterization of the meshes used in the thermo-hydraulic simulation of a radiator with a height of 0.8 m

	Number of cells	Number of nodes
Radiator with N1 (7 plates)	3708968	1761114
Plate with N2 (12 plates)	9065726	3591454
Plate with N3 (20 plates)	15125223	6040112

Table 7 – Characterization of the meshes used in the thermo-hydraulic simulation of a radiator with a height of 1.5 m

	Number of cells	Number of nodes
Radiator with N1 (7 plates)	4567649	2771501
Plate with N2 (12 plates)	10426737	5230058
Plate with N3 (20 plates)	17416704	8757633

Table 8 – Characterization of the meshes used in the thermo-hydraulic simulation of a radiator with a height of 3 m

	Number of cells	Number of nodes
Radiator with N1 (7 plates)	6090098	4616168
Plate with N2 (12 plates)	13061026	8441135
Plate with N3 (20 plates)	21805610	14112777

As expected, the mesh complexity increases with the number of plates and their height.

4.3.3 Simulation Settings

In these thermo-hydraulic simulations, the energy equation was activated, and so was gravity (with an acceleration of -9.8 $m \cdot s^{-2}$ in the y direction).

The chosen fluid flow model was, once again, the laminar one. The flow rates for these simulations were calculated based on the previous flow rates per plate multiplied by the number of plates per radiator, resulting in the following values:

Table 9 – Flow rate values (Q) pertaining to each plate number. Underlined flow rates had Re > 4000 at the radiator inlet

	Q_0 / $m^3 h^{-1}$	Q_1 / $m^3 h^{-1}$	Q_2 / $m^3 h^{-1}$	Q_3 / $m^3 h^{-1}$
N1	1.21	2.74	<u>6.10</u>	<u>9.49</u>
N2	2.08	<u>4.69</u>	<u>10.46</u>	<u>16.26</u>
N3	3.46	<u>7.82</u>	<u>17.43</u>	<u>27.10</u>

It is worth noting that, to equalize the interval between flow rate values, the flow rate generated by v1 (Q_0) was not considered. Instead Q_1 was selected, which is the average between Q_0 and Q_2.

The underlined flow rates were clearly in turbulent flow regimen when entering the radiator domain. As such the following solution was implemented: all simulations were set using the laminar model. This was because despite the fluid's turbulent entrance, it later subdivides along multiple channels, heavily reducing its Re. This meant that the simulation domain was still predominantly laminar. However, for the flow rates with an inlet Re > 4000, a power-law based inlet velocity profile was defined in an UDF, to simulate a turbulent velocity profile. For the remaining flow rates, a parabolic velocity profile was written in said UDF. Lastly, it is worth mentioning that the no-slip condition was implemented at the wall.

As for the thermal aspects, the inlet flow rate was set to have a temperature of 60 ºC and all oil thermophysical properties were defined using an UDF supplied by Efacec. It is worth noting that all used UDFs are mentioned in Appendix CA The wall boundary condition was defined as a convective wall. In this setup, the external convective heat transfer coefficient was set as described in section 4.2.3, and the free stream temperature was of 20 ºC. In this boundary condition, the effects of heat conduction are present. The external heat transfer coefficient includes both the air resistance and the metal resistance. However, as mentioned earlier, the low thickness of the steel case and its high conductivity greatly reduce the impact of the conductive resistance in this boundary condition.

5 Results and discussion

In this chapter follows a description of the results that were obtained throughout this work. In each section of this chapter, the results of CFD simulations are presented. Then a thorough analysis of said results follows, in which these results are processed, explained, and correlated. The results in this section were obtained through CFD thermo-hydraulic studies of radiators, with 7, 12 and 20 plates. Lastly, the results of the conjoined correlation of all obtained values through machine learning are presented and evaluated.

5.1 CFD Simulations: Thermo-hydraulic studies of radiator design

5.1.1 Pressure Drop

Here follows an in-depth analysis of how the pressure drop is affected by multiple aspects of transformer design and operation.

Effect of the number of plates and plate height

Below, in the following list of figures, the influence of the number of plates and flow rate is analyzed. Since the pressure results between AN, AF1 and AF2 featured great overlap, this meant that the ventilation type had little effect on the pressure drop within the fluidic system. As such the polynomial correlations of ΔP and $\dot{m}$ were only done for one convection type (AF2 was chosen).

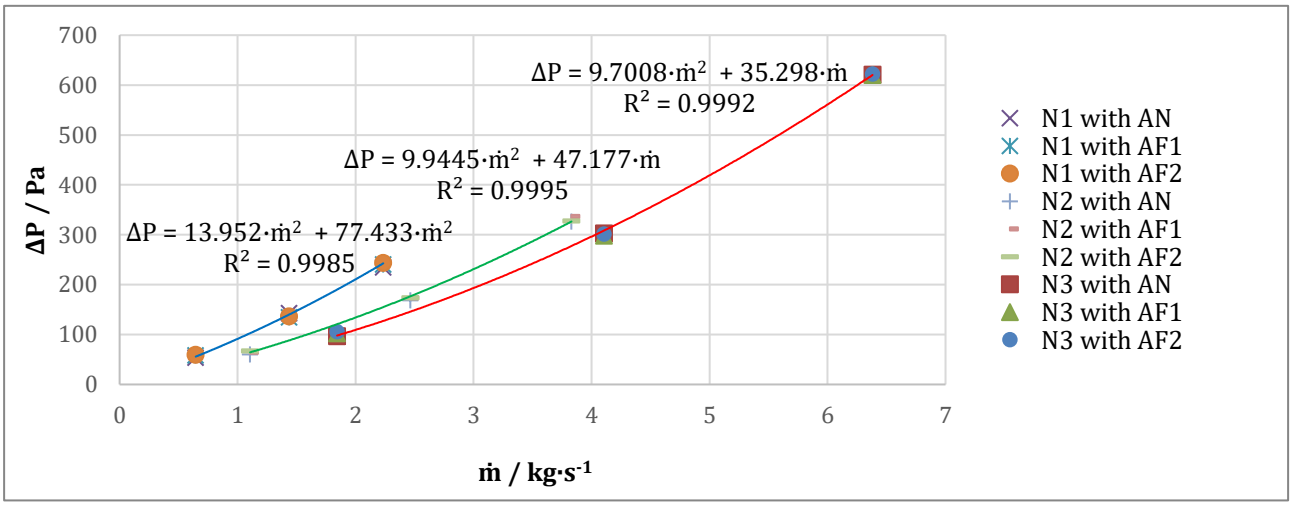


Figure 22 - Correlations for pressure drop (ΔP) as a function of flow rate for three numbers of plates for a height of 1.5 m

The results for the rest of the heights (0.8 m and 3 m) had similar features. These can be found in Appendix J.

All these regressions had a set intercept to 0, with the exception of the polynomial regression for N1. This was because with an intercept to 0, it would have a negative 2nd order term, which would indicate unphysical behavior. As such, this polynomial equation was created with a small independent term, for it to be later usable. This error was most likely caused by a small numerical deviation, given that these regressions are so close to being fully linear, at least in this range of flow rate values, the smallest numerical error can lead to a negative 2nd order term. Either way, all produced correlations feature high coefficients of determination, which corroborates the model expressed by Equation (1).These equations provide insight into hydraulic aspects of transformer design. With them, one can predict pressure drop using flow rate, for all these designs.

The next round of graphs was made as a means of studying the effect of plate height in the overall pressure drop.

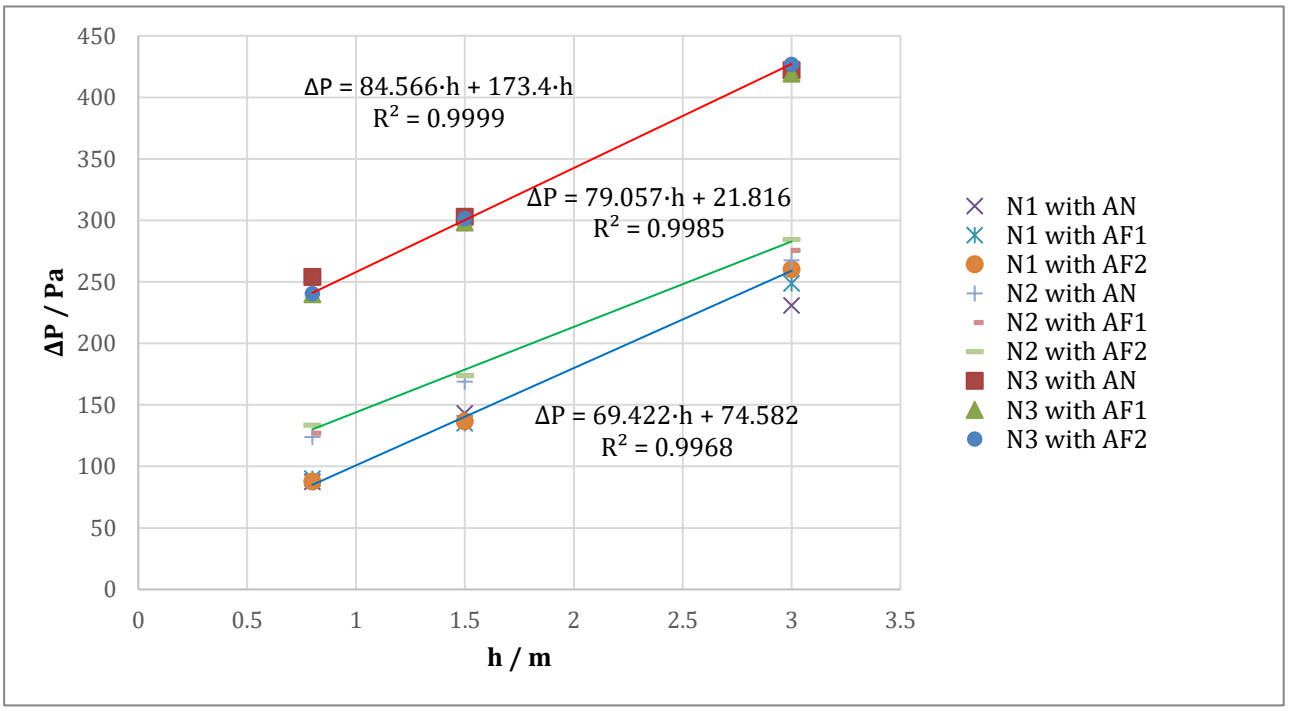


Figure 23 - Correlations for pressure drop (ΔP) as a function of flow rate for three numbers of plates for the flow rate Q2

Through these results one can see that the pressure drop can be linearly correlated with plate height. This is to be expected, given that pressure drop scales linearly with the length of the fluidic system, according to Bernoulli's equation. The results for the remaining flow rates (Q1 and Q3) had similar features. These can be found in Appendix J.

5.1.2 Outlet Temperature and Dissipated Losses

In this section, the output temperature and overall heat dissipation rate obtained through CFD in all variations of radiator design and operation is presented and studied.

Effect of plate height

Below are presented the results of outlet temperature drop and energy dissipation rate with plate height:

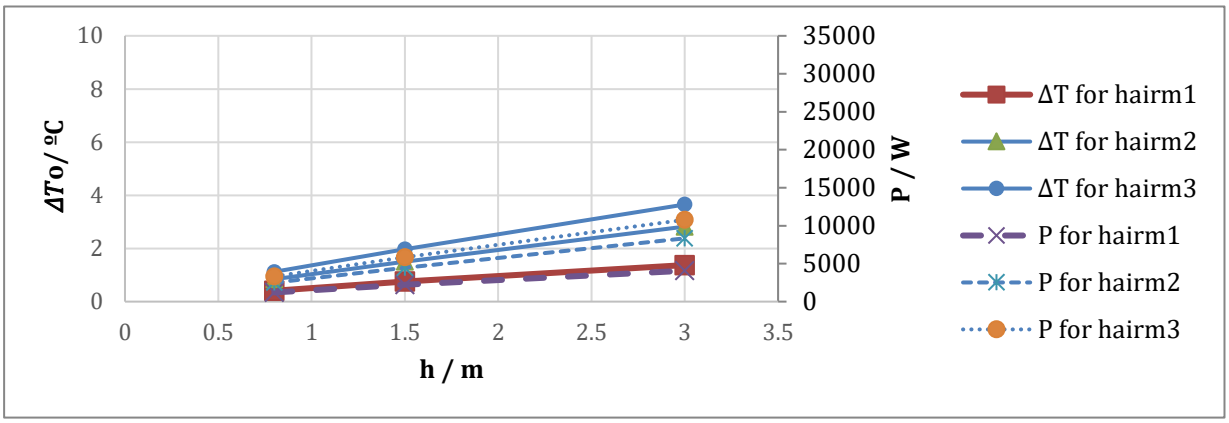


Figure 24 - Output temperature and energy dissipation rate as a function of plate height with varying external convective heat transfer coefficients for a radiator of 7 plates and Q2

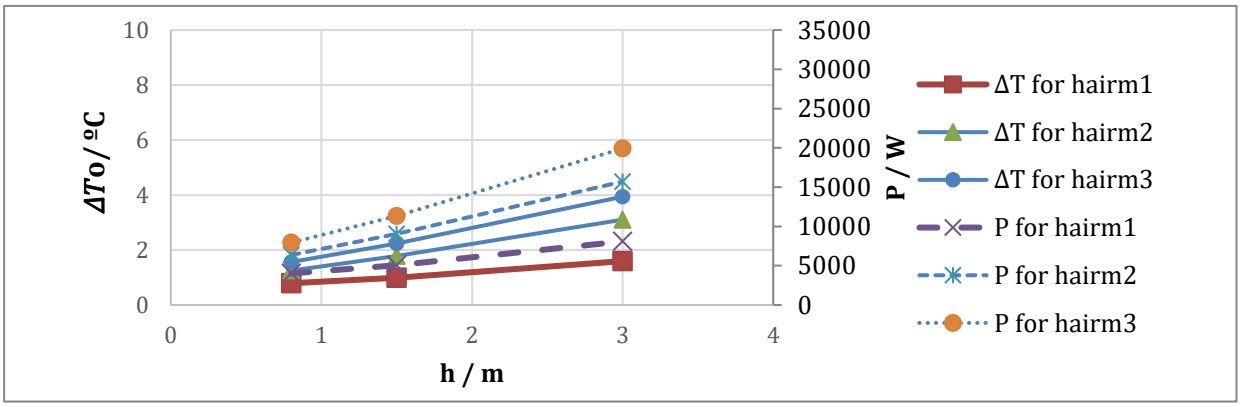


Figure 25 - Output temperature and energy dissipation rate as a function of plate height with varying external convective heat transfer coefficients for a radiator of 12 plates and Q2

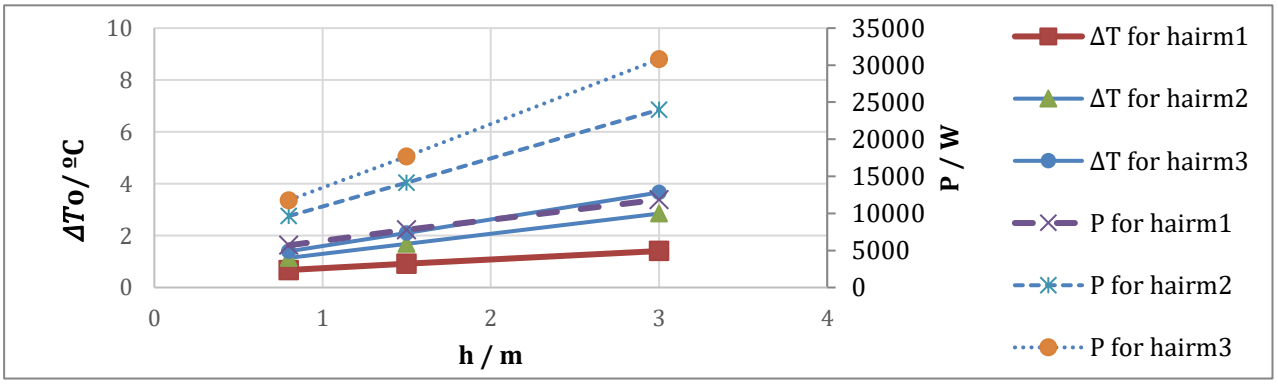


Figure 26 - Output temperature and energy dissipation rate as a function of plate height with varying external convective heat transfer coefficients for a radiator of 20 plates and Q2

The obtained results point to an almost linear relationship between power and plate for this range of heights. This means that increasing plate height (within this range of values) to

increase the dissipation of energy is an adequate solution, since the dissipated power continues to rise without stagnation. It is noteworthy to note that this was an expected result since a constant boundary condition of inlet temperature was assumed in all simulated cases. In addition, we can see that the number of plates and plate height reduces the impact that the convection style has on the temperature drop.

Effect of the flow rate

In this section are presented the values of output temperature drop and energy dissipation rate as a function of mass flow rate. These results are important because the increase in oil flow rate may be used to increase the cooling of the transformer.

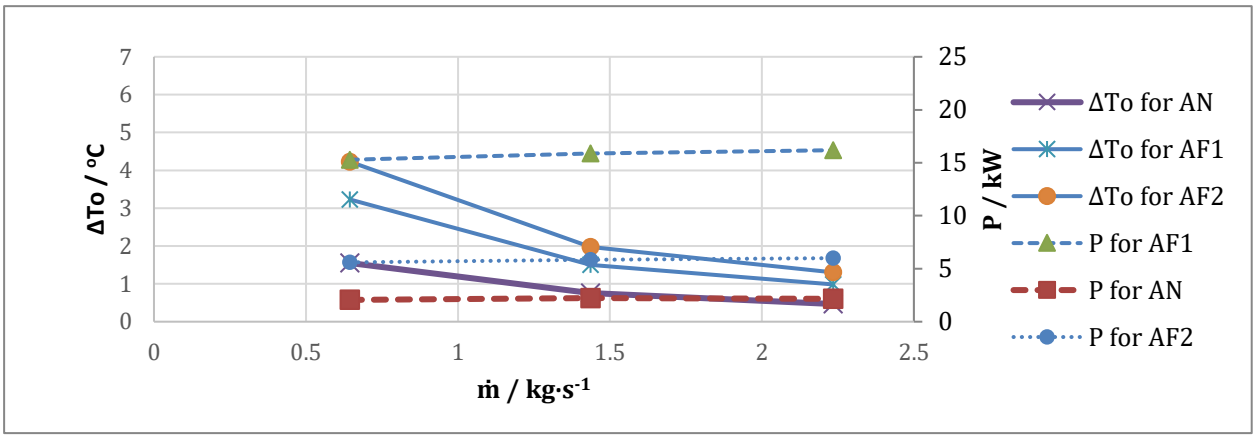


Figure 27 - Output temperature and energy dissipation rate as a function of plate height with varying external convective heat transfer coefficients for a radiator of 7 plates and a height of 0.8 m

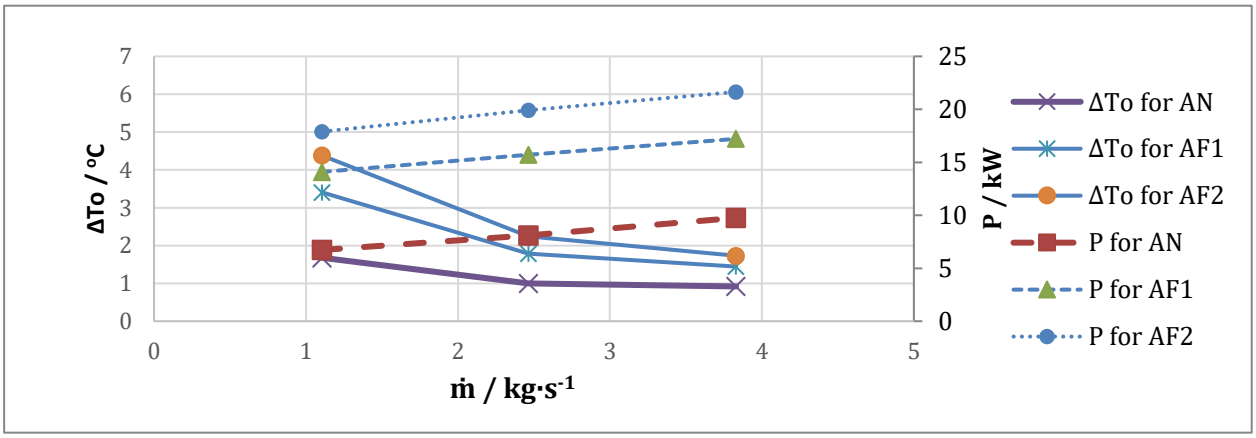


Figure 28 - Output temperature and energy dissipation rate as a function of plate height with varying external convective heat transfer coefficients for a radiator of 7 plates and a height of 1.5 m

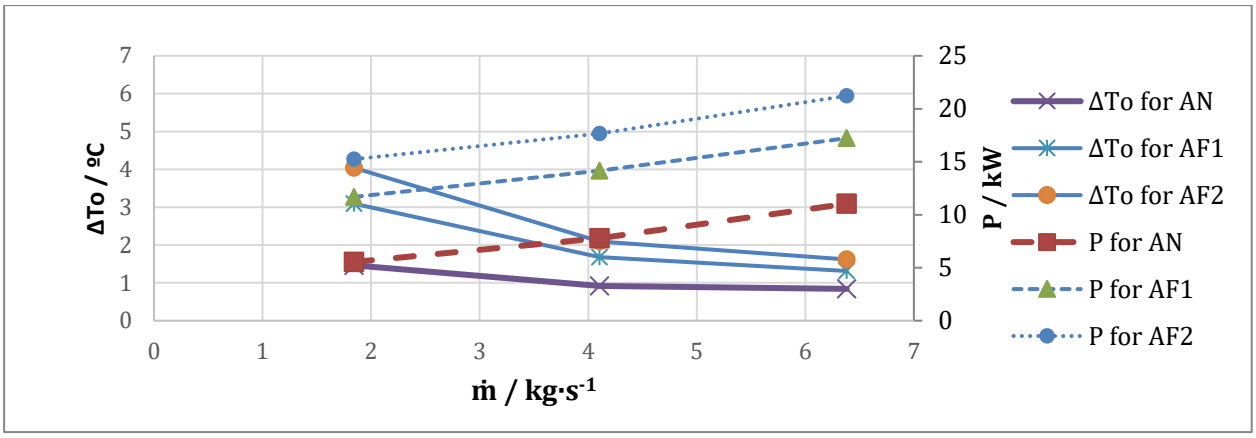


Figure 29 - Output temperature and energy dissipation rate as a function of plate height with varying external convective heat transfer coefficients for a radiator of 7 plates and a height of 3 m

From these results we can see that mass flow rate has, as expected, a positive influence in the energy dissipation. This is to be expected, Equation (8) states that the total heat dissipation scales with the mass flow rate. However, if the oil flows through the radiator at a higher speed, this means that each fluid element will have spent less time being cooled. As such, outlet temperature drop shrinks with the increase in mass flow rate, as it can be seen in the graphs above. In addition, the smaller the radiator gets, less time each fluid element spends being cooled. As such, flow rate increases have lower effects in energy dissipation rate.

5.2 Machine Learning: Simulator Performance and Results

In this chapter are presented the results of machine learning algorithms, and the models that were generated by them.

In this tool, four input variables must be specified, for the calculation of four output variables.

The input variables are:

- Plate number; in m
- Plate height; in m
- Oil flow rate; in $m^3 \cdot s^{-1}$
- External heat transfer coefficient; in $W \cdot m^{-2} \cdot K^{-1}$

The output variables are:

- Pressure Drop; in Pa
- Outlet Temperature; in ºC
- Dissipated Power; in W
- Oil heat transfer coefficient; in $W \cdot m^{-2} \cdot K^{-1}$
- Overall Heat transfer coefficient; in $W \cdot m^{-2} \cdot K^{-1}$

5.2.1 Algorithm Evaluation

The first step in this task is to select the most adequate algorithm for each variable among five different metrics. The tested algorithms were linear regression, ridge regression, polynomial regression, random forests, and support vector machines. An important aspect of this task is data scarcity. Algorithms such as ridge regression or linear regression were favored over algorithms that tend to overfit, which includes random forests or support vector machines. The evaluation of each algorithm applied to each output variable is presented in the following tables. In each the medium absolute error (MAE), the medium square error (MSE), the root medium square error (RMSE) and the coefficient of determination were used as evaluation parameters.

Table 10 – Evaluation of Machine Learning regression algorithms for pressure drop (ΔP).

ΔP				
	MAE	MSE	RMSE	R2
linear regression	81.68	11386.75	106.71	0.70
ridge regression	81.64	11387.16	106.71	0.70
polynomial regression	67.12	8398.74	91.64	0.78
Support vector machines	59.18	7250.98	85.15	0.81
Random forest (Chosen)	18.90	1054.53	32.47	0.97

In the case of the pressure drop, values of 0 were present in the dataset. As such, MAPE often produced completely disproportionately large values, since the residuals were being divided by 0. The values of R2 were quite low for all algorithms except Random Forests. As such, this algorithm was chosen to predict pressure drop values.

Table 11 – Evaluation of Machine Learning regression algorithms for Power output (Power).

Power					
	MAE	MSE	RMSE	R2	MAPE
linear regression	2012.40	6274598.60	2504.91	0.87	0.36
ridge regression	2013.16	6277572.77	2505.51	0.87	0.36
Polynomial regression (Chosen)	528.60	455757.04	675.10	0.99	0.10
Support vector machines	1914.74	9858264.08	3139.79	0.80	0.33
Random forest	413.22	414572.29	643.87	0.99	0.05

In this parameter, polynomial regression had a very high performance, comparable to that of Random forests. As such, polynomial regression was chosen, since it tends to overfit less than Random forests, an important factor when there is data scarcity.

Table 12 – Evaluation of Machine Learning regression algorithms for outlet temperature (T_o)

T_o					
	MAE	MSE	RMSE	R2	MAPE
linear regression	0.64	0.75	0.87	0.72	0.01
ridge regression	0.64	0.75	0.87	0.72	0.01
polynomial regression	0.31	0.16	0.40	0.94	0.01
Support vector machines	0.43	0.71	0.84	0.74	0.01
Random forest (Chosen)	0.18	0.07	0.27	0.97	0.00

Similarly to what happened with the pressure drop prediction, the values of R2 were quite low for all algorithms except Random Forests. As such, this algorithm was chosen to predict pressure drop values.

Table 13 – Evaluation of Machine Learning regression algorithms for oil convective heat transfer coefficient

h_{oil}					
	MAE	MSE	RMSE	R2	MAPE
linear regression	0.12	0.02	0.15	1.00	0.02
ridge regression (Chosen)	0.12	0.02	0.15	1.00	0.02
polynomial regression	0.07	0.01	0.11	1.00	0.01
Support vector machines	1.18	5.01	2.24	0.66	0.13
Random forest	0.03	0.00	0.05	1.00	0.00

In this parameter, all algorithms features high scores. As such, ridge regression was chosen, since it is the one least likely to overfit.

Table 14 – Evaluation of Machine Learning algorithms for overall heat transfer coefficient

U					
	MAE	MSE	RMSE	R2	MAPE
linear regression	0.03	0.00	0.04	1.00	0.01
ridge regression	0.03	0.00	0.04	1.00	0.01
polynomial regression (chosen)	0.02	0.00	0.03	1.00	0.01
svm	0.63	1.27	1.13	0.71	0.13
Random forest	0.01	0.00	0.01	1.00	0.00

In this parameter, all algorithms features high scores. As such, the polynomial regression algorithm was chosen.

With the algorithms selected, a training dataset was created from the CFD data, and the models were created by Python programming. Lastly, a GUI was implemented using tkinter and Python, leading to the creation of a graphical interface (Figure 30)

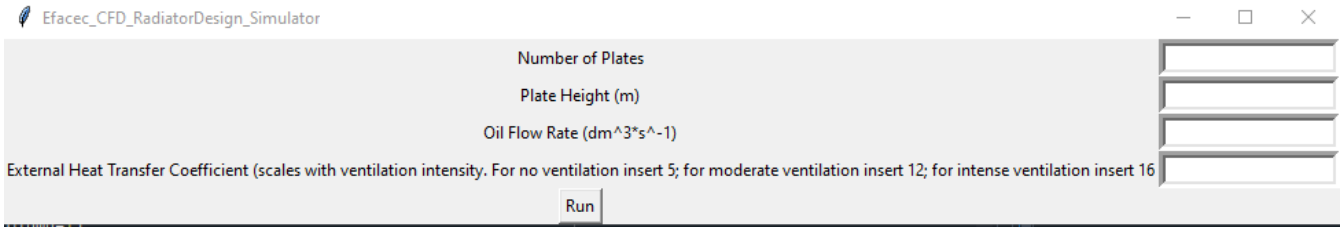


Figure 30 – Simulator GUI

In the four input boxes depicted in Figure 30, the user can insert values of the simulation variables to predict output values, as shown in Figure 31.

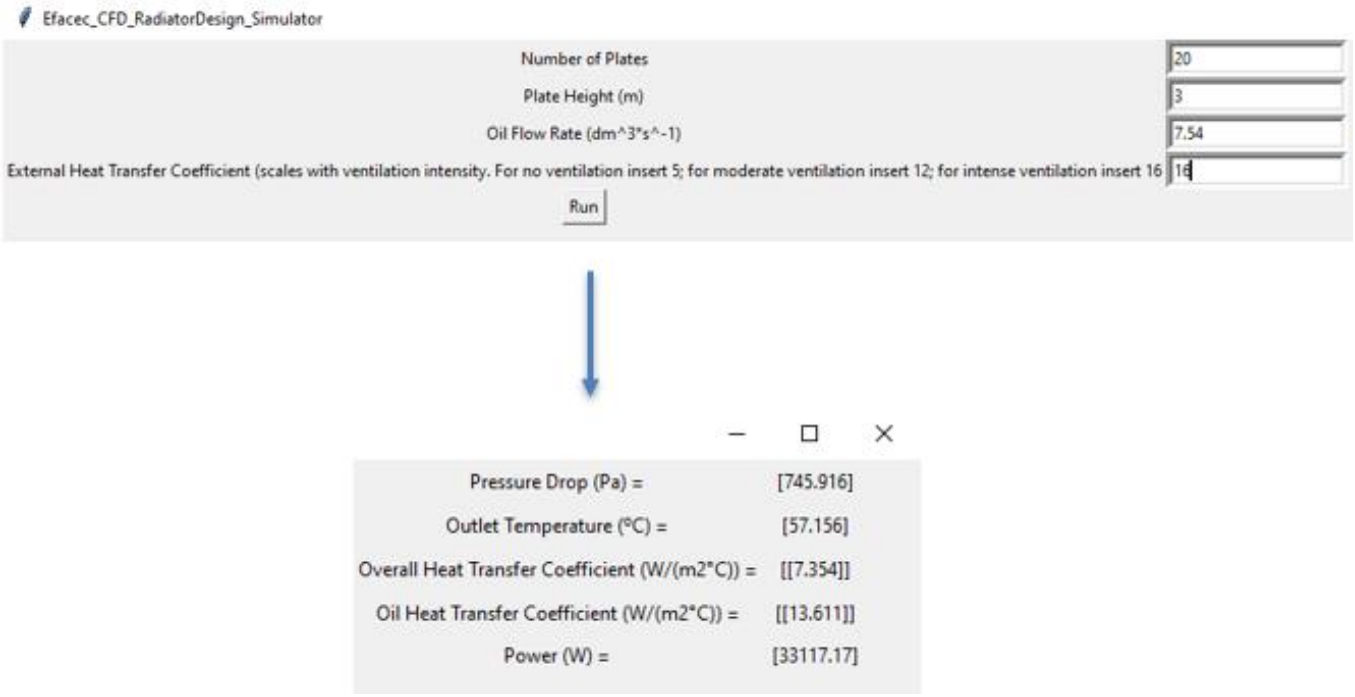


Figure 31 – Simulator operation

As Figure 31 depicts, the simulator was capable of performing a "run".

6 Conclusion

In conclusion, in the present work, the influence of design aspects and operation settings in the performance of external cooling systems was studied. To this end, a CFD-based methodology was used to simulate combinations of different values of number of radiator plates, plate height, inlet flow rate and external convection type. From these simulations, values of pressure drop, output temperature, oil convective heat transfer coefficient, overall heat transfer coefficient and dissipated power were obtained.

The pressure drop was found to scale linearly with the plate height and number of plates, and quadratically with the flow rate. These behaviors are to be expected, given Bernoulli's equation. In addition, it was found that thermal factors had little influence on this output variable.

The outlet temperature and the dissipated losses were found to scale in a linear fashion with the plate height. This is quite useful information for the design of radiators. However, it was found that the number of plates and plate height reduces the impact that the convection style has on the temperature drop. The increase in flow rate causes the energy dissipation rate to rise, but the outlet temperature drop decreases.

The machine learning simulator was found to be a very promising tool. Multiple algorithms were tested, whose performance was assessed using multiple evaluation parameters. It is however, worth noting that the data produced throughout the present work is quite scarce, and therefore not sufficient to make for a reliable model. However, this can be corrected by future work, in which more data can be fed to improve the simulator's performance

7 Assessment of the work done

7.1 Objectives Achieved

The study of the variation of geometrical properties and operation settings in the external cooling of core type power transformers was successfully studied, and the prediction of the thermal performance of the transformer external cooling process was obtained using machine learning was carried out.

7.2 Other Work carried out

Before starting to handle radiator geometries, an introductory CFD exercise was performed, to get started with the usage of Fluent. In this exercise, a thermohydraulic simulation of a simple oil pipe was carried out, to learn how to use Fluent for heat transfer studies. This exercise was done both on Fluent and openFOAM.

7.3 Future Work

As future work, it would be advisable to conduct these studies this study using a wider range of parameters, in pursuance of a broader notion regarding the effect of external cooling on the thermo-hydraulic behavior of a core type power transformer. In addition, further work within the same parameters would also be advisable, to strengthen the performance of the machine learning simulator.

In addition, it may be of interest for other variables to be studied, such as the inlet temperature and its interaction with the system cooling performance.

7.4 Final Assessment

The fruits of the present work provided further information regarding the influence of the external cooling system design and operation on the thermal performance of a core-type power transformer. However, more results should be obtained to better understand the phenomena. The machine learning simulator has also proved to be quite promising. However, more data needs to be provided, in order for it to work in larger ranges of values, and to not overfit so much.

Through this work, I learned plenty about CFD, fluid mechanics, transport phenomena and data analysis.

I also had the chance to explore a field that was relatively new to me: Machine Learning. It was a great experience, and it opened my eyes to something that I might want to explore in the future.

8 References

[1] A. Baggini and F. Bua, "Power transformers energy efficiency programs: A critical review," *2015 IEEE 15th Int. Conf. Environ. Electr. Eng. EEEIC 2015 - Conf. Proc.*, pp. 1961–1965, Jul. 2015, doi: 10.1109/EEEIC.2015.7165474.

[2] J. Il Jeong, J. S. An, and C. S. Huh, "Accelerated aging effects of mineral and vegetable transformer oils on medium voltage power transformers," *IEEE Trans. Dielectr. Electr. Insul.*, vol. 19, no. 1, pp. 156–161, Feb. 2012, doi: 10.1109/TDEI.2012.6148514.

[3] "Efacec main website," Feb. 24, 2022. https://www.efacec.pt/ (accessed Feb. 24, 2022).

[4] R. Neves and C. Filipe, "Efacec carrega Porsche eléctrico com potência recorde," Jul. 21, 2016.

[5] "Transformer Basics and Transformer Principles." https://www.electronics-tutorials.ws/transformer/transformer-basics.html (accessed May 11, 2022).

[6] "Types of Electric Transformers." https://www.iqsdirectory.com/articles/electric-transformer/types-of-electric-transformers.html (accessed May 22, 2022).

[7] J. Winders, *Power transformers: principles and applications*. CrC Press, 2002.

[8] "Why Power Transformers are a Necessity in the Modern World - Elect Power." https://www.electpower.com/why-power-transformers-are-a-necessity-in-the-modern-world/ (accessed May 22, 2022).

[9] "Efacec vai apresentar nova geração de soluções de mobilidade elétrica – O Jornal Económico." https://jornaleconomico.pt/noticias/efacec-vai-apresentar-nova-geracao-de-solucoes-de-mobilidade-eletrica-716160 (accessed Jun. 06, 2022).

[10] "2021 A Complete Guide to Power Plant Transformer | Daelim." https://daelim-electric.com/power-plant-transformer/ (accessed Apr. 25, 2022).

[11] "Transformadores - Efacec." https://www.efacec.pt/transformadores/ (accessed Sep. 25, 2022).

[12] P. M. da C. Martins, "Numerical investigation of thermal behaviour of core plates in core type transformers," University of Porto, 2019.

[13] P. Evans, "How Transformers Work," *The Engineering Mindset*, Nov. 12, 2019.

[14] "Transformers: Basics, Maintenance, and Diagnostics," 2005.

[15] L. de F. A. e T. Rodrigues, "Numerical analysis of water distribution inside a power

transformer winding A Master ' s dissertation," University of Porto, 2018.

[16] C. H. Cha, J. K. Kim, and K. Y. Kweon, "Investigation of the thermal head effect in a power transformer," in *2009 Transmission & Distribution Conference & Exposition: Asia and Pacific. IEEE*, 2009, pp. 5–8. doi: 10.1109/TD-ASIA.2009.5356811.

[17] X. Liu, Y. Yang, F. Yang, and A. jadoon, "Numerical research on the losses characteristic and hot-spot temperature of laminated core joints in transformer," *Appl. Therm. Eng.*, vol. 110, pp. 49–61, Jan. 2017, doi: 10.1016/J.APPLTHERMALENG.2016.08.158.

[18] "Cooling of Transformers - Owlcation." https://owlcation.com/stem/Cooling-of-transformers (accessed Mar. 16, 2022).

[19] International Electrotechnical Commission, "IEC 60076-2 Power Transformers –Part 2: Temperature rise for liquid-immersed transformers." 2011.

[20] E. O. Aluyor and M. Ori-Jesu, "Biodegradation of mineral oils-A review," *African J. Biotechnol.*, vol. 8, no. 6, pp. 915–920, 2009, Accessed: May 02, 2022. [Online]. Available: http://www.academicjournals.org/AJB

[21] M. Srivastava, S. K. Goyal, and A. Saraswat, "Ester oil as an alternative to mineral transformer insulating liquid," *Mater. Today Proc.*, vol. 43, pp. 2850–2854, Jan. 2021, doi: 10.1016/J.MATPR.2021.01.066.

[22] J. P. B. Baltazar, "Modelling Vertical Plate Radiators for Electric Transformers EFACEC," University of Porto, 2014.

[23] "Specific Heat Capacity and Water | U.S. Geological Survey." https://www.usgs.gov/special-topics/water-science-school/science/specific-heat-capacity-and-water (accessed Aug. 26, 2022).

[24] "Specific Heat Capacities of Air - (Updated 7/26/08)." https://www.ohio.edu/mechanical/thermo/property_tables/air/air_Cp_Cv.html (accessed Aug. 26, 2022).

[25] "Transformer cooling methods." https://www.electricalclassroom.com/transformer-cooling-methods/#13-oil-forced-water-forced-ofwf-cooling (accessed Jun. 08, 2022).

[26] "OFWF Transformer Enclosures Oil to water cooled transformers".

[27] "Purpose of Radiator in Transformer? - Electrical Concepts." https://electricalbaba.com/purpose-of-radiator-in-transformer/ (accessed Sep. 22, 2022).

[28] Y. J. Kim and M. Y. Ha, "A study on the performance of different radiator cooling systems in large-scale electric power transformer," *J. Mech. Sci. Technol.*, vol. 31, no. 7, pp.

3317–3328, Jul. 2017, doi: 10.1007/s12206-017-0622-2.

[29] R. Godina, D. João Paulo da Silva Catalão Coorientador, and D. João Carlos de Oliveira Matias, "UNIVERSIDADE DA BEIRA INTERIOR Smart Operation of Transformers for Sustainable Electric Vehicles Integration and Model Predictive Control for Energy Monitoring and Management Engenharia e Gestão Industrial".

[30] M. G. Kim, S. M. Cho, and J. K. Kim, "Prediction and evaluation of the cooling performance of radiators used in oil-filled power transformer applications with non-direct and direct-oil-forced flow," *Exp. Therm. Fluid Sci.*, vol. 44, pp. 392–397, 2013, doi: 10.1016/j.expthermflusci.2012.07.011.

[31] G. C. Nogueira *et al.*, "Thermal Analysis of Power Transformers with Different Cooling Systems Using Computational Fluid Dynamics," *J. Control. Autom. Electr. Syst.*, vol. 33, no. 1, pp. 359–368, Feb. 2022, doi: 10.1007/s40313-021-00848-0.

[32] S. Zhao, Q. Liu, M. Wilkinson, G. Wilson, and Z. Wang, "A Reduced Radiator Model for Simplification of ONAN Transformer CFD Simulation," *IEEE Trans. Power Deliv.*, pp. 1–1, 2022, doi: 10.1109/TPWRD.2022.3142889.

[33] P. A. Córdoba, E. A. Dari, and N. Silin, "NATURAL CONVECTION IN A REPRESENTATIVE SECTION OF AN ONAN DISTRIBUTION TRANSFORMER," pp. 7–10, 2017.

[34] B. Galletti, A. Blaszczyk, and W. Wu, "CFD Based Sensitivity Study of Cooling Performance of Transformer Radiators," in *6th International Advanced Research Workshop on Transformers*, 2019, no. 6, pp. 1–6. doi: 10.23919/ARWtr.2019.8930189.

[35] "Transformer Cooling - globecore.com." https://globecore.com/oil-heating/cooling-of-transformer/ (accessed May 12, 2022).

[36] W. Van der Veken, S. B. Paramane, R. Mertens, V. Chandak, and J. Codde, "Increased Efficiency of Thermal Calculations via the Development of a Full Thermohydraulic <?Pub _newline?> Radiator Model," *IEEE Trans. Power Deliv.*, vol. 31, no. 4, pp. 1473–1481, Aug. 2016, doi: 10.1109/TPWRD.2015.2501431.

[37] L. Wang, W. Zuo, Z.-X. Yang, Z. Cai, P. Ma, and Z. Ye, "CFD-Based Heat Dissipation Efficiency Monitoring for Radiator in Different Air-Cooling Modes," in *2021 5th International Conference on System Reliability and Safety (ICSRS)*, Nov. 2021, pp. 155–160. doi: 10.1109/ICSRS53853.2021.9660692.

[38] S. B. Paramane, K. Joshi, W. Van Der Veken, and A. Sharma, "CFD study on thermal performance of radiators in a power transformer: Effect of blowing direction and offset of fans," *IEEE Trans. Power Deliv.*, vol. 29, no. 6, pp. 2596–2604, 2014, doi: 10.1109/TPWRD.2014.2347292.

[39] B. Kwon, F. Ejaz, and L. K. Hwang, "Machine learning for heat transfer correlations," *Int. Commun. Heat Mass Transf.*, vol. 116, p. 104694, Jul. 2020, doi: 10.1016/J.ICHEATMASSTRANSFER.2020.104694.

[40] A. Singh, N. Thakur, and A. Sharma, "A review of supervised machine learning algorithms," in *2016 3rd International Conference on Computing for Sustainable Global Development (INDIACom)*, 2016, pp. 1310–1315.

[41] "sklearn.linear_model.LinearRegression — scikit-learn 1.1.2 documentation." https://scikit-learn.org/stable/modules/generated/sklearn.linear_model.LinearRegression.html (accessed Sep. 09, 2022).

[42] G. C. McDonald, "Ridge regression," *Wiley Interdiscip. Rev. Comput. Stat.*, vol. 1, no. 1, pp. 93–100, Jul. 2009, doi: 10.1002/WICS.14.

[43] "sklearn.linear_model.Ridge — scikit-learn 1.1.2 documentation." https://scikit-learn.org/stable/modules/generated/sklearn.linear_model.Ridge.html (accessed Sep. 09, 2022).

[44] A. M. M. L. S. de Sousa, "Predictive Analysis of Flight Times," Faculdade de engenharia da Universiade do Porto, 2020.

[45] J. Pedro, C. Leal, and M. Moreira, "Travel Time Prediction for the Planning of Mass Transit Companies: a Machine Learning Approach," 2008.

[46] A. J. Smola and B. Schölkopf, "A tutorial on support vector regression," *Stat. Comput.*, vol. 14, no. 3, pp. 199–222, Aug. 2004, doi: 10.1023/B:STCO.0000035301.49549.88.

[47] A. Pečkov, "A MACHINE LEARNING APPROACH TO POLYNOMIAL REGRESSION".

[48] L. Breiman, "Random Forests," vol. 45, pp. 5–32, 2001.

[49] T. G. Dietterich, "Ensemble Methods in Machine Learning", Accessed: Sep. 15, 2022. [Online]. Available: http://www.cs.orst.edu/~tgd

[50] C. Chiastra, S. Morlacchi, S. Pereira, G. Dubini, and F. Migliavacca, "Computational fluid dynamics of stented coronary bifurcations studied with a hybrid discretization method," *Eur. J. Mech. - B/Fluids*, vol. 35, pp. 76–84, Sep. 2012, doi: 10.1016/J.EUROMECHFLU.2012.01.011.

[51] R. Koomullil, B. Soni, and R. Singh, "A comprehensive generalized mesh system for CFD applications," *Math. Comput. Simul.*, vol. 78, no. 5–6, pp. 605–617, Sep. 2008, doi: 10.1016/J.MATCOM.2008.04.005.

[52] M. K. Thompson and J. M. Thompson, "Meshing," in *ANSYS Mechanical APDL for Finite*

Element Analysis, Elsevier, 2017, pp. 181–199. doi: 10.1016/B978-0-12-812981-4.00006-X.

[53] "What is Python? Executive Summary | Python.org." https://www.python.org/doc/essays/blurb/ (accessed Sep. 09, 2022).

[54] K. Jolly, *Machine learning with scikit-learn quick start guide: classification, regression, and clustering techniques in Python*. Packt Publishing Ltd, 2018.

[55] "NumPy documentation — NumPy v1.23 Manual." https://numpy.org/doc/stable/ (accessed Sep. 14, 2022).

[56] "Package overview — pandas 1.4.4 documentation." https://pandas.pydata.org/docs/getting_started/overview.html (accessed Sep. 14, 2022).

[57] F. Lundh, "An introduction to tkinter," *URL www. pythonware. com/library/tkinter/introduction/index. htm*, 1999.

[58] A. H. H. Al-Kayiem and M. A. Ibrahim, "The influence of the equivalent hydraulic diameter on the pressure drop prediction of annular test section," *IOP Conf. Ser. Mater. Sci. Eng.*, vol. 100, no. 1, Dec. 2015, doi: 10.1088/1757-899X/100/1/012049.

[59] N. Rott, "Note on the History of the Reynolds Number," *http://dx.doi.org/10.1146/annurev.fl.22.010190.000245*, vol. 22, no. 1, pp. 1–12, Nov. 2003, doi: 10.1146/ANNUREV.FL.22.010190.000245.

[60] B. Rehm, D. Consultant, A. Haghshenas, A. S. Paknejad, and J. Schubert, "Situational Problems in MPD," *Manag. Press. Drill.*, pp. 39–80, Jan. 2008, doi: 10.1016/B978-1-933762-24-1.50008-5.

[61] W. Cao, W. Huang, and F. Jiang, "Numerical study on variable thermophysical properties of heat transfer fluid affecting EGS heat extraction," *Int. J. Heat Mass Transf.*, vol. 92, pp. 1205–1217, Jan. 2016, doi: 10.1016/J.IJHEATMASSTRANSFER.2015.09.081.

[62] I. Santos, P. F. Oliveira, and C. R. E. Mansur, "Factors that affect crude oil viscosity and techniques to reduce it: A review," *Brazilian J. Pet. gas*, vol. 11, no. 2, pp. 115–130, 2017.

[63] A. Salama, "Velocity Profile Representation for Fully Developed Turbulent Flows in Pipes: A Modified Power Law," *Fluids 2021, Vol. 6, Page 369*, vol. 6, no. 10, p. 369, Oct. 2021, doi: 10.3390/FLUIDS6100369.

[64] "Navier-Stokes equation | Definition & Facts | Britannica." https://www.britannica.com/science/Navier-Stokes-equation (accessed Sep. 26, 2022).

[65] "Shared topology in ANSYS." http://help.spaceclaim.com/dsm/4.0/en/Content/ANSYS_SharedTopology.htm (accessed Sep. 15, 2022).

[66] L. Rayward and J. P. Little, "A subject-specific FEM to predict deep tissue mechanical stresses when supine: Development of efficient contact interfaces using Shared Topology," *J. Biomech.*, vol. 137, May 2022, doi: 10.1016/J.JBIOMECH.2022.111085.

[67] W. El-Bouri, I. Deiab, K. Khanafer, and E. Wahba, "Numerical and experimental analysis of turbulent flow and heat transfer of minimum quantity lubrication in a turning process using discrete phase model," *Int. Commun. Heat Mass Transf.*, vol. 104, pp. 23–32, May 2019, doi: 10.1016/J.ICHEATMASSTRANSFER.2019.02.012.

[68] G. E. Matt, A. Brewer, and M. Sklar, "External Validity," *Int. Encycl. Educ.*, pp. 521–527, Jan. 2010, doi: 10.1016/B978-0-08-044894-7.01700-0.

[69] H. K. Esfeh, A. Azarafza, and M. K. A. Hamid, "On the computational fluid dynamics of PEM fuel cells (PEMFCs): an investigation on mesh independence analysis," *RSC Adv.*, vol. 7, no. 52, pp. 32893–32902, Jun. 2017, doi: 10.1039/C7RA03236F.

[70] "ANSYS FLUENT 12.0 Theory Guide - 18.4.3 Pressure-Velocity Coupling." https://www.afs.enea.it/project/neptunius/docs/fluent/html/th/node373.htm (accessed Sep. 26, 2022).

[71] "ANSYS FLUENT 12.0 Theory Guide - 18.3.3 Evaluation of Gradients and Derivatives." https://www.afs.enea.it/project/neptunius/docs/fluent/html/th/node368.htm (accessed Sep. 26, 2022).

[72] "ANSYS FLUENT 12.0 Theory Guide - 18.3.1 Spatial Discretization." https://www.afs.enea.it/project/neptunius/docs/fluent/html/th/node366.htm (accessed Sep. 26, 2022).

[73] "Solver Settings Customer Training Material," 2010.

[74] "Transformer Radiator | tradekorea." https://www.tradekorea.com/product/detail/P487730/Transformer-Radiator.html (accessed May 02, 2022).

Appendix A - User Defined Functions

It is worth noting that all these functions were submitted to Fluent as part of the same file. In order for these to be interpreted, they must be written in the same document and then each of them is accessed thorough Fluent's interface

A.1. Density

For reasons of confidentiality , this appendix was omitted.

A.2. Specific Heat

For reasons of confidentiality , this appendix was omitted.

A.3. Thermal Conductivity

For reasons of confidentiality , this annex was omitted.

A.4. Dynamic Viscosity

For reasons of confidentiality , this annex was omitted.

A.5. Parabolic inlet velocity profile for laminar flow

DEFINE_PROFILE(inlet_z_vel, thread, index)

```
{
real z[ND_ND];
real x;
real y;
real a;
face_t f;
begin_f_loop(f, thread)
{
F_CENTROID(z,f,thread);
x = z[0];
y = z[1];
a = pow(x*x+y*y,0.5);
F_PROFILE(f, thread, index) = 2*0.07653*(1-(a*a/(0.05625*0.05625)));
}
end_f_loop(f, thread)
}
```

This function was written for an inlet parabolic velocity profile with an average velocity of 0.0765 $m \cdot s^{-1}$.

A.5. Parabolic inlet velocity profile for turbulent flow

DEFINE_PROFILE(inlet_z_vel, thread, index)

```
{
real z[ND_ND];
real x;
real y;
real a;
real Uav,Umax,K,Kn,Ko;
face_t f;
begin_f_loop(f, thread)
{
F_CENTROID(z,f,thread);
x = z[0];
y = z[1];
a = pow(x*x+y*y,0.5);
Kn = 0.1429;
Uav = 0.7573;
Umax = Uav/0.875;
F_PROFILE(f, thread, index) = pow((1-(a*a/(0.05625*0.05625))),Kn)*Umax;
}
end_f_loop(f, thread)
}
```

This function was written for an average velocity of 0.757 $m \cdot s^{-1}$.

Appendix B - CFD Simulations: Hydraulic studies of a single radiator plate

As a first step, a unique hydraulic simulation of a single radiator plate was performed. These simulations were meant as intermediate steps to later advance to more elaborate simulation work. This section is described in Appendix I.

B.1. Geometry

The base geometry inherent to these simulations was that of a radiator plate, as it can be seen below in Figure 32.

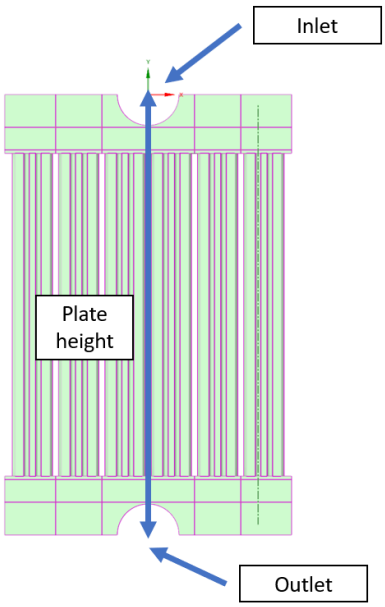


Figure 32 – Plate geometry

Below, in Figure 33, are depicted schematics wich describe in detail the radiator plate's geometry.

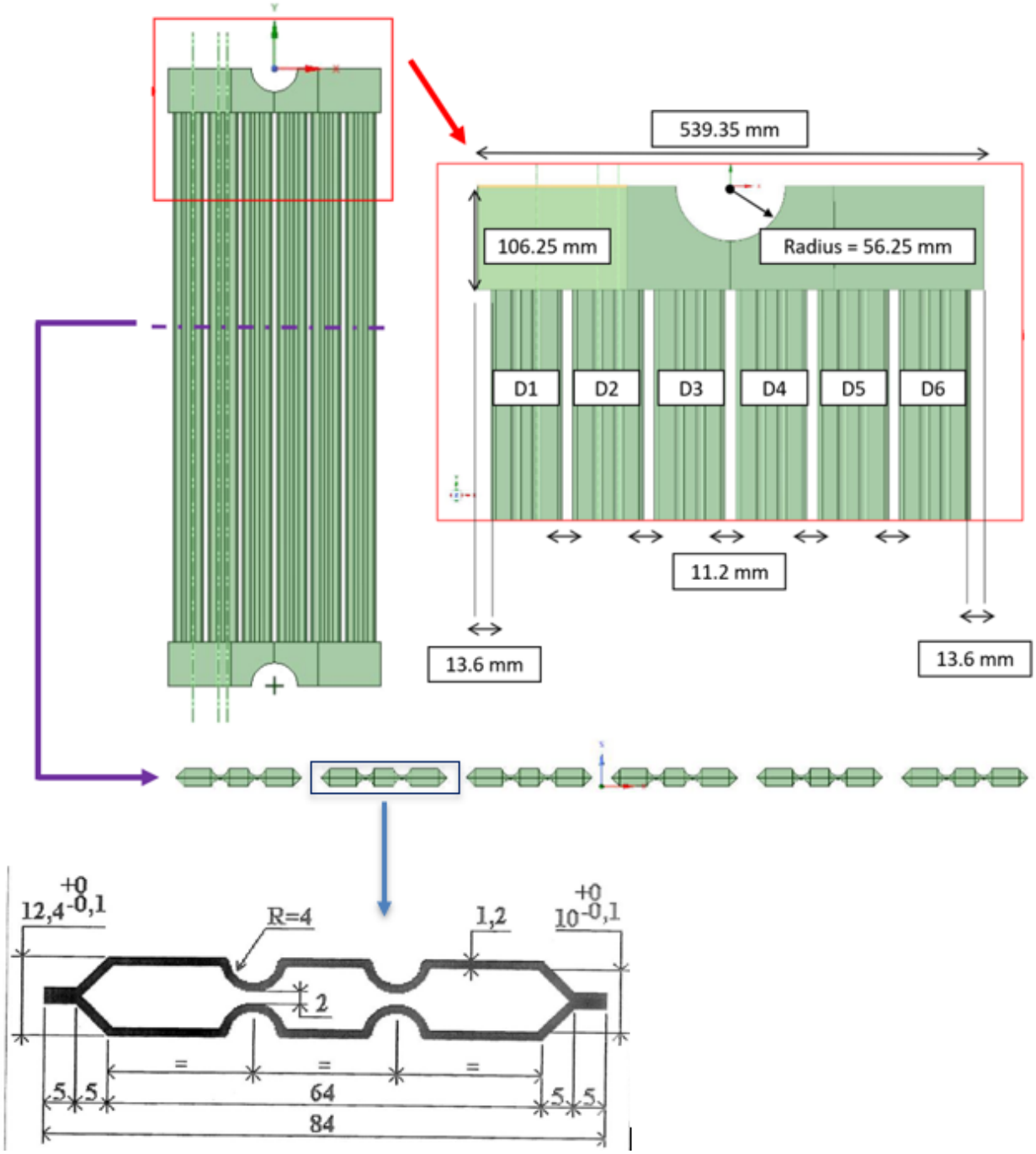


Figure 33 – Full plate geometrical specifications

These dimensions were then used to draw all simulated geometries in SpaceClaim 2021 R2.

As it can be seen in Figure 32, the project geometry was subdivided into multiple partitions, to allow for better regional control and for a structured hexahedral mesh to form more easily. The boundaries between these partitions have shared topology.

Shared topology is a specification within SpaceClaim, that allows for the generation of a conformal mesh where bodies meet, and it is the only way to be certain that the intersection of bodies is meshed perfectly [65]. This solution has been found to increase computational efficiency and accuracy [66] and eliminates the need for contact regions [67].

As mentioned before, plate height is a relevant factor in the hydraulic performance of a cooling system, as such, geometries of three different heights were conceived: 0.8 m, 1.5 m and 3 m. The heights of 0.8 m and 3 m were, respectively, the minimum and maximum heights featured in the company's internal bibliography. This is was an important criterion in their choosing, since correlations of an interpolative nature tend to perform in a superior way than those of an extrapolative nature [68].

B.2. Mesh

The aforementioned geometry was exported to ANSYS Workbench's Meshing Module. Through this module, mesh independence tests were conducted. Mesh independence analysis is used to show that a solution is independent of the geometry grid size [69]. This analysis is conducted by gradually increasing mesh resolution and evaluating the change in output values. This analysis is of paramount importance, since it allows one to characterize how mesh-dependent are the obtained results.

For this study, a nearly fully hexahedral mesh was produced, made up of mostly structured cells. Below in Table 15 are presented the mesh characteristics for the three plate geometries that were simulated:

Table 15 – Mesh characteristics for simulated plate geometries

	Number of cells	**Number of faces**	**Number of nodes**
Plate with h1 (0.8 m)	1705513	5226956	1810933
Plate with h2 (1.5 m)	2884721	8880094	3107175
Plate with h3 (3 m)	5411502	16701393	5877285

Simulation Settings

In this section, the simulation settings of the single hydraulic plate are detailed. It is worth noting that all numerical settings can be found in Appendix E.For these simulations, the laminar model was selected. This was because for all selected flow rates, the inlet Re was kept well below 2000. The energy equation remained switched off, since it was a purely hydraulic simulation. Only one domain was set, the oil domain. In this material, viscosity and density were defined using the oil properties at 60ºC. These are stated below, in Table 16.

Table 16Table 16 – Oil physical properties at 60ºC

ρ **/ kg·m^{-3}**	μ **/ mPa·s**
846.4	4.6

The three simulated flow rates were chosen based on Efacec's radiator catalog. The models were the following: ONAF 350 MVA, ODAF 40 MVA and ODAF 300 MVA. The estimated oil flow rate per plate was calculated and then divided by the inlet area, resulting in the following inlet velocities, inserted in Table 17.

Table 17 - Inlet velocities for a single radiator plate

v1 / m·s^{-1}	v2 / m·s^{-1}	v3 / m·s^{-1}
0.0272	0.0615	0.213

These were used to define the plate's inlet. The velocity profile was set as uniform. No changes from default were made to the radiator walls. The outlet was defined as a pressure outlet. This is an option present in fluent that allows the setting of a fixed pressure at the fluid outlet. In this case, it was set to 0 Pa.

B.3. Pressure Drop and Velocity Magnitude Distribution

Initially, a uniquely hydraulic CFD simulation of a single radiator plate was conducted, where the fluid pressure drop and the fluid velocity magnitude were the output variables of interest.

Figure 20 depicts the pressure drop (ΔP) in function of the flow rate (Q) for three different heights.

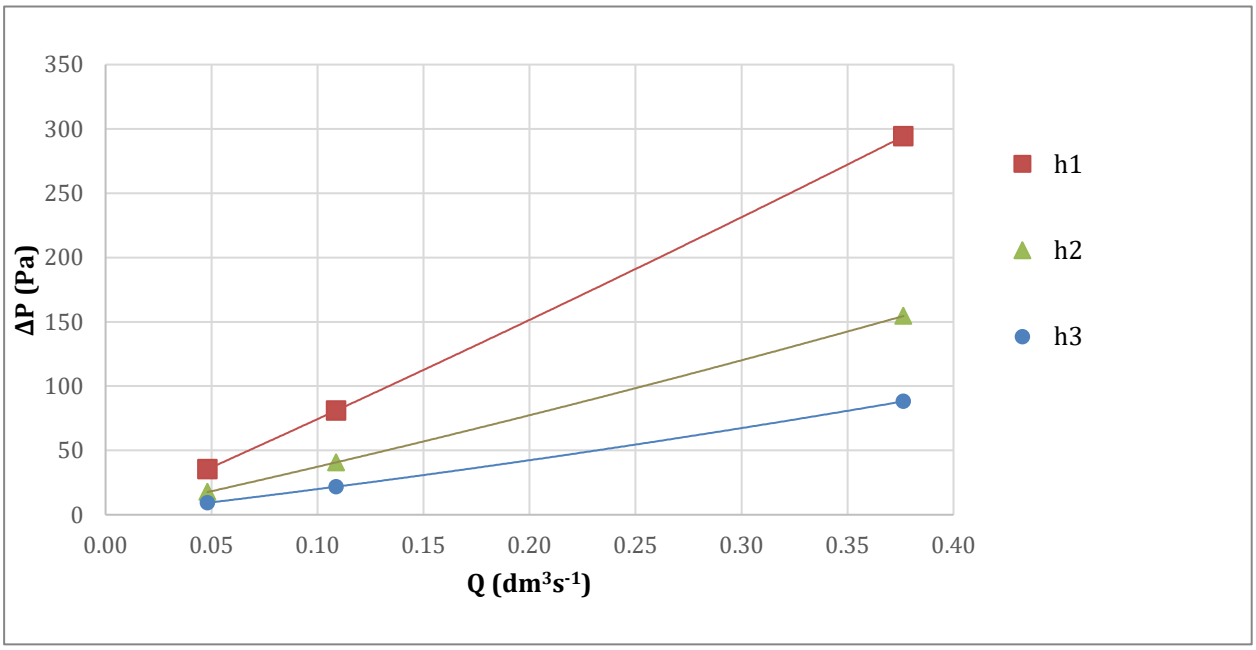


Figure 34 - Pressure drop (ΔP) in function of the flow rate (Q) in a single radiator plate for three different plate heights (h). The lines indicate second order polynomial regressions.

The pressure drop increases with both flow rate and plate height (Figure X). The following expressions are the depicted polynomial regressions fitted to the simulation data (for Q in $m^3 s^{-1}$ and ΔP in Pa):

These regressions (Equations X-Y) feature very high coefficients of determination, although it is worth noting that they were made from 3 points plus a set intercept to 0. This condition was placed because physically it makes sense that an immobilized fluid does not feature a pressure drop. The 2nd order term (a) suffers very little changes despite changes in plate height, whilst the 1st order term (b) increases with it.This happens because when plate height is increased the length of the fluidic system (l) also increases, which, according to Equation (3), will lead to an increase in b. As for a, none of the variables in Equation (2) change, so essentially it remained the same.

In addition, to further study the effect of plate height, the following graphics were created:

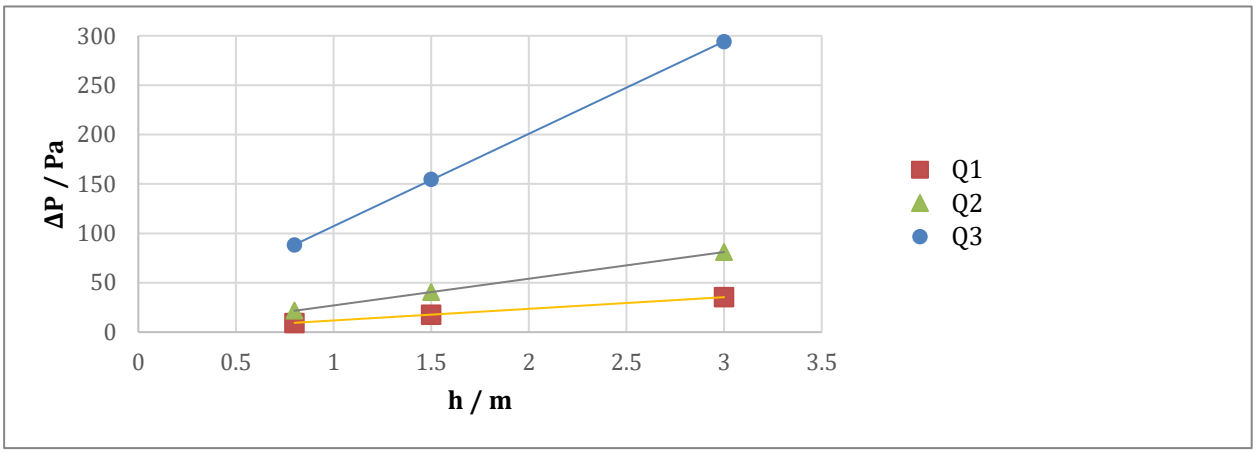


Figure 35 - Pressure drop (ΔP) in function of plate height (h) in a single radiator plate for three different flow rates. The lines indicate linear regressions.

Through Bernoulli's equation, it is known that pressure drop scales linearly with the length of the path of the fluid. As such, 1st order regressions were used to fit the data. The equations of said regressions are as following:

- Flow Rate Q_1: $\Delta P = 93.528 \cdot h + 13.715$
- Flow Rate Q_2: $\Delta P = 27.028 \cdot h$
- Flow Rate Q_3: $\Delta P = 11.79 \cdot h$

As it can be seen these regressions all feature very high coefficients of determination. As such, one can conclude that the linear model is suitable for the understanding of the effect of plate height.It is worth noting that for the two lowest flow rates the independent terms were quite small. This means that localized losses are somewhat unimportant in this geometry. This is something to be expected, given the absence of elements such as elbows, valves or bends. As

such, in the regressions of the two lowest flow rates, the intercept was set to 0, to make for more compact expressions.

As mentioned in the beginning of this section, another variable of interest was the velocity magnitude distribution. In this topic, contour analysis is a very powerful tool.

In this section are represented contours of velocity magnitude for the simulated plate geometries. The visualization of these data might provide some insight on how to design more hydraulically efficient plate geometries, in order to avoid dead volumes and so forth.

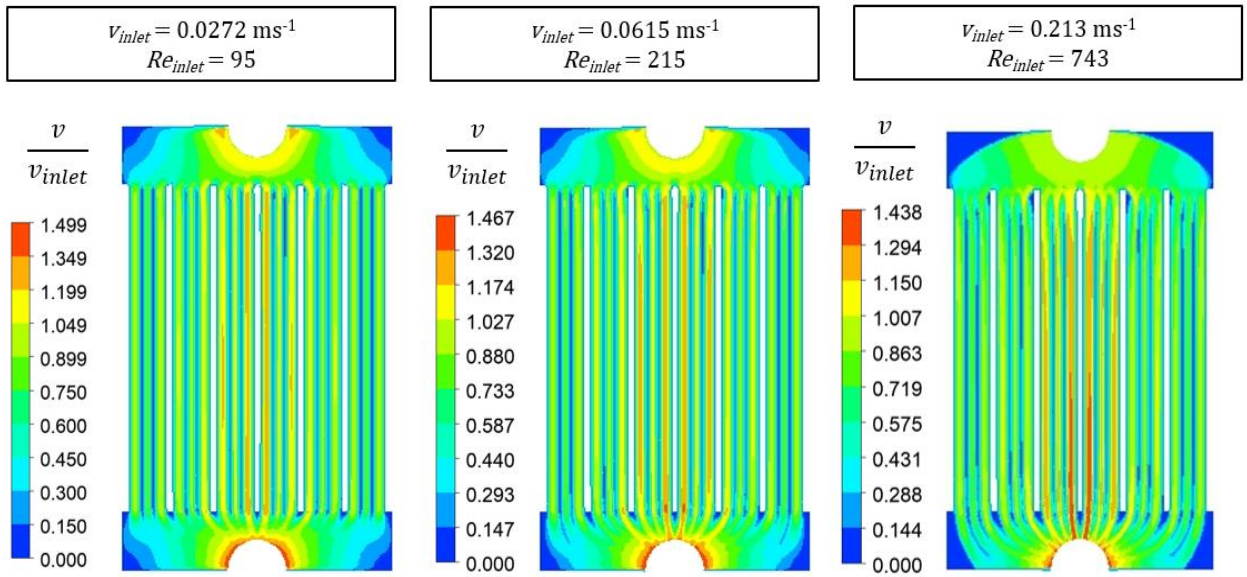


Figure 36 – Contours plots of velocity magnitude normalized by each simulation's inlet velocity. Plate features a height of 0.8 m.

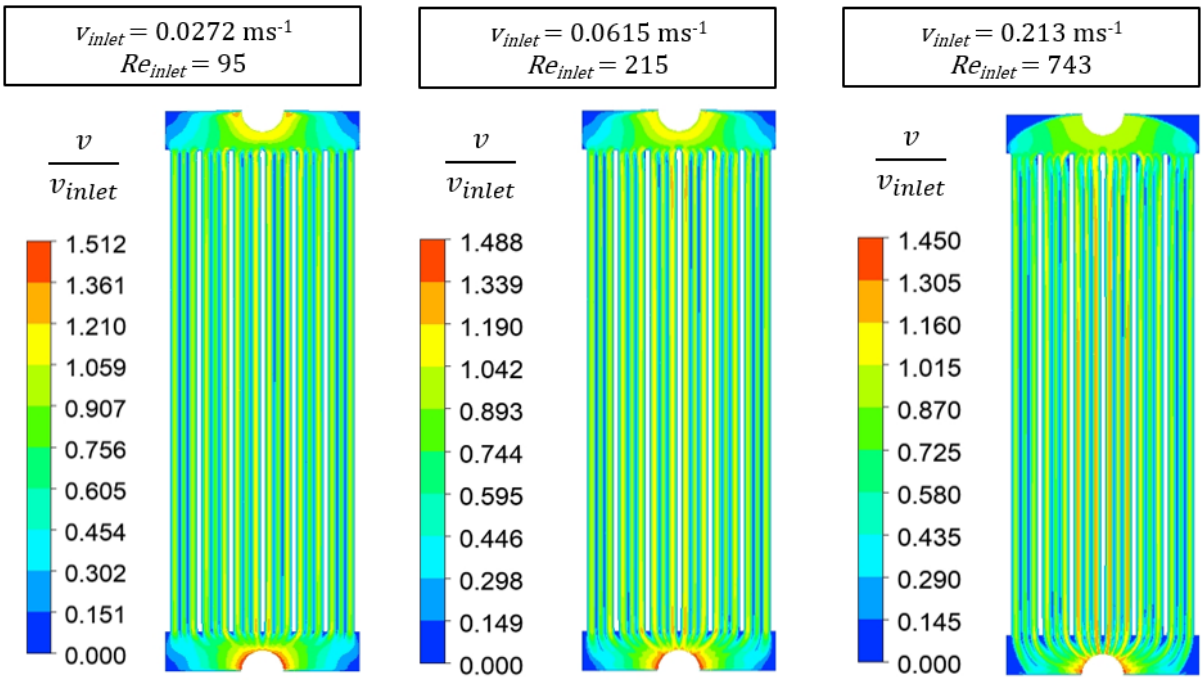


Figure 37 – Contours plots of velocity magnitude normalized by each simulation's inlet velocity. Plate features a height of 1.5 m.

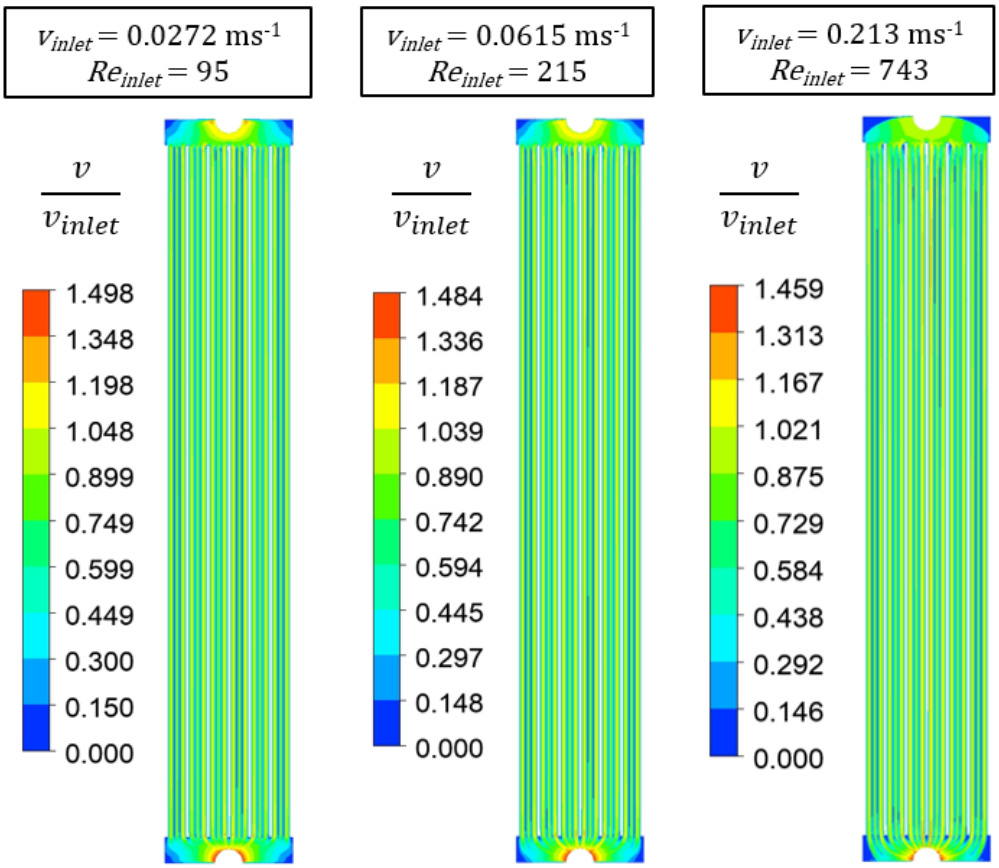


Figure 38- Contours plots of velocity magnitude normalized by each simulation's inlet velocity. Plate features a height of 3 m.

Through this second round of contour plots, one can see that the increase in inlet velocity creates greater contrasts of velocity magnitude throughout the plate. This means when velocity is increased, there is a greater tendency for recirculation zones to form, particularly near the edges of the plate. These are patches of fluid that are not being adequately mobilized and absorb mechanical energy. Eliminating these zones would constitute an improvement to the efficiency of the radiator. Plates with a curved or inclined distributor, as shown below in Figure 25, counter this effect, for their corners have a shape similar to the flow of the oil. In addition, these kinds of plate designs require less steel to make, which is means they are more economically attractive.



Figure 39 – Radiator plates with inclined distributor zones and curved corners [74]

B.4. Velocity Distribution

In the series of pictures below follow a collection of contour plots of the velocity magnitude divided by the maximum inlet velocity of all three that were simulated (that is, the inlet velocity inherent to Q_{3SP}). These plots allow one to visualize the stark difference in overall velocity magnitude between them.

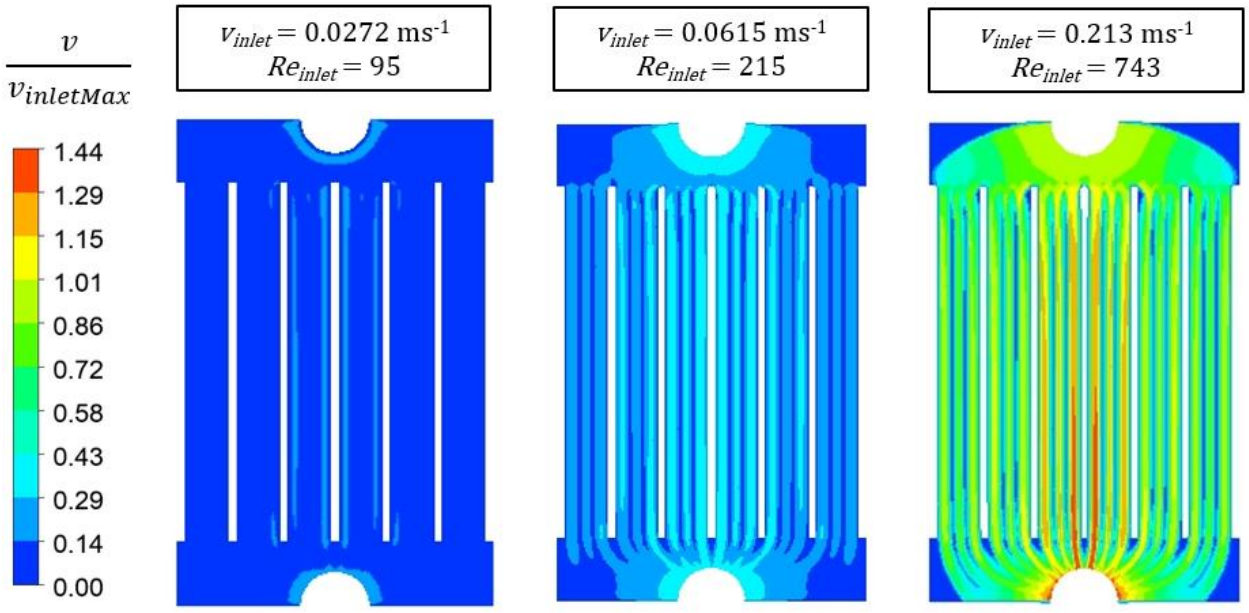


Figure 40 - Contours of velocity magnitude normalized by the maximum inlet velocity (0.213 ms^{-1}). Plate features a height of 800 mm

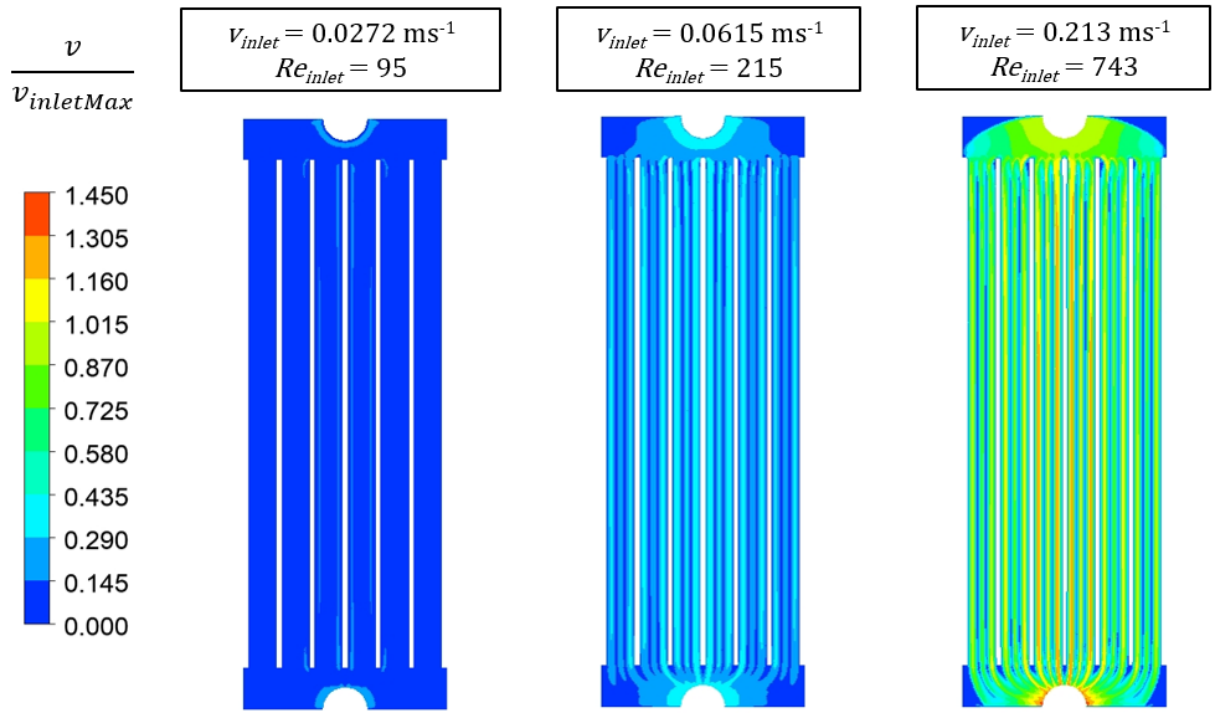


Figure 41 - Contours of velocity magnitude normalized by the maximum inlet velocity (0.213 ms^{-1}). Plate features a height of 800 mm

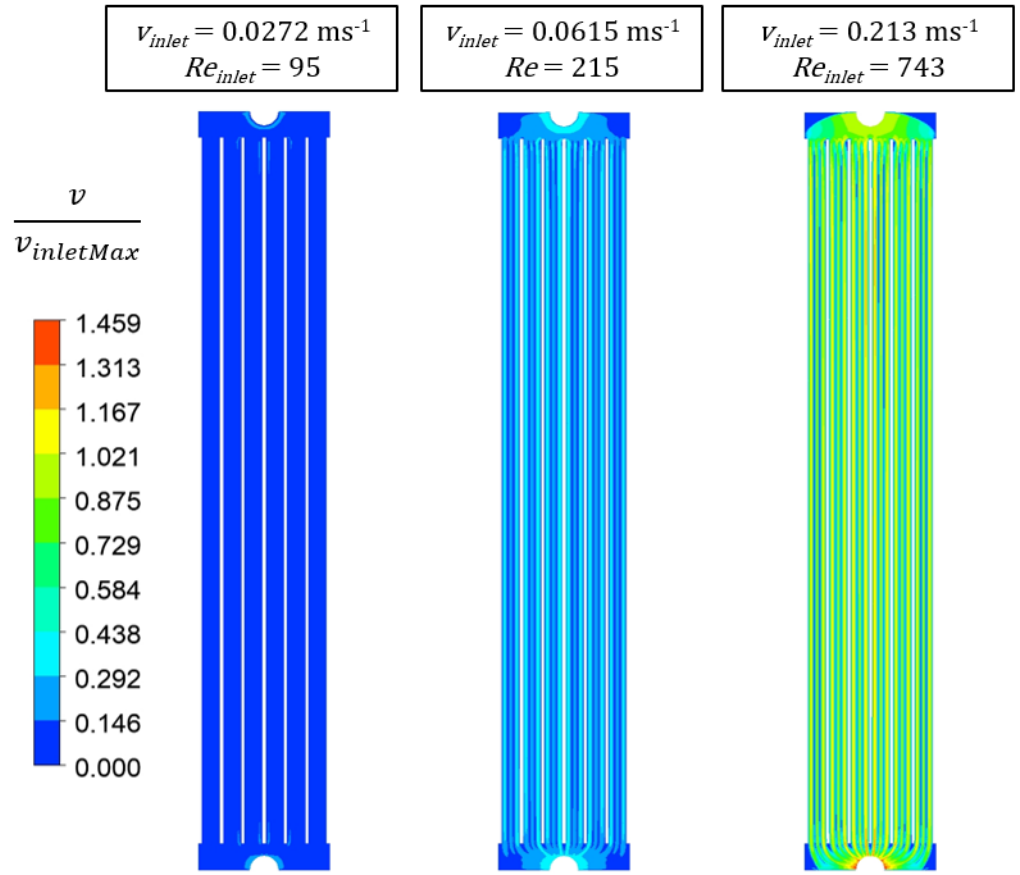


Figure 42 - Contours of velocity magnitude normalized by the maximum inlet velocity (0.213 ms^{-1}). Plate features a height of 800 mm

Another aspect of velocity distribution within the radiator plate is the flow rate distribution between the plate ducts. This analysis was done using the contours that were presented above and by the elaboration of graphs. In this first round of graphs are presented volume flow rate distributions, maintaining a constant total inlet flow rate and varying heights within the same graph

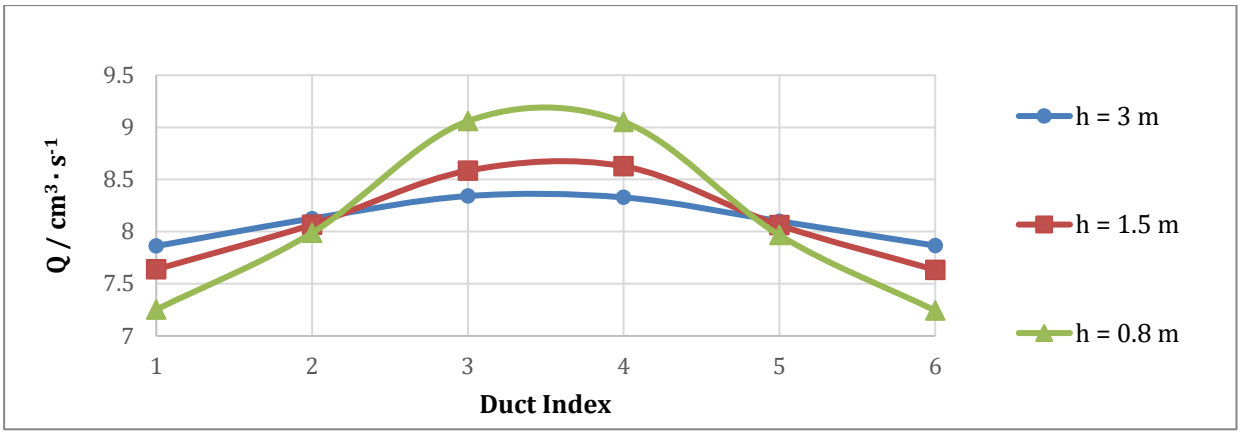


Figure 43 - Volume flow rate distribution between plate ducts with an inlet flow rate of 0.048 dm3s-1

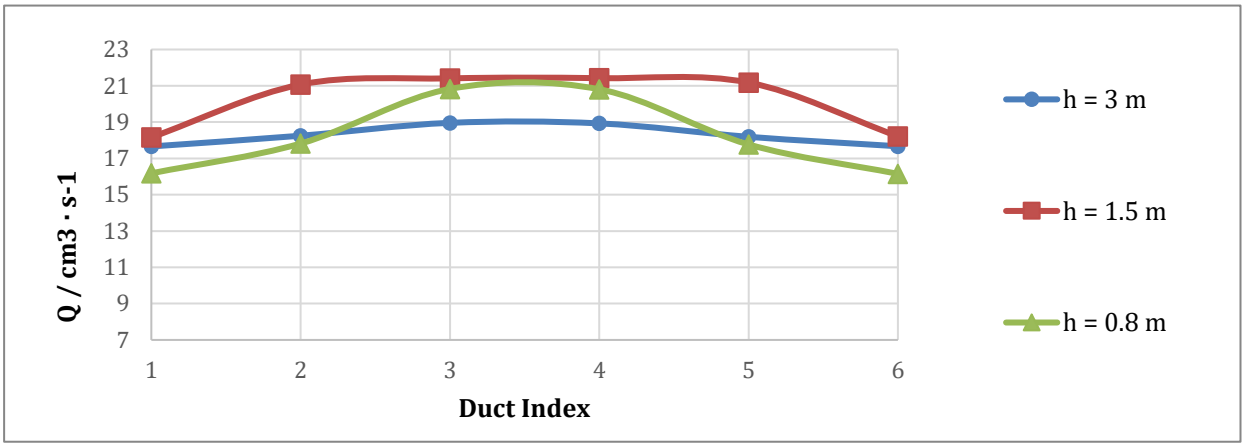


Figure 44 - Volume flow rate distribution between plate ducts between plate ducts with an inlet flow rate Q_2 = 0.11 dm^3s^{-1}

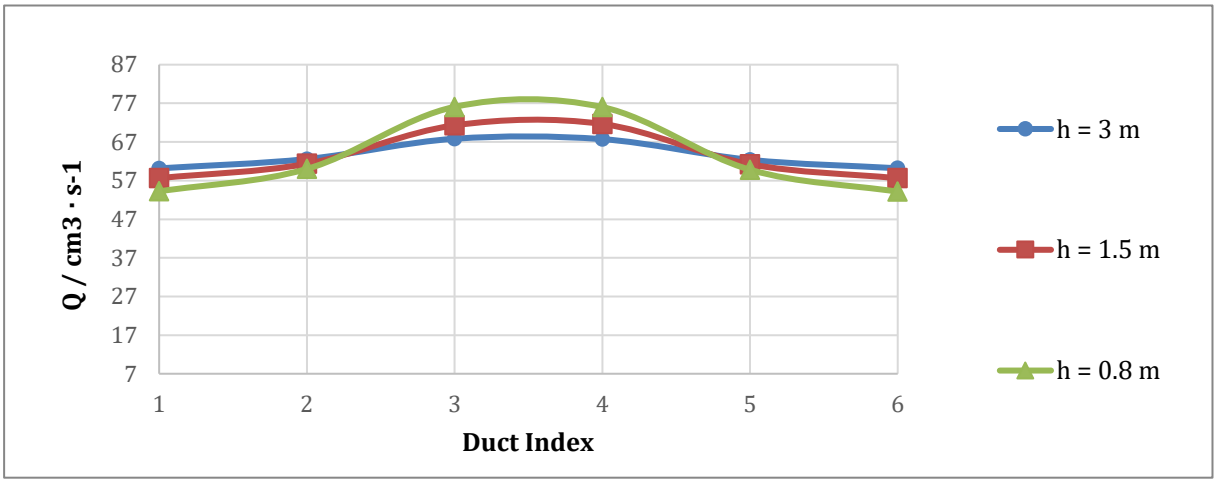
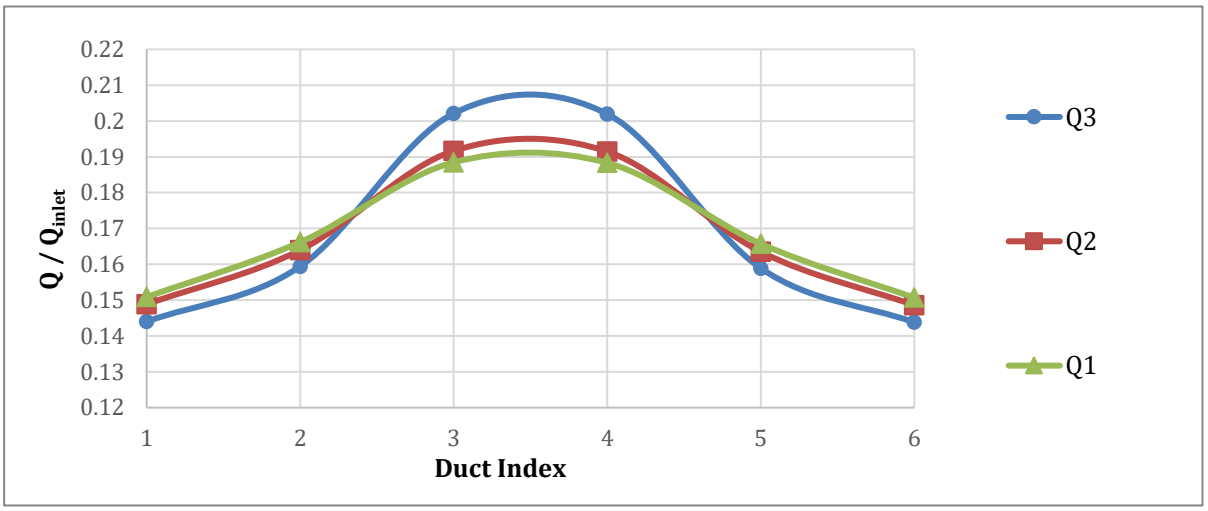
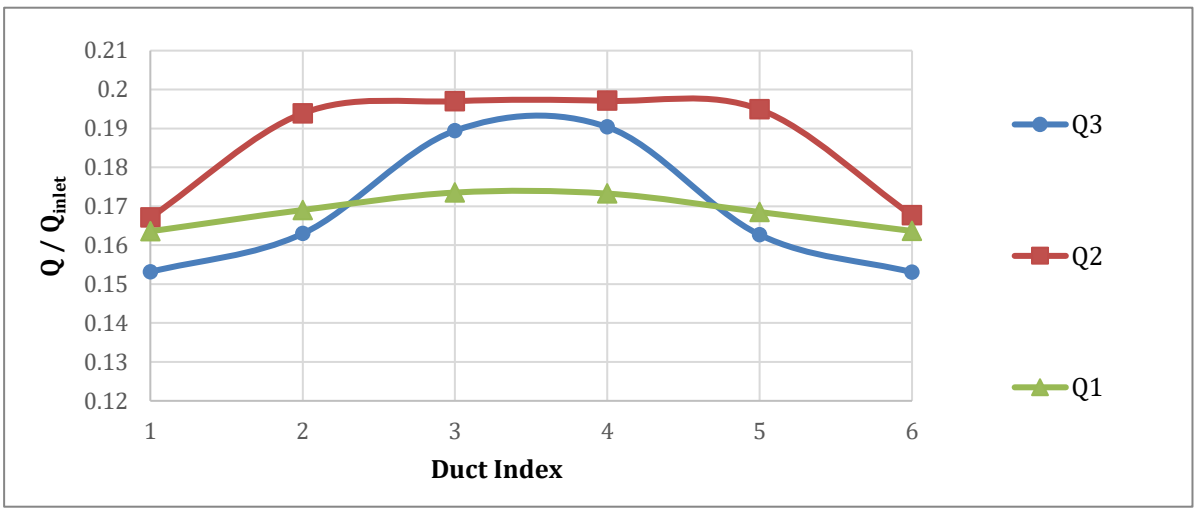


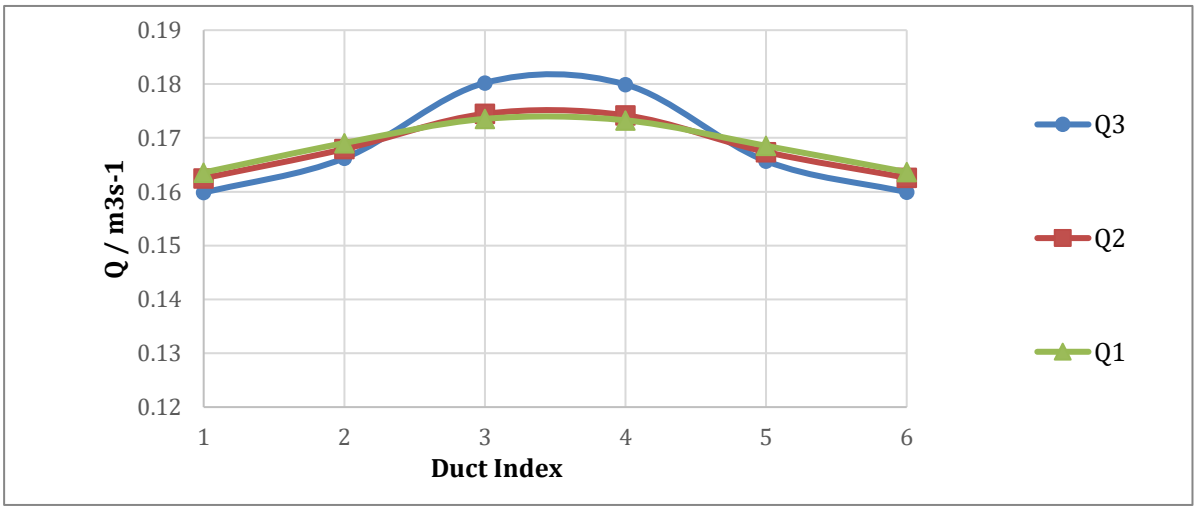
Figure 45 - Volume flow rate distribution between plate ducts between plate ducts with an inlet flow rate Q_2 = 0.376 dm^3s^{-1}

As it can be seen, increasing plate height makes the flow rate distribution more even among the ducts.

In the next round of graphs, the y-axis will have values of volume flow rate normalized by each inlet flow rate maintaining a constant total inlet flow rate and varying inlet flow rates within the same graph.







Through analysis of these graphs it can be seen that increasing inlet flow rate makes for a more uneven distribution of oil among the plate ducts.

B.5. Pressure drop contour plots

In the following figures are depicted contours of static pressure for the simulated plate heights. It is once again worth noting that these are values of relative pressure.

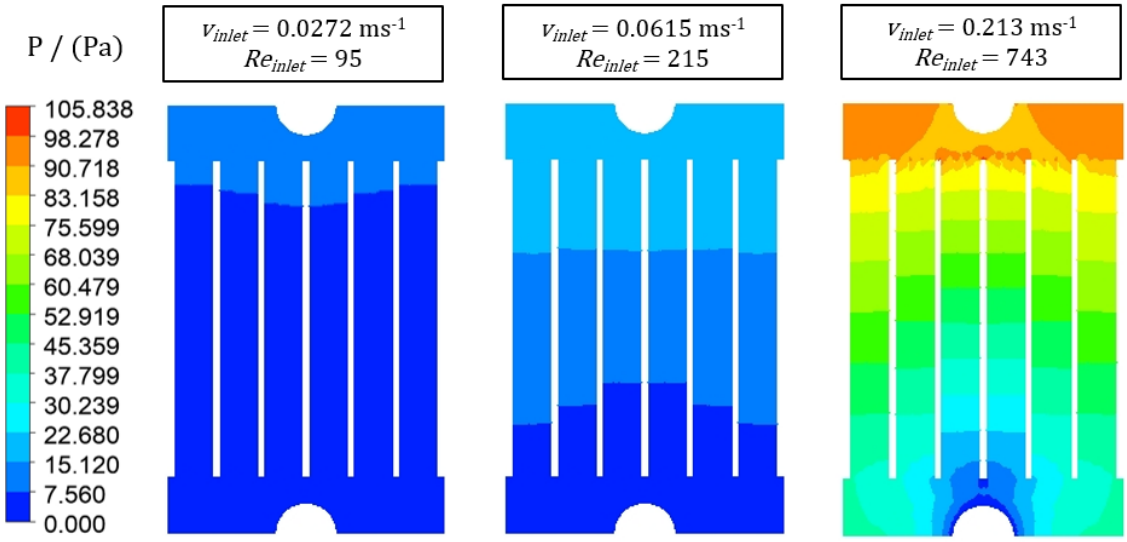


Figure 46 - Contours of static pressure obtained from hydraulic CFD simulations of a single radit. Plate features a height of 800 mm

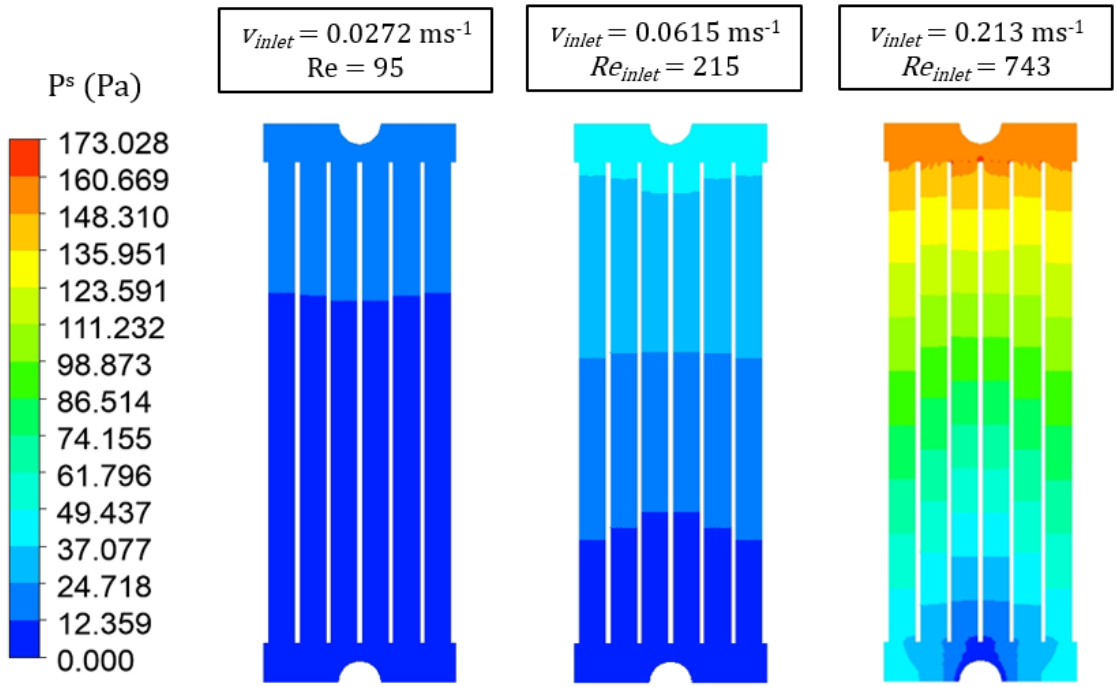


Figure 47 - Contours of static pressure obtained from hydraulic CFD simulations of a single radiator plate. Plate features a height of 1.5 m.

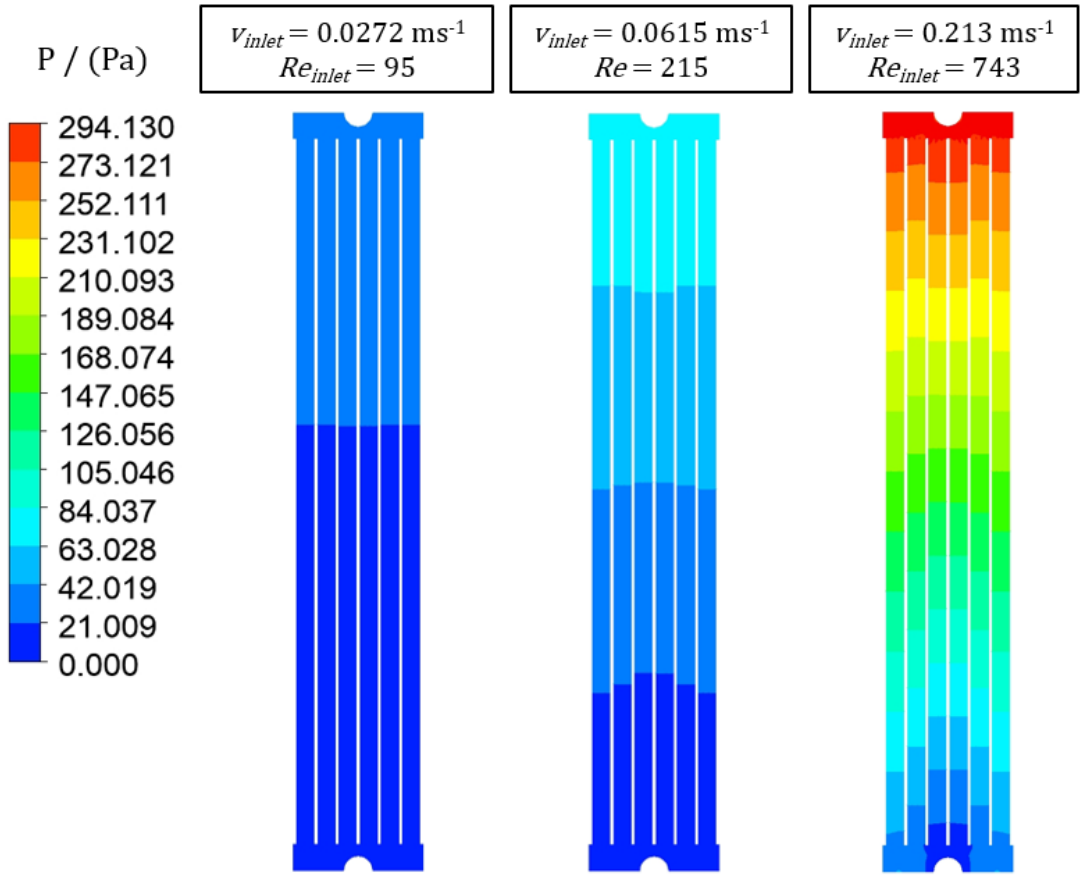


Figure 48 – Contours of static pressure obtained from hydraulic CFD simulations of a single radiator plate. Plate features a height of 3 m.

Appendix C - Mesh full Settings and Numerical Settings

C.1. Single Plate Hydraulic Simulations

Meshing Aspects

The plate geometry is presented below, in Figure 49. In this figure are also depicted the within the plate and the duct from where data was taken in order to conduct mesh independence tests.Figure 49

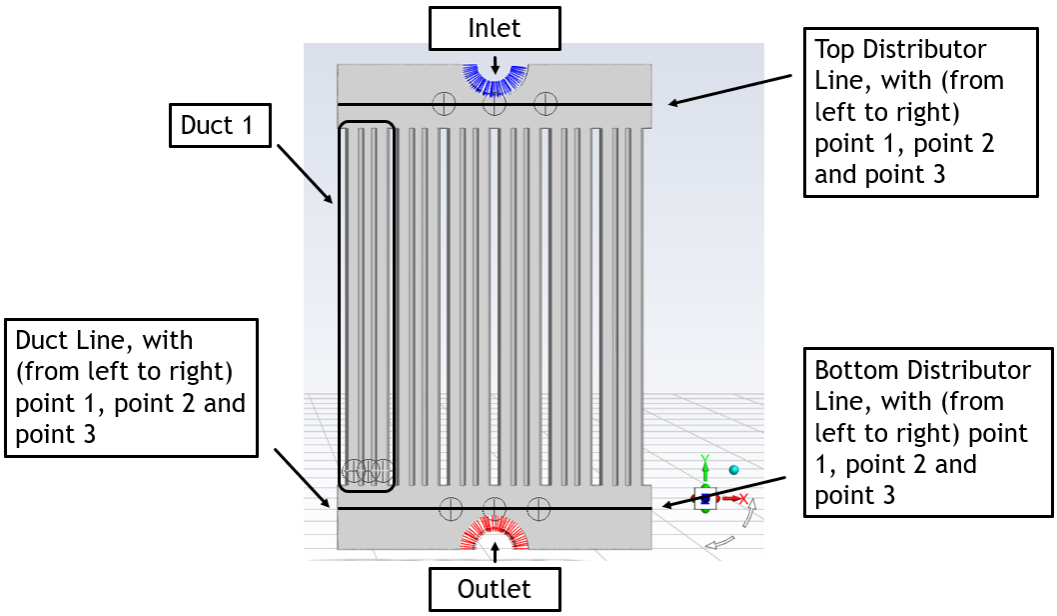


Figure 49 - Plate geometry with mesh independence testing zones

Firstly, mesh independence tests of the radiator duct were conducted. Below, in Figure 50, the geometry of the tested model is depicted:

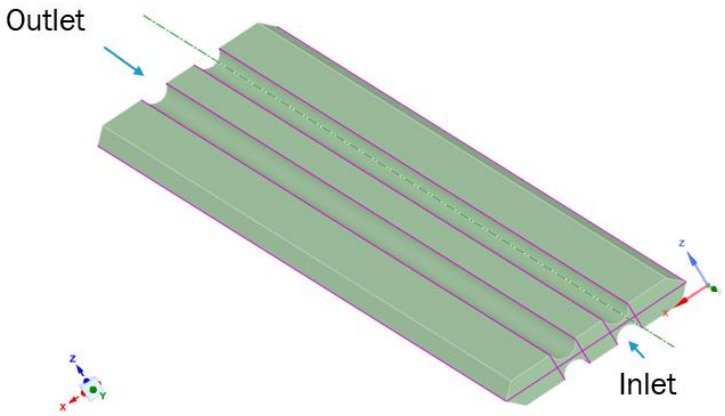


Figure 50 - Duct Geometry

In Figure 51 are plotted the results of the duct mesh independence tests and in Table 5 is a comparison of the obtained values.

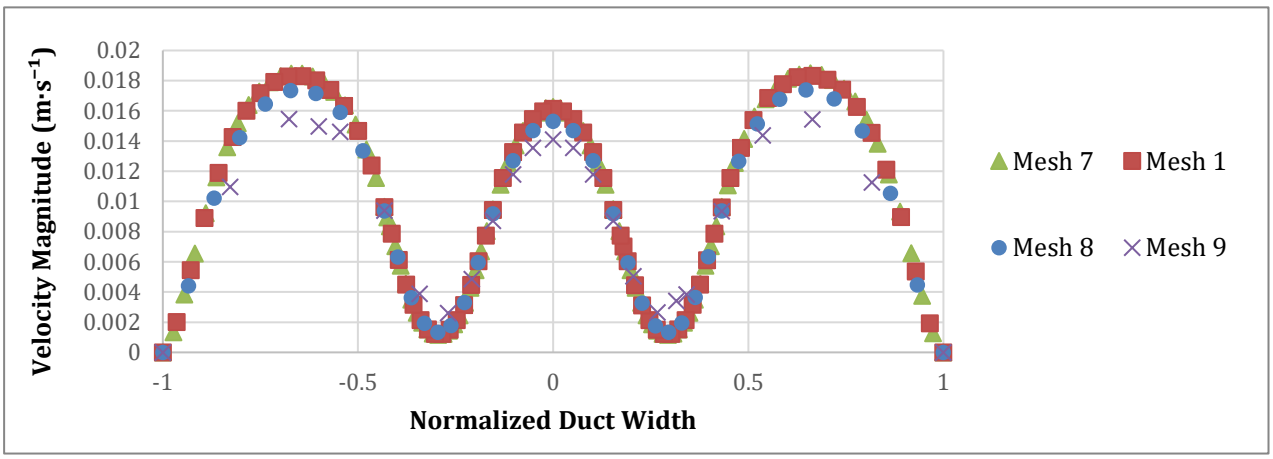


Figure 51 - Velocity profile Duct mesh Independence tests

Table 18 - Mesh performance comparison for duct mesh independence tests

These results were then analyzed and Mesh 1 was selected. The next step was to conduct tests on the distributor. The results of these are reported in the following figures and tables.

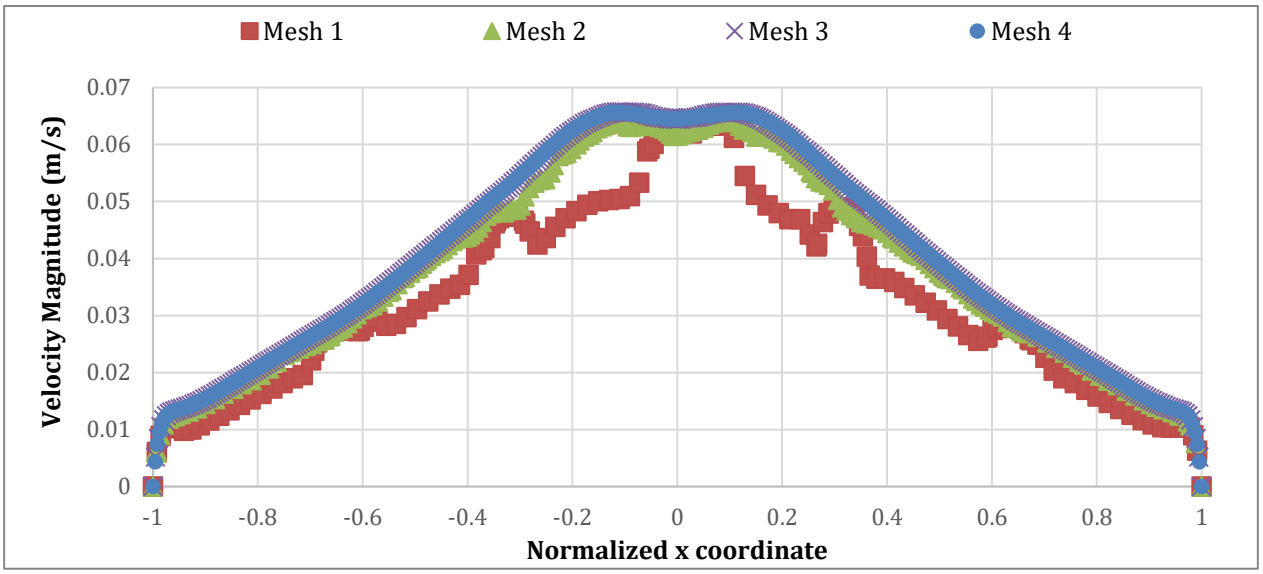


Figure 52 - Velocity magnitude profiles obtained from the top distributor line in the hydraulic mesh tests

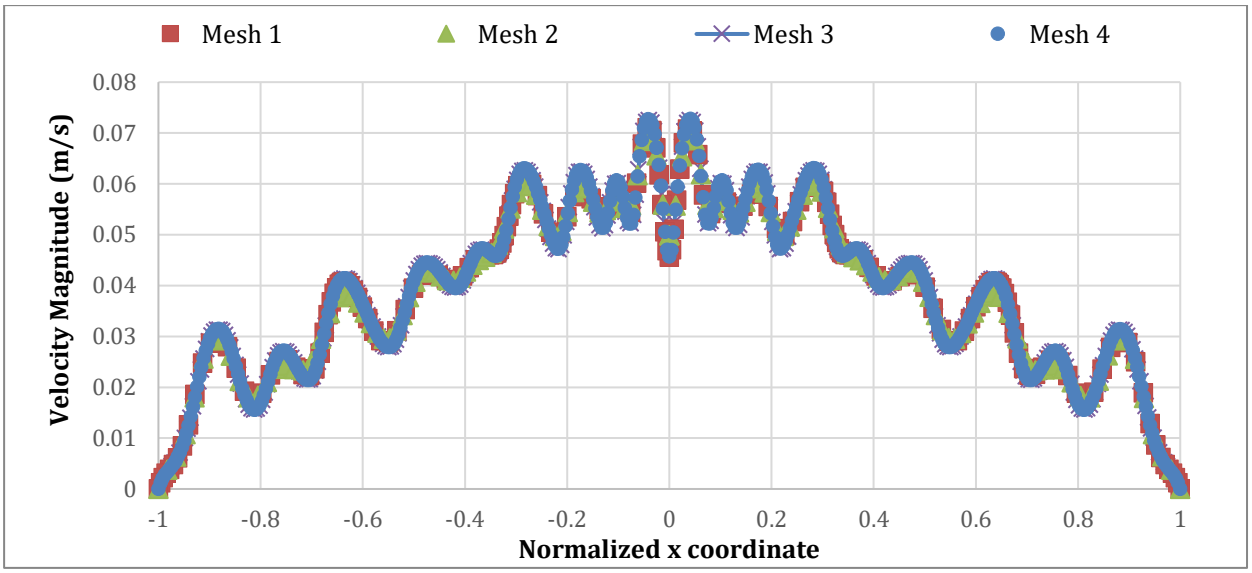


Figure 53 – Velocity magnitude profiled obtained from the bottom distributor line in the hydraulic mesh tests

These results were then analyzed, and Mesh 3 was the one that was selected to carry out further thermo-hydraulic simulations.

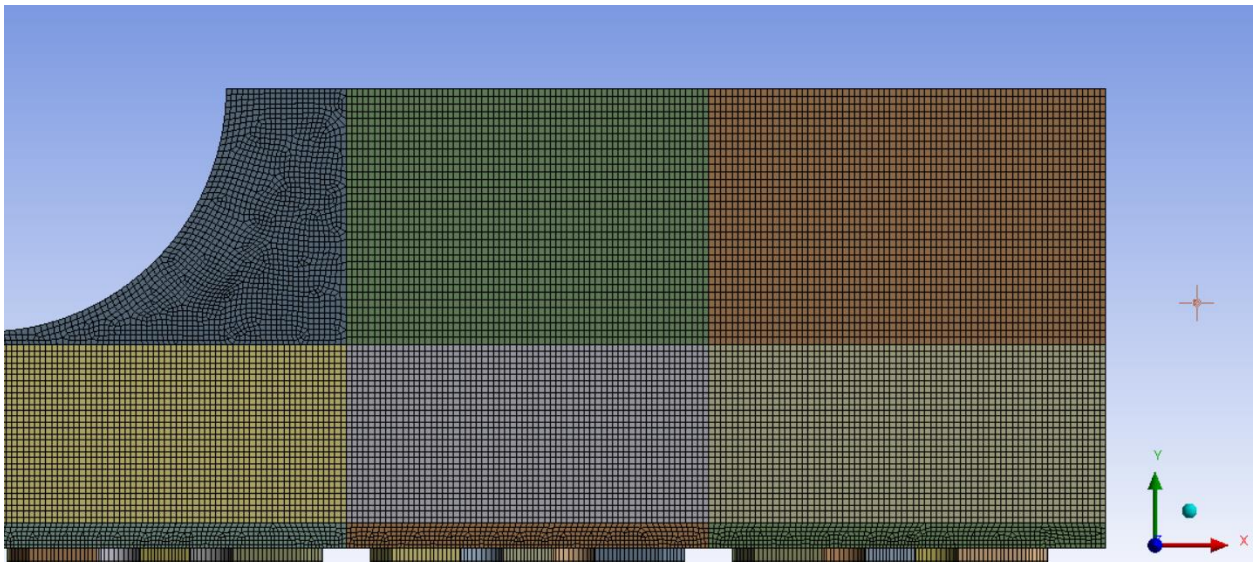


Figure 54 – View of the right side of the hydraulic mesh distributor

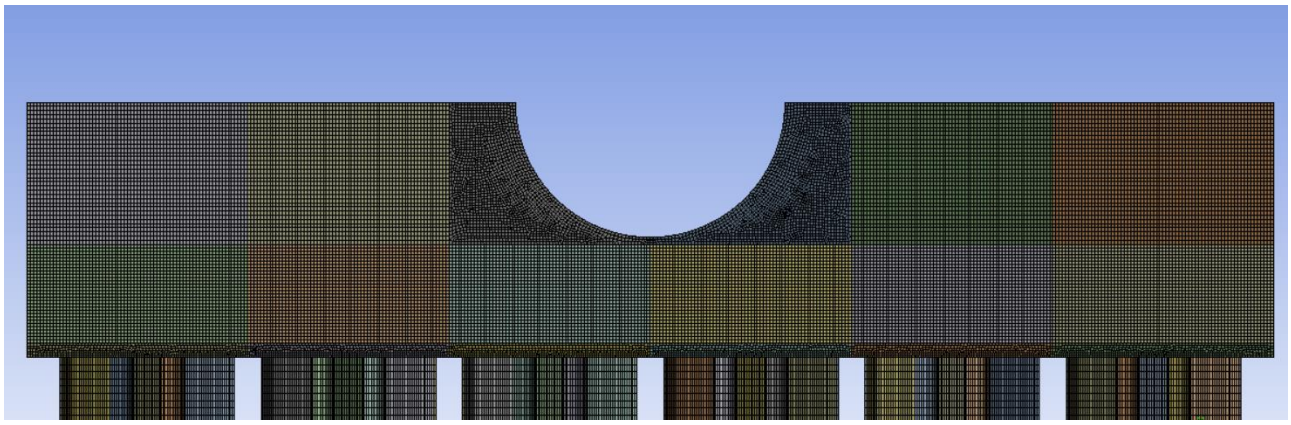


Figure 55 – View of the left side of the hydraulic mesh distributor

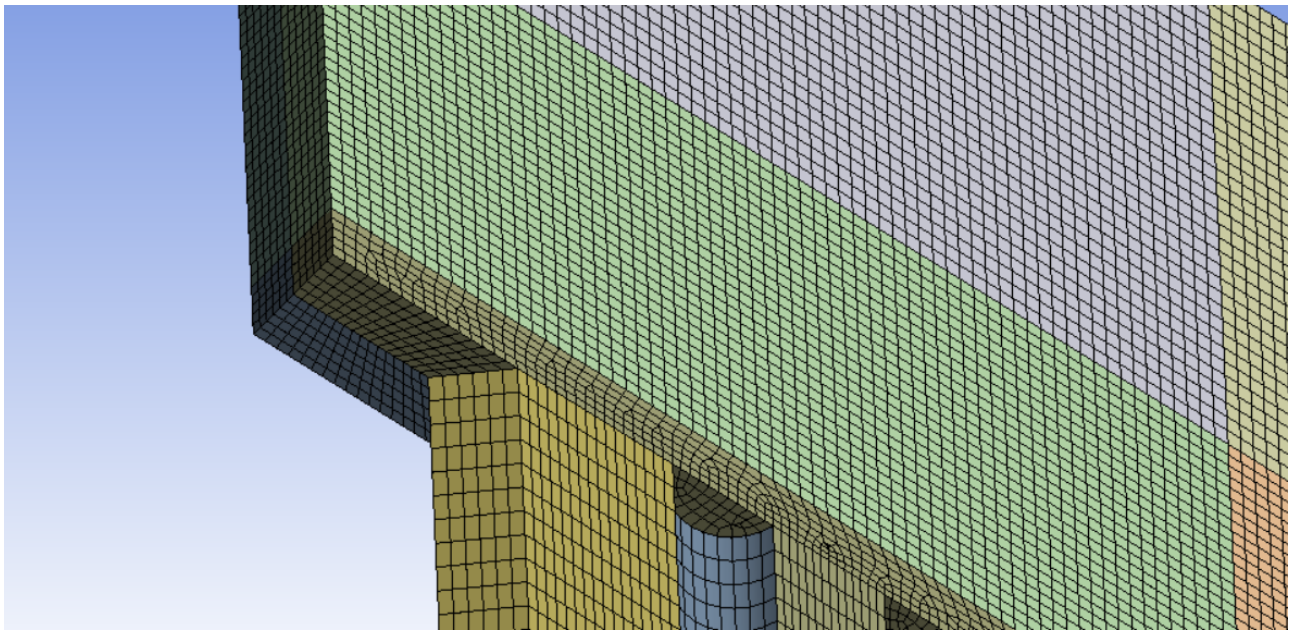


Figure 56 – View of a corner of the distributor of the hydraulic mesh

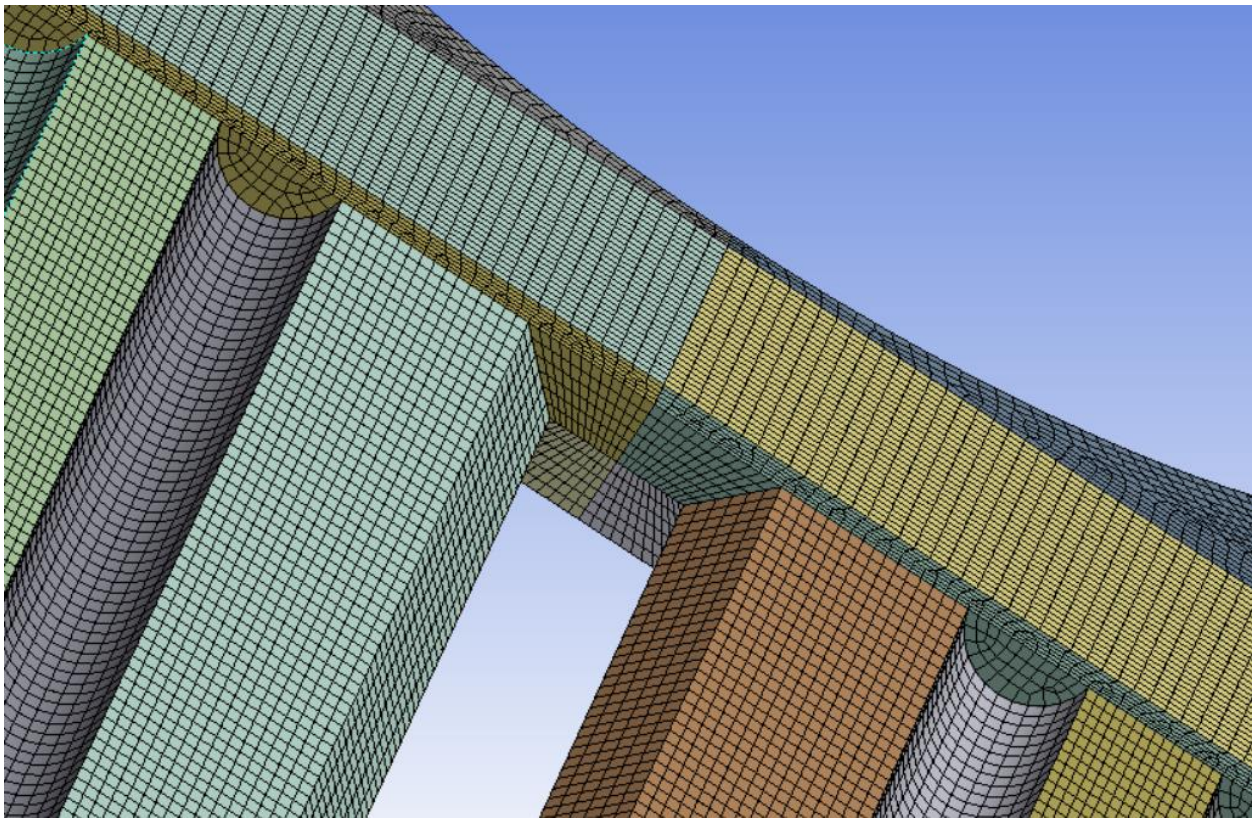


Figure 57 – View of a detail of the hydraulic mesh

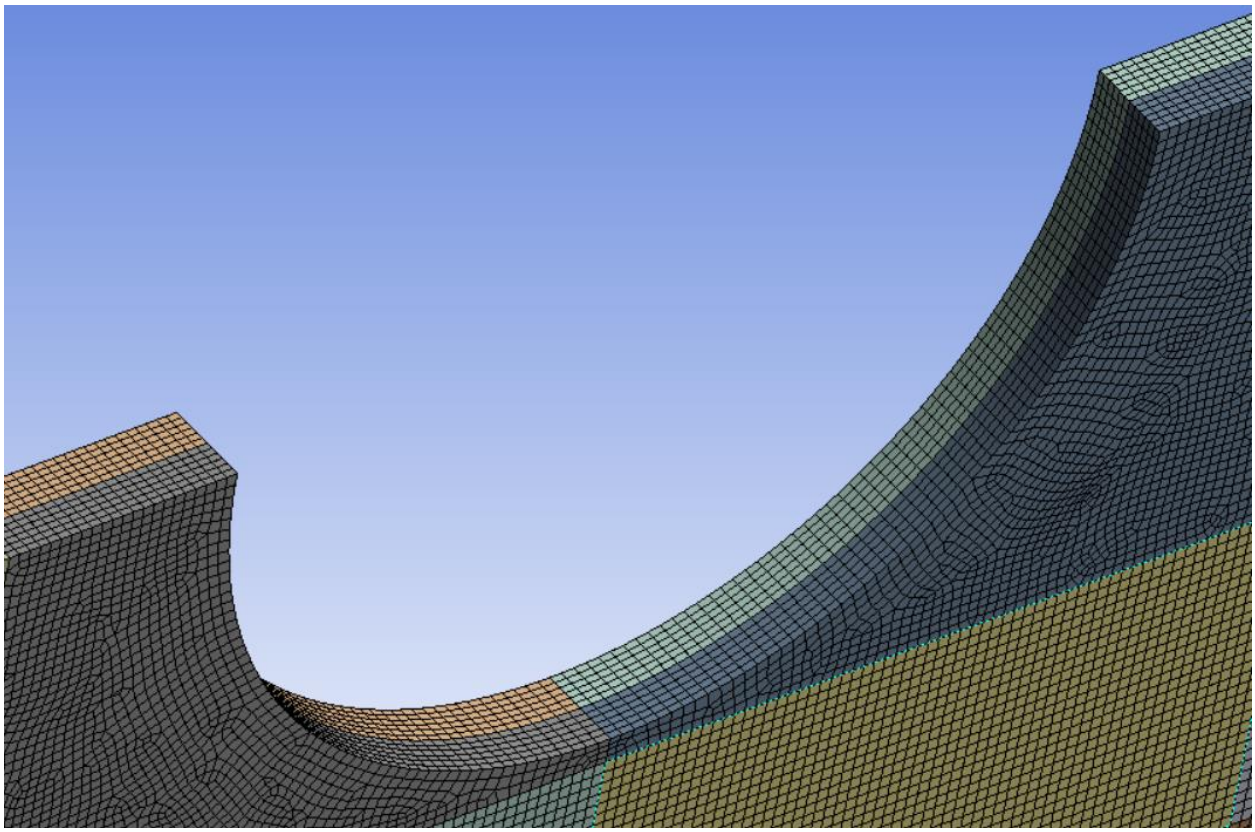


Figure 58 – View of the inlet of the hydraulic mesh

Numerical Aspects

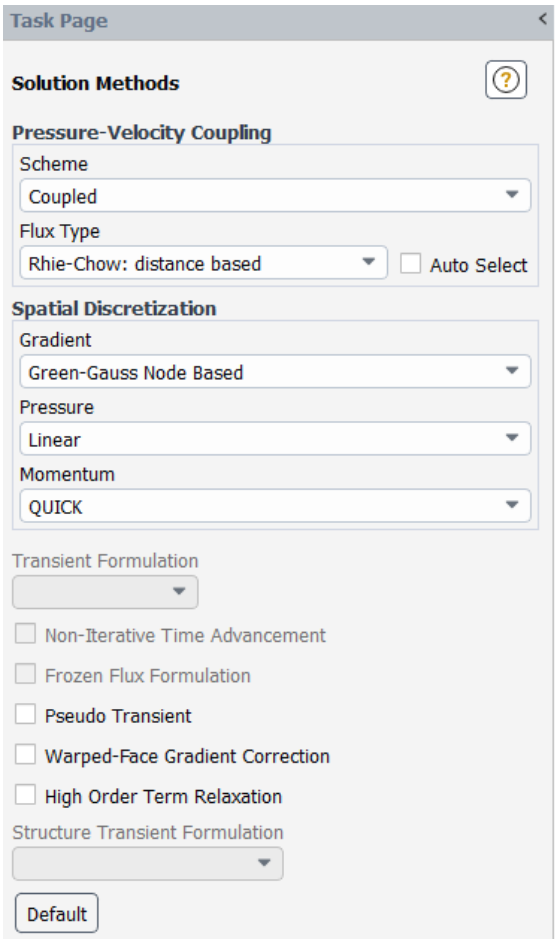


Figure 59 – Numerical settings of the single plate hydraulic simulations

The steady-state option was chosen to solve these simulations.

Using the "Coupled" option for the Scheme settings offers some advantages over the non-coupled or segregated approach. This option selects the pressure-based coupled solver. The coupled scheme obtains a robust and efficient single phase implementation for steady-state flows, with superior performance compared to the segregated solution schemes. This pressure-based coupled algorithm offers an alternative to the density-based and pressure-based segregated algorithm with SIMPLE-type pressure-velocity coupling [70].

Gradients are needed not only for constructing values of a scalar at the cell faces, but also for computing secondary diffusion terms and velocity derivatives. The chosen gradient option was the "Green-Gauss Node Based" option. The node-based gradient is known to be more accurate than the cell-based gradient particularly on irregular (skewed and distorted) unstructured meshes, however, it is relatively more expensive to compute than the cell-based gradient scheme [71]. This was chosen due concerns of unstructured zones near the edges of the mesh.

The QUICK is suited for quadrilateral and hexahedral meshes, where unique upstream and downstream faces and cells can be identified [72]. It was chosen for its accuracy, for it features 3rd-order accuracy [73].

C.2. Radiator thermo-hydraulic simulations

The next step in these proceedings was to conduct thermo-hydraulic simulations of all relevant geometries and conditions. However, these next simulations were performed using much larger and complex geometries. This not only presents an increase to the number of cells but to the difficulties and speed of the convergence. As such, new mesh tests were performed, in order to obtain a coarser mesh that would work in terms of time and processing power.In these tests, given the increased experience with CFD tools, both the ducts and the distributor were tested at the same time.

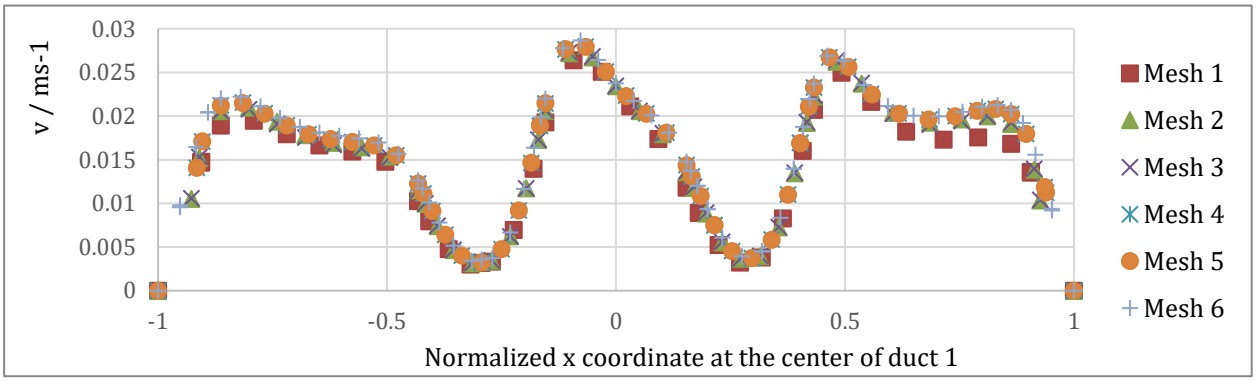


Figure 60 – Thermo-hydraulic Duct Mesh independence tests

Comparing the thermo-hydraulic duct mesh tests from Figure 60 with the hydraulic dust mesh tests from Figure 51, one can see that the velocity profiles obtained for the thermo-hydraulic mesh tests are slightly distorted to left. This is because in these second tests, the entire plate was simulated and the values were taken from duct 1, as depicted in Figure 49, meaning the fluid was launched to the left side of the plate. In the tests from Figure 51, the duct was simulated separately, as such the velocity came with a straight trajectory.

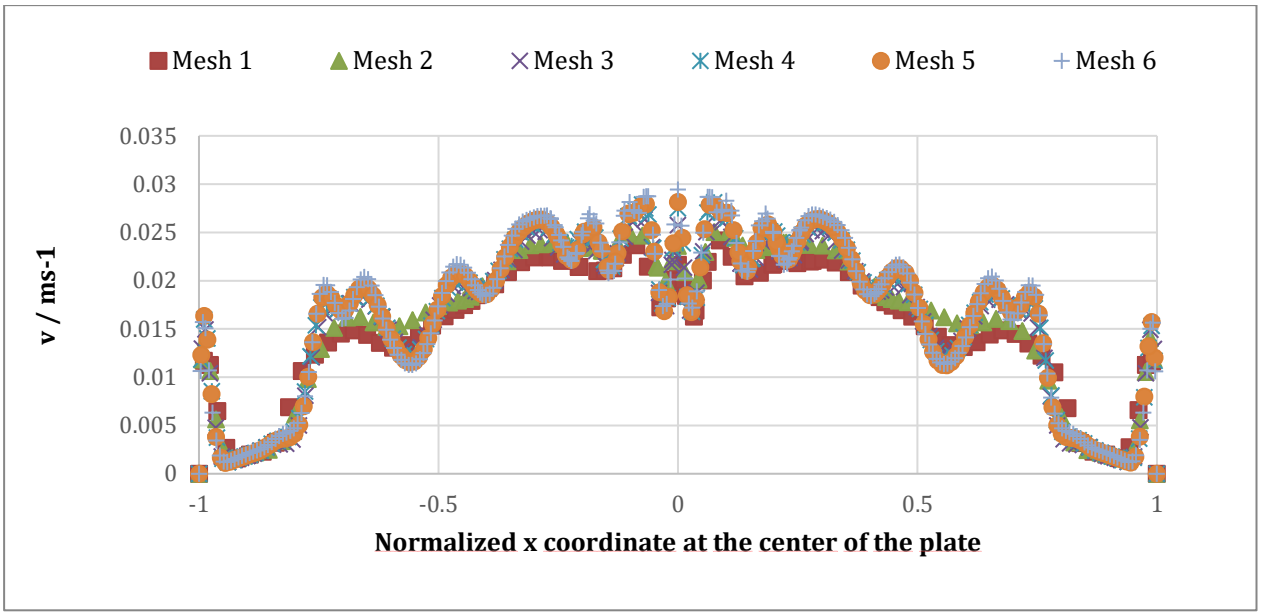


Figure 61 - Velocity magnitude profiled obtained from the bottom distributor line in thermo-hydraulic mesh tests

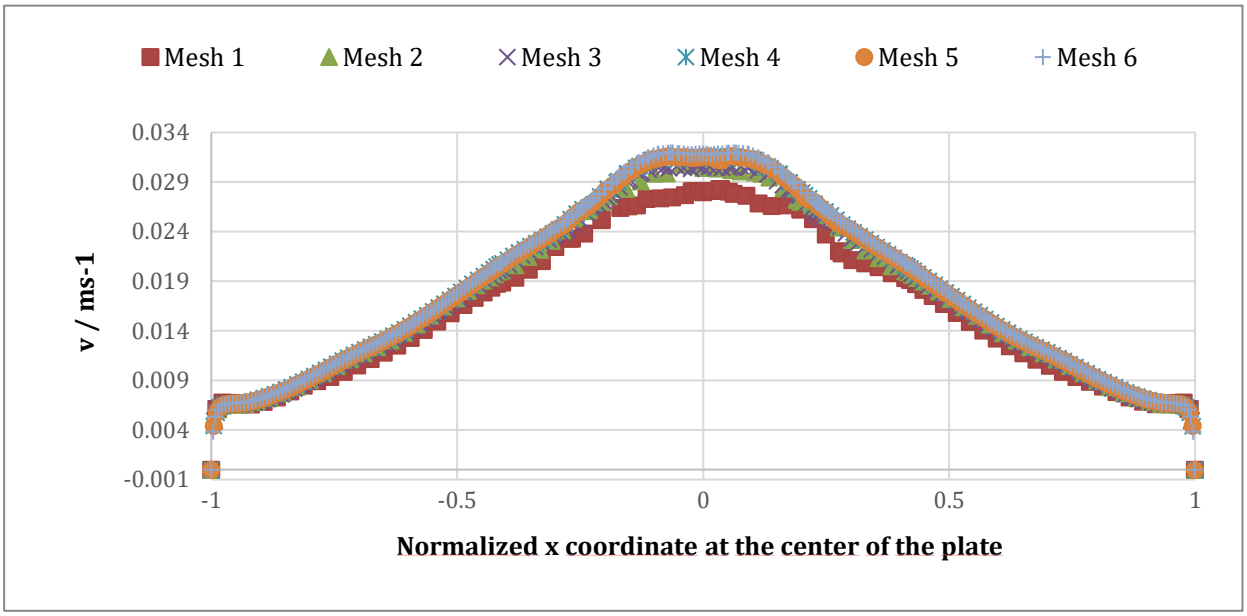


Figure 62 – Velocity magnitude profiles obtained from the top distributor line in thermo-hydraulic mesh tests

These results were then analyzed, and Mesh 3 was the one that was selected to carry out further thermo-hydraulic simulations.

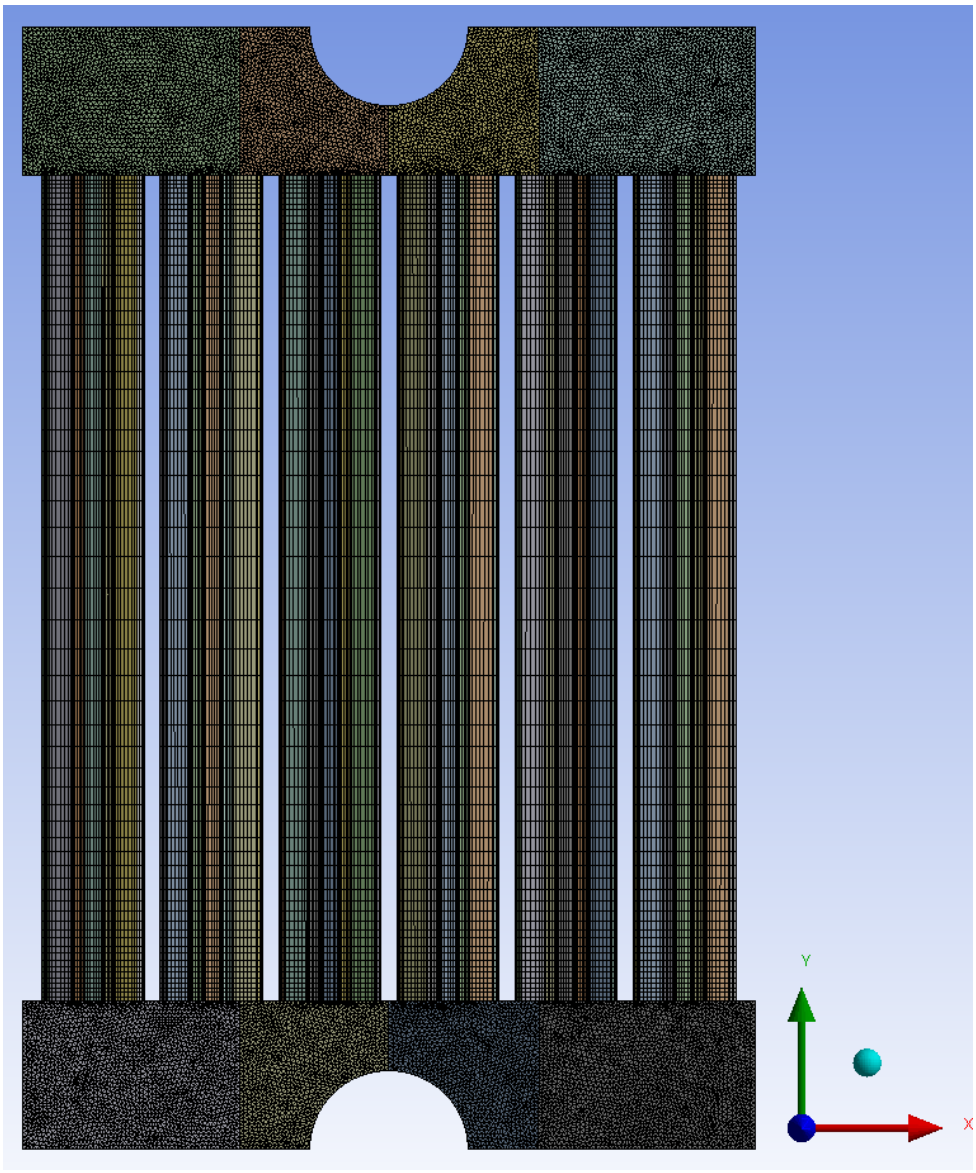


Figure 63 – Frontal view of the thermo-hydraulic plate mesh

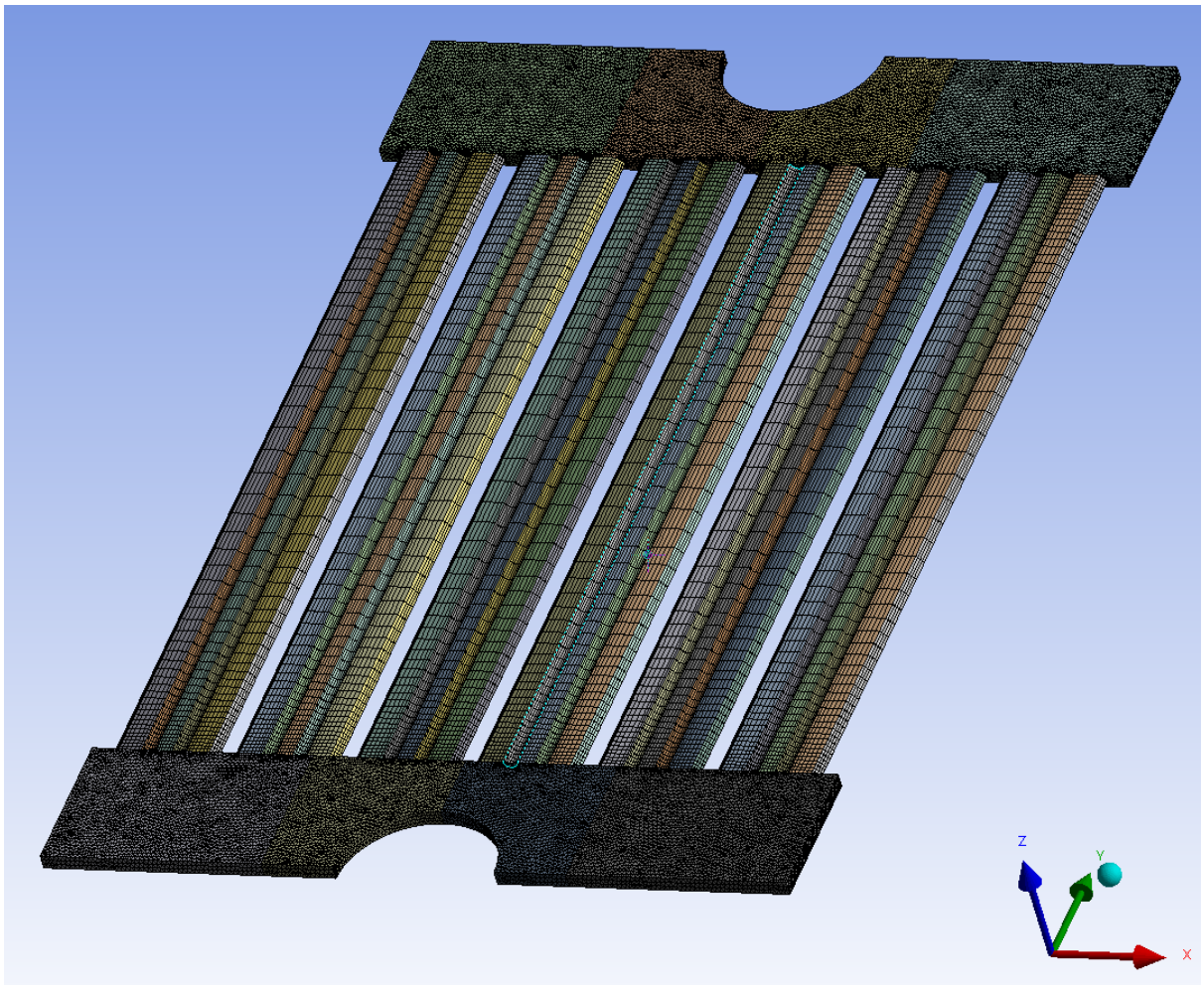


Figure 64 – Overall view of the thermo-hydraulic plate mesh

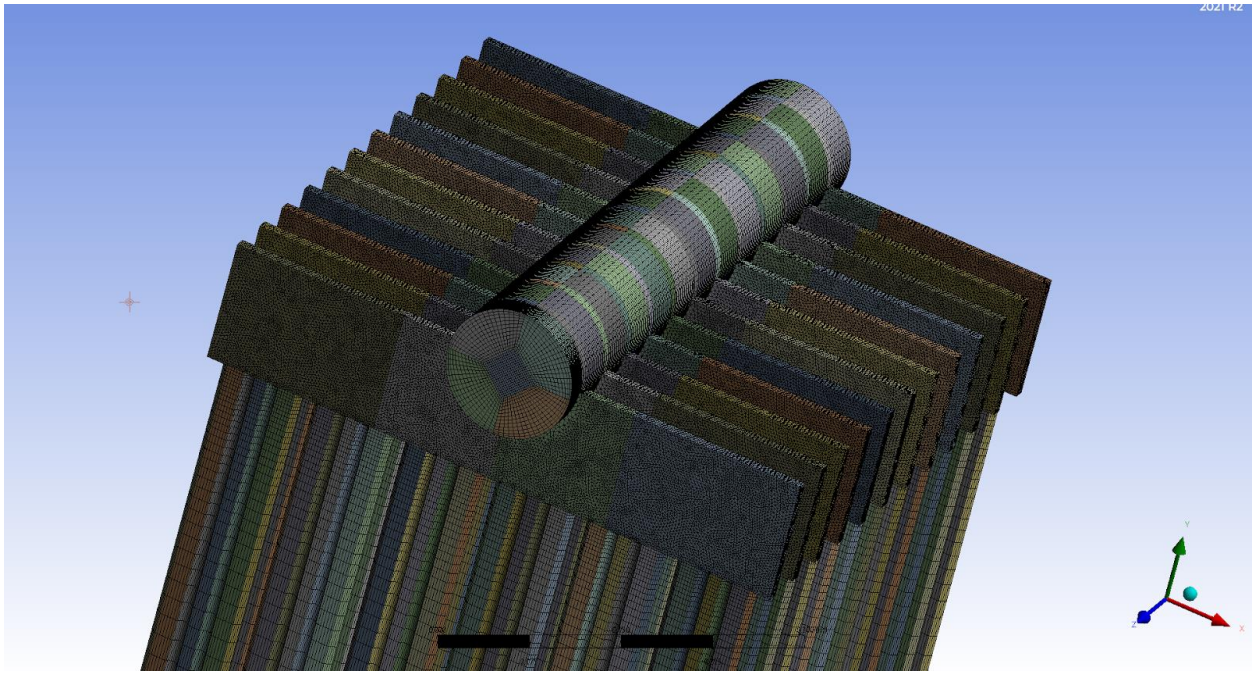


Figure 65 – Top view of the radiator mesh with 7 plates and a height of 0.8 m

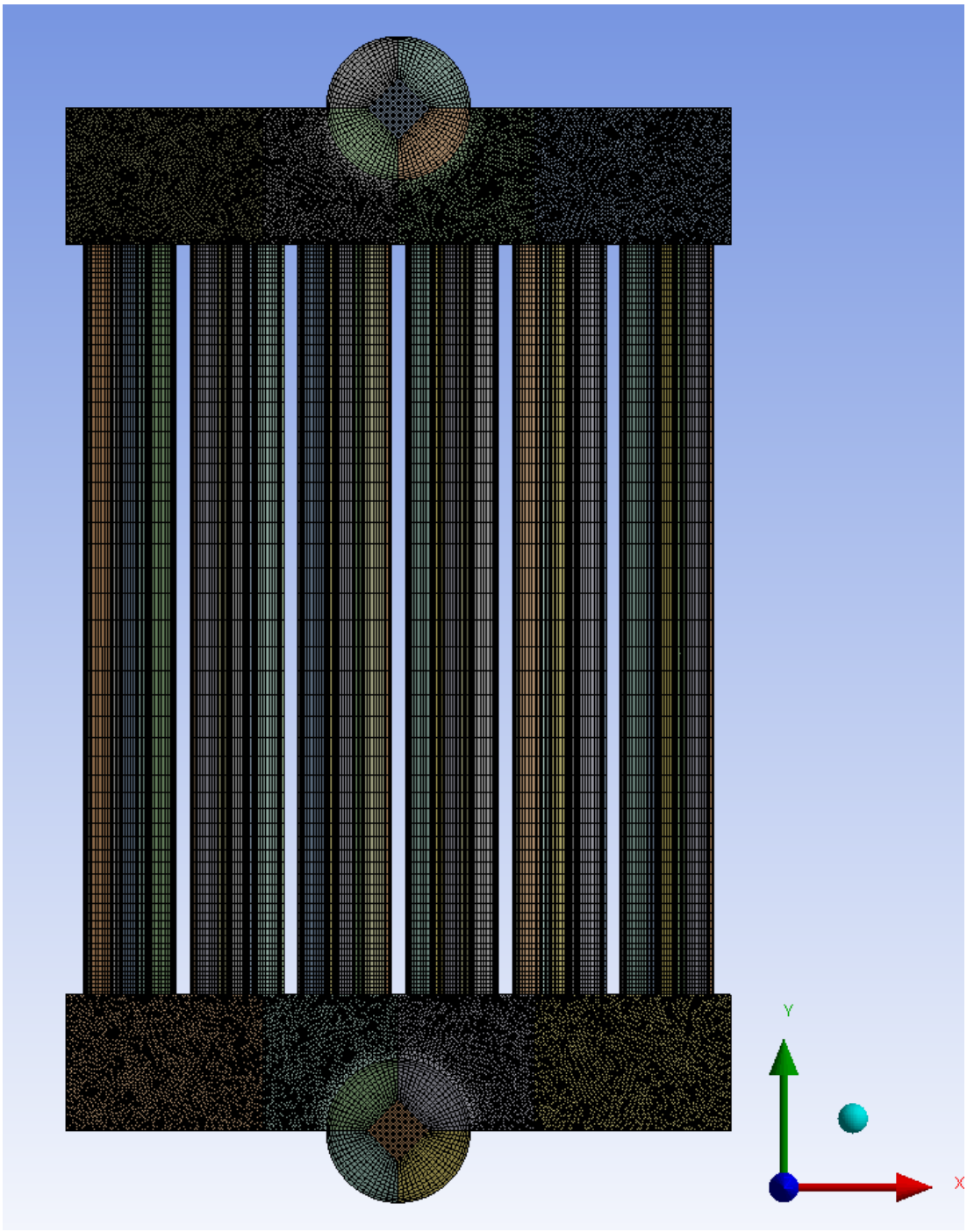


Figure 66 – Front view of the radiator mesh with 7 plates and a height of 0.8 m

Numerical Aspects

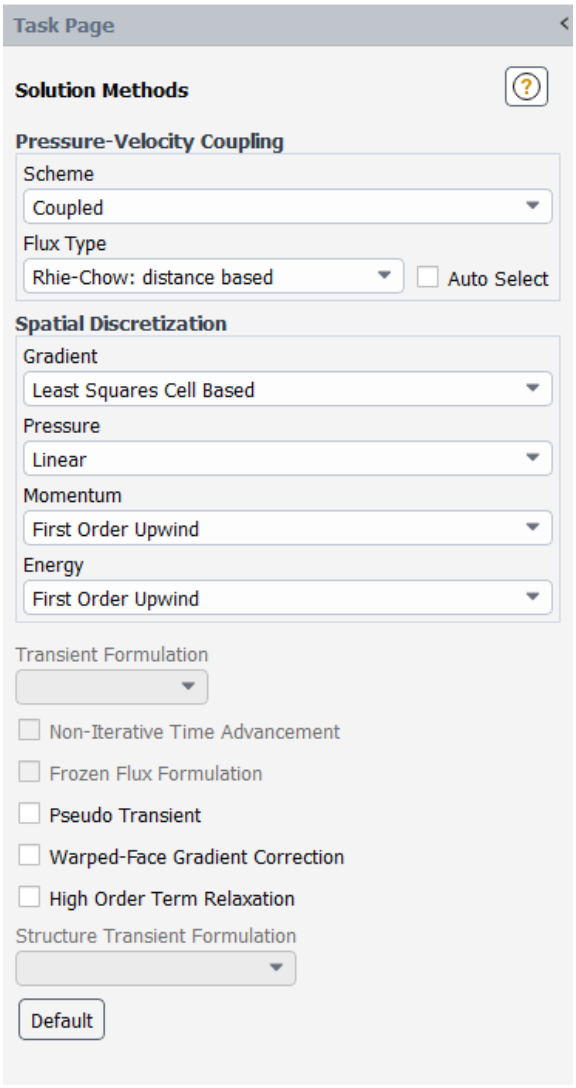


Figure 67 - Numerical settings of thermo-hydraulic simulations

The steady-state option was chosen to solve these simulations.

Using the "Coupled" option for the Scheme settings offers some advantages over the non-coupled or segregated approach. This option selects the pressure-based coupled solver. The coupled scheme obtains a robust and efficient single phase implementation for steady-state flows, with superior performance compared to the segregated solution schemes. This pressure-based coupled algorithm offers an alternative to the density-based and pressure-based segregated algorithm with SIMPLE-type pressure-velocity coupling [70].

Gradients are needed not only for constructing values of a scalar at the cell faces, but also for computing secondary diffusion terms and velocity derivatives. The chosen gradient option was the "Least Squares Cell Based" option. The cell-based gradient is known to be less accurate than the node-based gradient particularly on irregular (skewed and distorted) unstructured

meshes, however, it is relatively more easy to compute than the cell-based gradient scheme [71]. This was chosen due concerns of unstructured zones near the edges of the mesh.

The “linear” option does not produce the most accurate results compared to QUICK, but the previous alternatives resulted in convergence difficulties.

For energy and momentum, the 1st order upwind option was selected. When first-order accuracy is desired, quantities at cell faces are calculated by assuming that the cell-center values of any field variable represent a cell-average value and hold throughout the cell, the quantities at the face quantities are identical to the quantities in the cell. This was chosen to make the simulations computationally undemanding, since the mesh was so large.

Appendix D - CFD Simulator Code

"""

Thermo-Hydraulic Performance CFD Radiator Simulator

Author: Gabriel Silva

"""

```
#importing libraries

import pandas as pd
import numpy as np
import sklearn
from sklearn.linear_model import Ridge
from sklearn.linear_model import LinearRegression
from sklearn.preprocessing import PolynomialFeatures
from sklearn.ensemble import RandomForestRegressor
from sklearn.pipeline import make_pipeline


#importing data. Note: These files contain the CFD-originated data based on which this simulator formulates predictions.
#in order to work on another device, these files must be adequally sourced in the lines below

thermo=pd.read_excel(r'C:\Users\Gabriel Silva\Efacec_CFD_simulator\Datasets\To_dataset.xlsx',sheet_name='Thermo')
hydra=pd.read_excel(r'C:\Users\Gabriel Silva\Efacec_CFD_simulator\Datasets\To_dataset.xlsx',sheet_name='Hydra')

#naming variables

x_thermo=thermo[["plate_number","height","vfr","hairm"]]
x_hydra=hydra[["plate_number","height","vfr","hairm"]]

x_thermov=x_thermo.values
x_hydrav=x_hydra.values

y_thermo_to=thermo[["to"]]
y_thermo_u=thermo[["u"]]
y_thermo_hoil=thermo[["hoil"]]
y_thermo_power=thermo[["power"]]

y_hydra_dp=hydra[["pressure_drop"]]

#To (outlet temperature) regressor

rndfor_to=RandomForestRegressor(n_estimators=100, random_state=42)
rndfor_to.fit(x_thermov, np.ravel(y_thermo_to))

#U (overall heat transfer coefficient) regressor
```

```
ridreg_u = Ridge(alpha=1.0)
ridreg_u.fit(x_thermov, y_thermo_u)

#hoil (oil heat transfer coefficient) regressor

ridreg_hoil = Ridge(alpha=1.0)
ridreg_hoil.fit(x_thermov, y_thermo_hoil)

#power (energy removal rate) regressor

degree=2
polyreg_power=make_pipeline(PolynomialFeatures(degree),LinearRegression())
polyreg_power.fit(x_thermov, np.ravel(y_thermo_power))

#dP (pressure drop) regressor

rndfor_dp=RandomForestRegressor(n_estimators=100, random_state=42)
rndfor_dp.fit(x_hydrav, np.ravel(y_hydra_dp))

#generating simulator GUI and activation

from tkinter import*
root=Tk()
root.title("Efacec_CFD_RadiatorDesign_Simulator")

Input_1 = Entry(root, borderwidth=5)
Input_2 = Entry(root, borderwidth=5)
Input_3 = Entry(root, borderwidth=5)
Input_4 = Entry(root, borderwidth=5)

Input_1.grid(row=0,column=1)
Input_2.grid(row=1,column=1)
Input_3.grid(row=2,column=1)
Input_4.grid(row=3,column=1)

Label_1 = Label(root, text="Number of Plates")
Label_2 = Label(root, text="Plate Height (m)")
Label_3 = Label(root, text="Oil Flow Rate (dm^3*s^-1)")
Label_4 = Label(root, text="External Heat Transfer Coefficient (scales with ventilation intensity. For no ventilation insert 5; for
moderate ventilation insert 12; for intense ventilation insert 16")

Label_1.grid(row=0,column=0)
Label_2.grid(row=1,column=0)
Label_3.grid(row=2,column=0)
Label_4.grid(row=3,column=0)
```

```
def myClick():

    inputlist = [Input_1.get(),Input_2.get(),Input_3.get(),Input_4.get()]

    y_thermo_to_pred=rndfor_to.predict(np.array(inputlist).reshape(-4,4))
    y_thermo_u_pred=ridreg_u.predict(np.array(inputlist).reshape(-4,4))
    y_thermo_hoil_pred=ridreg_hoil.predict(np.array(inputlist).reshape(-4,4))
    y_thermo_power_pred=polyreg_power.predict(np.array(inputlist).reshape(-4,4))

    y_hydra_dp_pred=rndfor_dp.predict(np.array(inputlist).reshape(-4,4))

    y_thermo_to_output=np.round(y_thermo_to_pred,3)
    y_thermo_u_output=np.round(y_thermo_u_pred,3)
    y_thermo_hoil_output=np.round(y_thermo_hoil_pred,3)
    y_thermo_power_output=np.round(y_thermo_power_pred,3)
    y_hydra_dp_output=np.round(y_hydra_dp_pred,3)



    dp = Label(root,text = "Pressure Drop (Pa) = ")
    dp_pred= Label(root,text=y_hydra_dp_output)

    to = Label(root, text="Outlet Temperature (ºC) = ")
    to_pred= Label(root,text=y_thermo_to_output)

    u = Label(root, text="Overall Heat Transfer Coefficient (W/(m2°C)) = ")
    u_pred= Label(root,text=y_thermo_u_output)

    hoil = Label(root, text="Oil Heat Transfer Coefficient (W/(m2°C)) = ")
    hoil_pred = Label(root,text=y_thermo_hoil_output)

    power = Label(root, text="Power (W) = ")
    power_pred = Label(root, text=y_thermo_power_output)

       dp.grid(row=0, column=3)
    dp_pred.grid(row=0, column=4)

    to.grid(row=1, column=3)
    to_pred.grid(row=1, column=4)

    u.grid(row=2, column=3)
    u_pred.grid(row=2, column=4)

    hoil.grid(row=3, column=3)
    hoil_pred.grid(row=3, column=4)

    power.grid(row=4, column=3)
    power_pred.grid(row=4, column=4)
```

```
    return

myButton = Button(root, text="Run", command=myClick)
myButton.grid(row=4,column=0)

root.mainloop()
```

Appendix E - Additional Pressure Drop Results obtained from thermo-hydraulic simulations

E.1. Correlations of pressure drop and mass flow rate

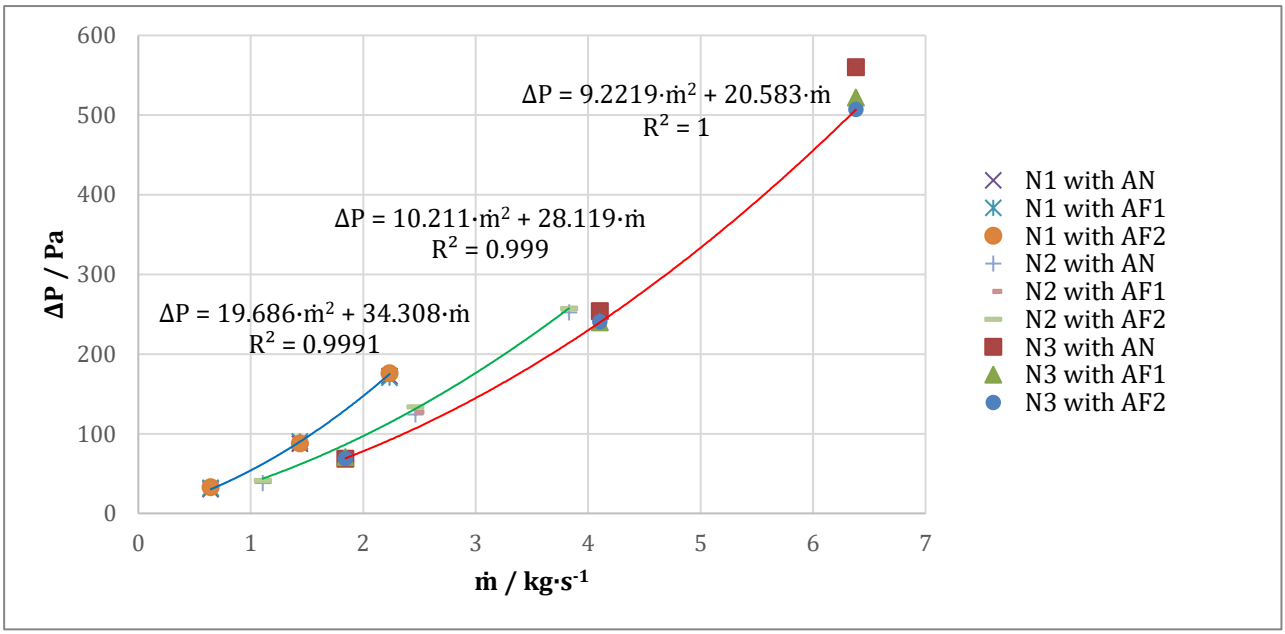


Figure 68 - Correlations for pressure drop (ΔP) as a function of flow rate for three numbers of plates for a height of 0.8 m

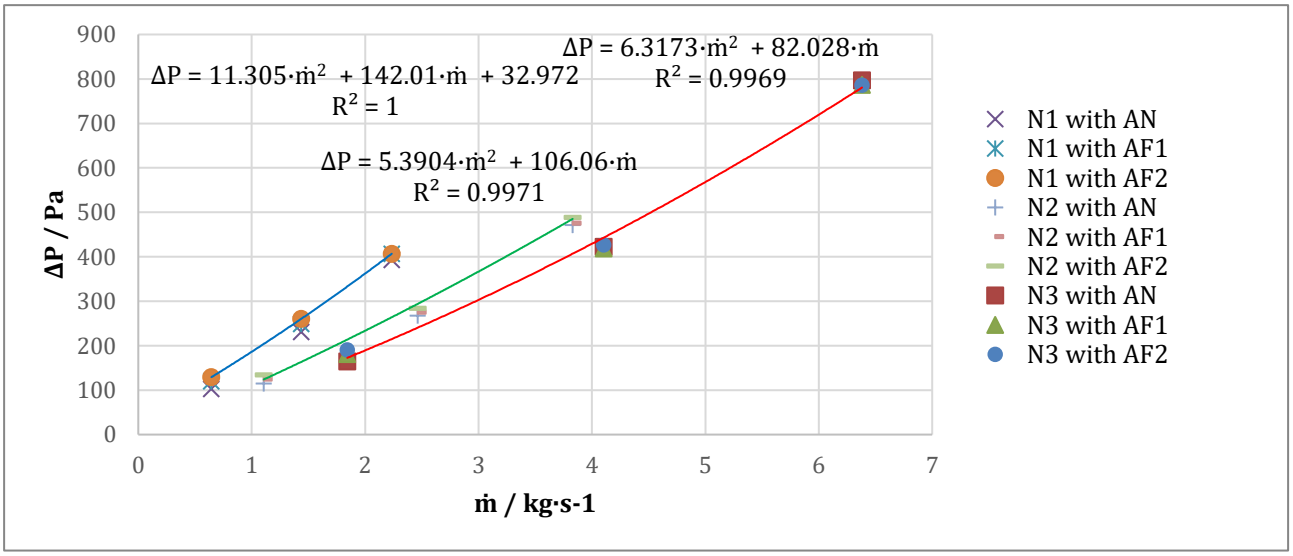


Figure 69 - Correlations for pressure drop (ΔP) as a function of flow rate for three numbers of plates for a height of 3 m

E.2. Correlations of pressure drop and plate height

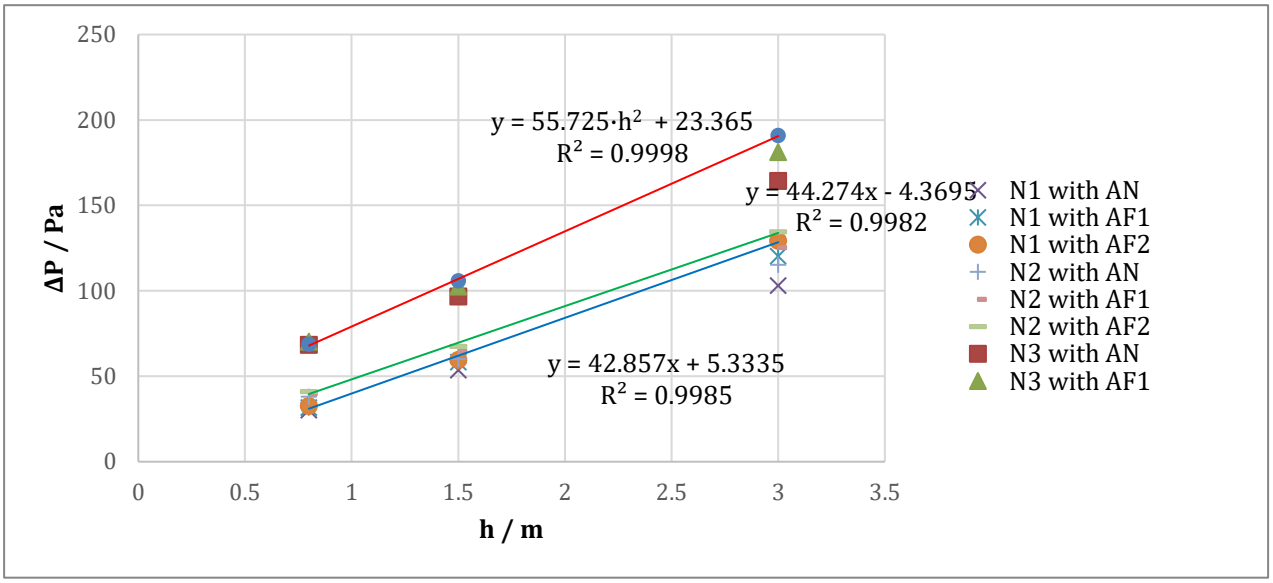


Figure 70 - Correlations for pressure drop (ΔP) as a function of flow rate for three numbers of plates for the flow rate Q1

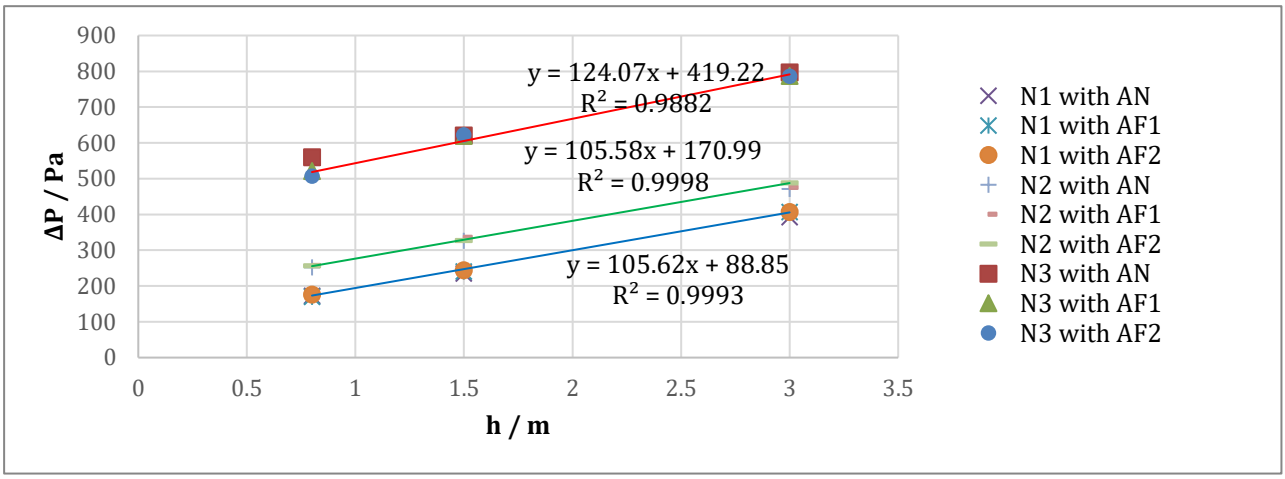


Figure 71 - Correlations for pressure drop (ΔP) as a function of flow rate for three numbers of plates for the flow rate Q3

Appendix F - Additional graphs regarding the effect of ventilation on oil convection (for radiators of 7 and 20 plates)

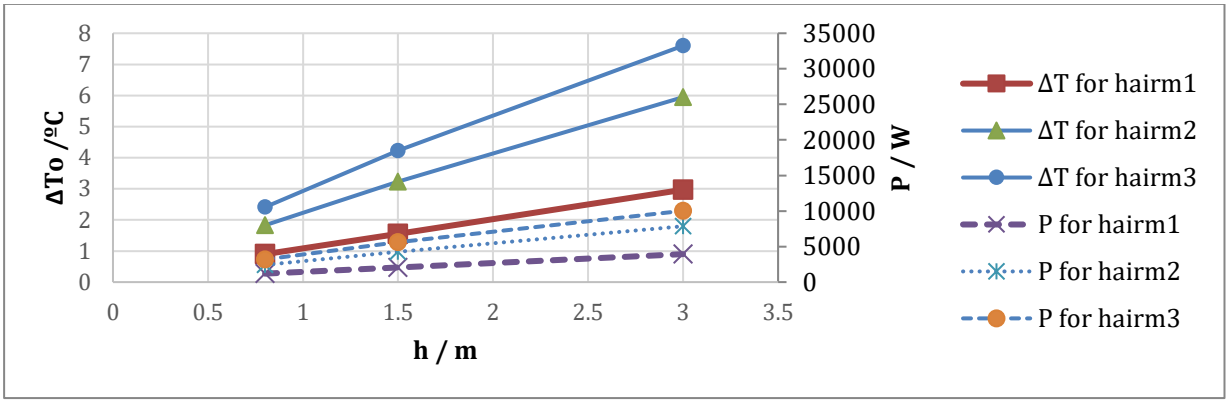


Figure 72 - Output temperature and energy dissipation rate as a function of plate height with varying external convective heat transfer coefficients for a radiator of 7 plates and Q1

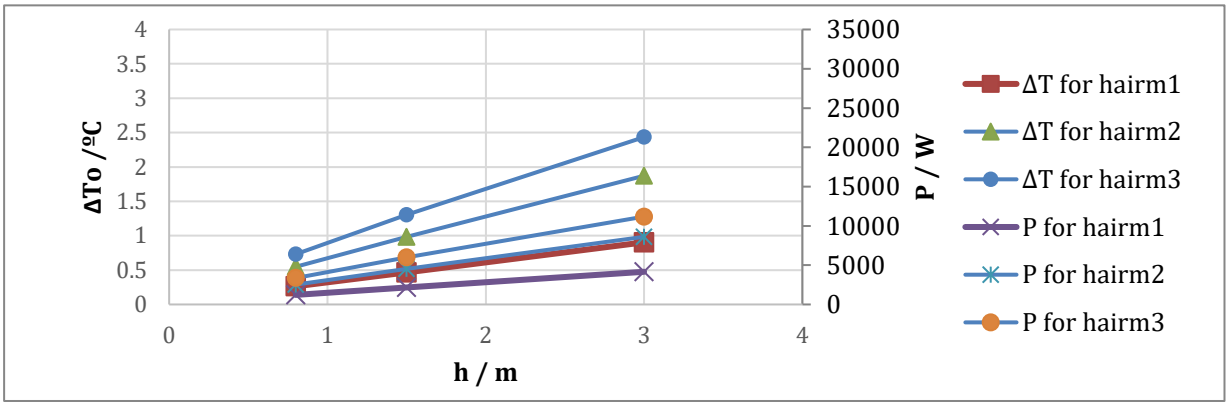


Figure 73 - Output temperature and energy dissipation rate as a function of plate height with varying external convective heat transfer coefficients for a radiator of 7 plates and Q3

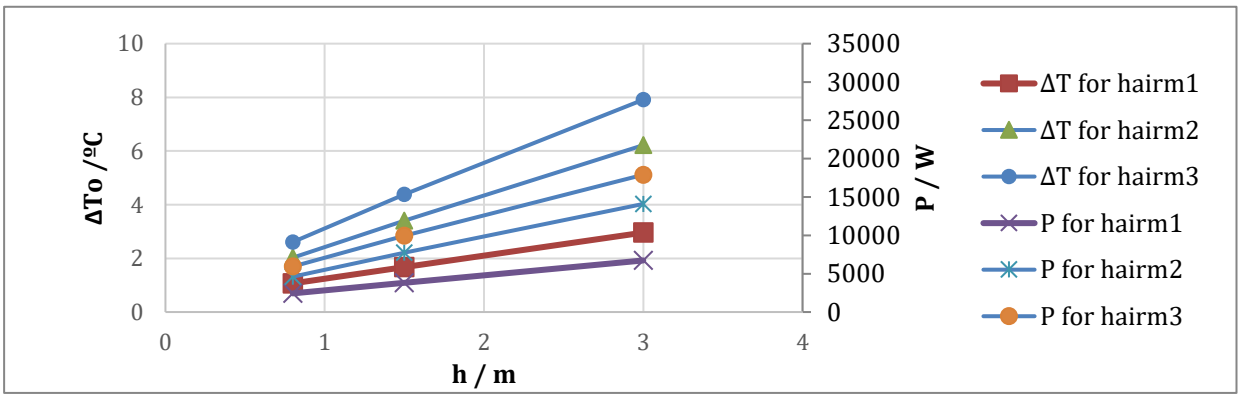


Figure 74 - Output temperature and energy dissipation rate as a function of plate height with varying external convective heat transfer coefficients for a radiator of 12 plates and Q1

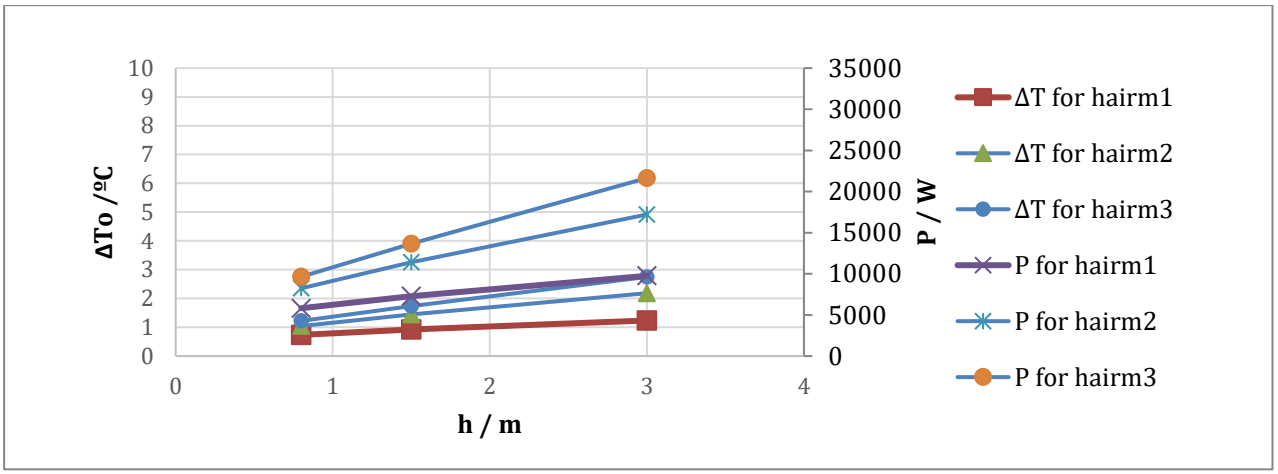


Figure 75 - Output temperature and energy dissipation rate as a function of plate height with varying external convective heat transfer coefficients for a radiator of 12 plates and Q3

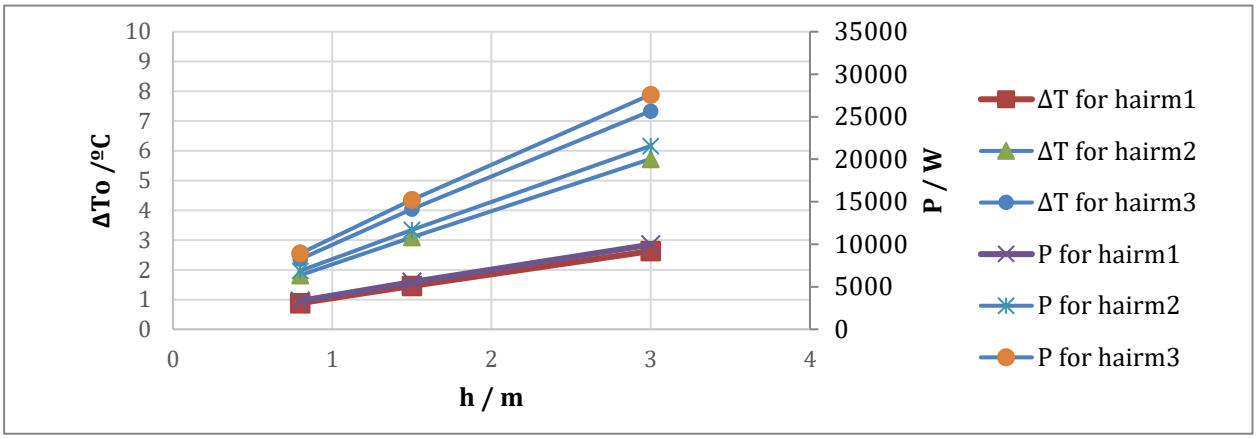


Figure 76 - Output temperature and energy dissipation rate as a function of plate height with varying external convective heat transfer coefficients for a radiator of 20 plates and Q1

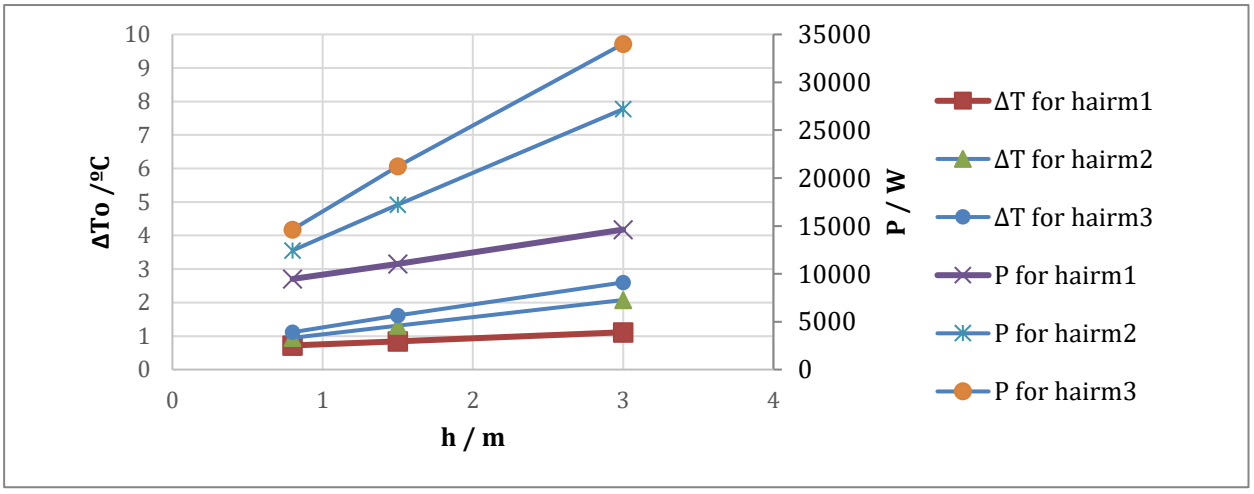


Figure 77 - Output temperature and energy dissipation rate as a function of plate height with varying external convective heat transfer coefficients for a radiator of 20 plates and Q3

Appendix G - Radiator Flow Rate Graphs per plate (12 plate radiator)

G.1. Height of 0.8 m

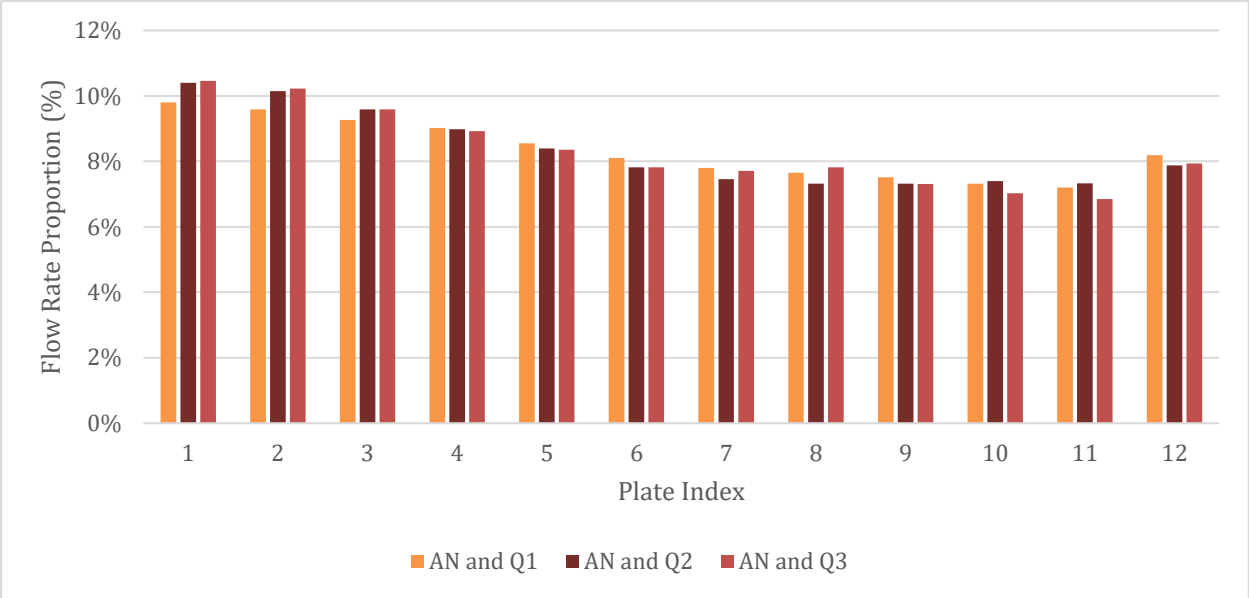


Figure 78 - Flow rate proportion per plate for AN

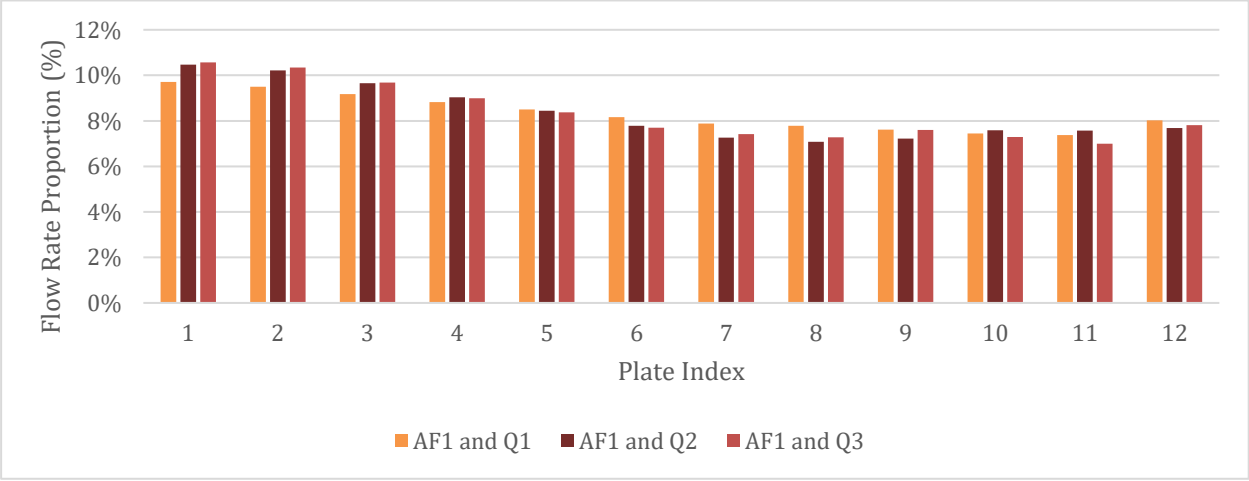


Figure 79 - Flow rate proportion per plate for AF1

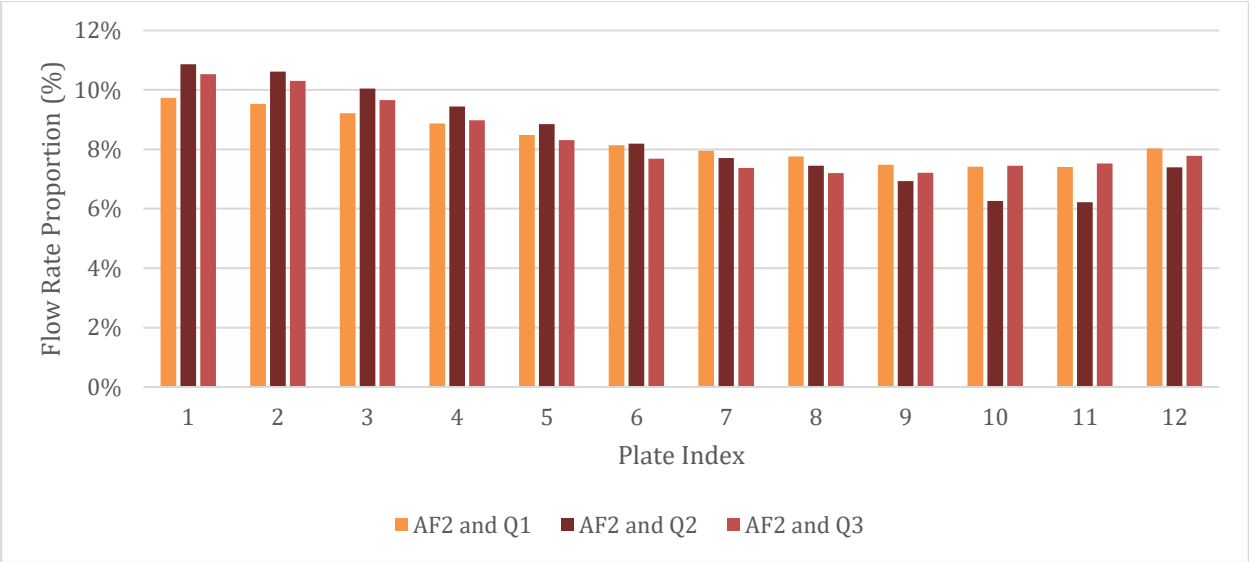


Figure 80 - Flow rate porportion per plate for AF2



Figure 81 - Flow rate proportion per plate for Q1



Figure 82 - Flow rate proportion per plate for Q2



Figure 83 - Flow rate proportion per plate for Q3

G.2. Height of 1.5 m

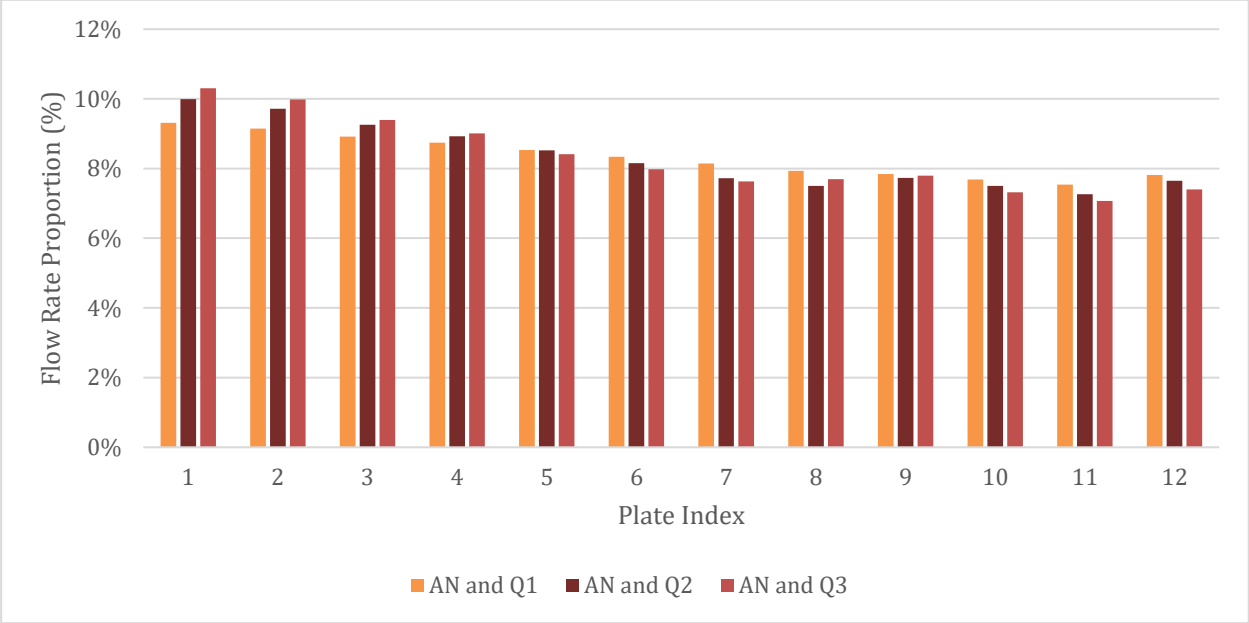


Figure 84 - Flow rate proportion per plate for AN

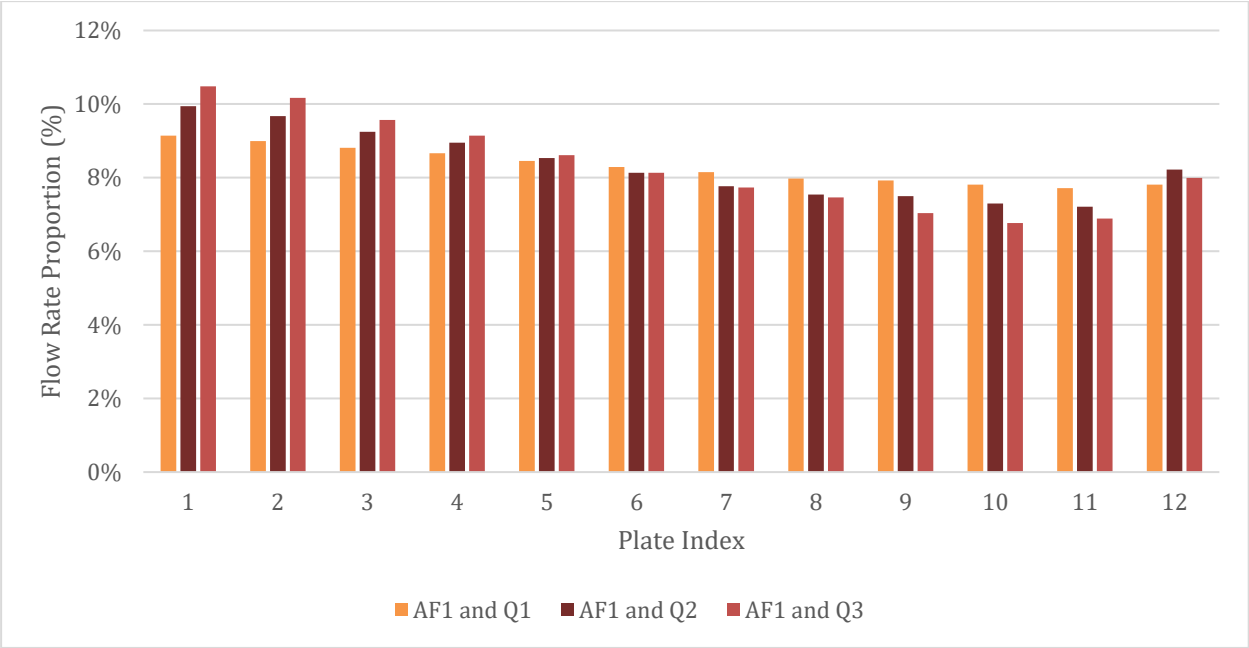


Figure 85 - Flow rate proportion per plate for AF1



Figure 86 - Flow rate proportion per plate for AF2

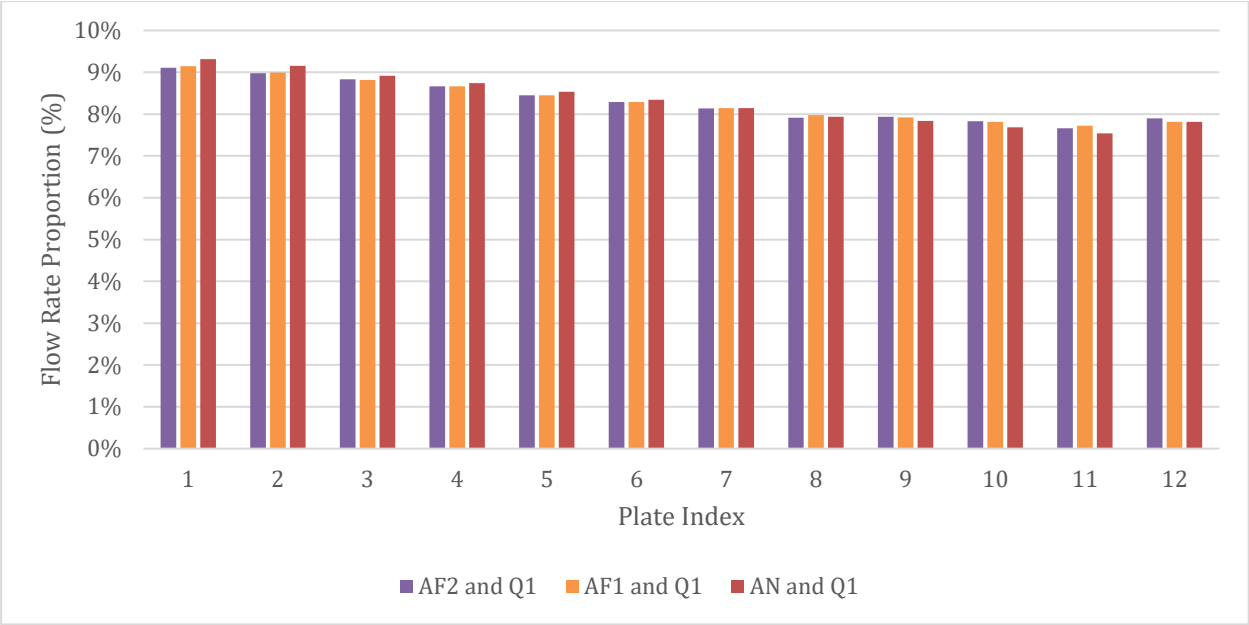


Figure 87 - Flow rate proportion per plate for Q1



Figure 88 - Flow rate proportion per plate for Q2

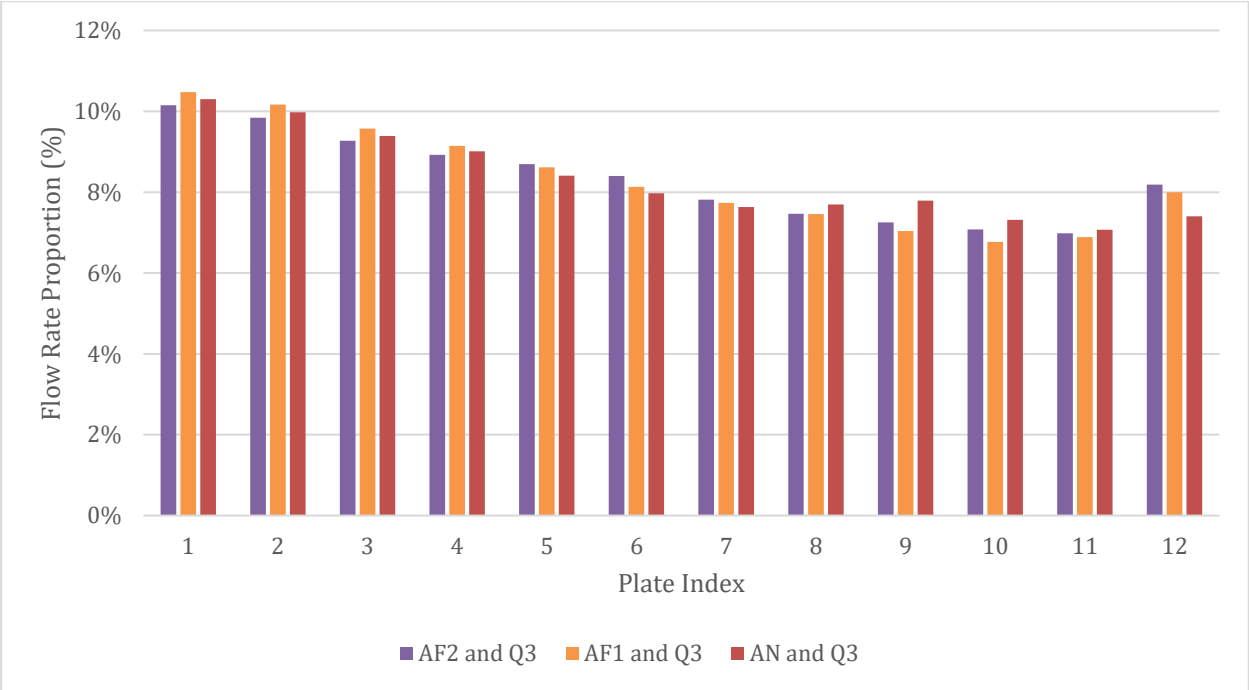


Figure 89 - Flow rate proportion per plate for Q3

G.3. Height of 3 m

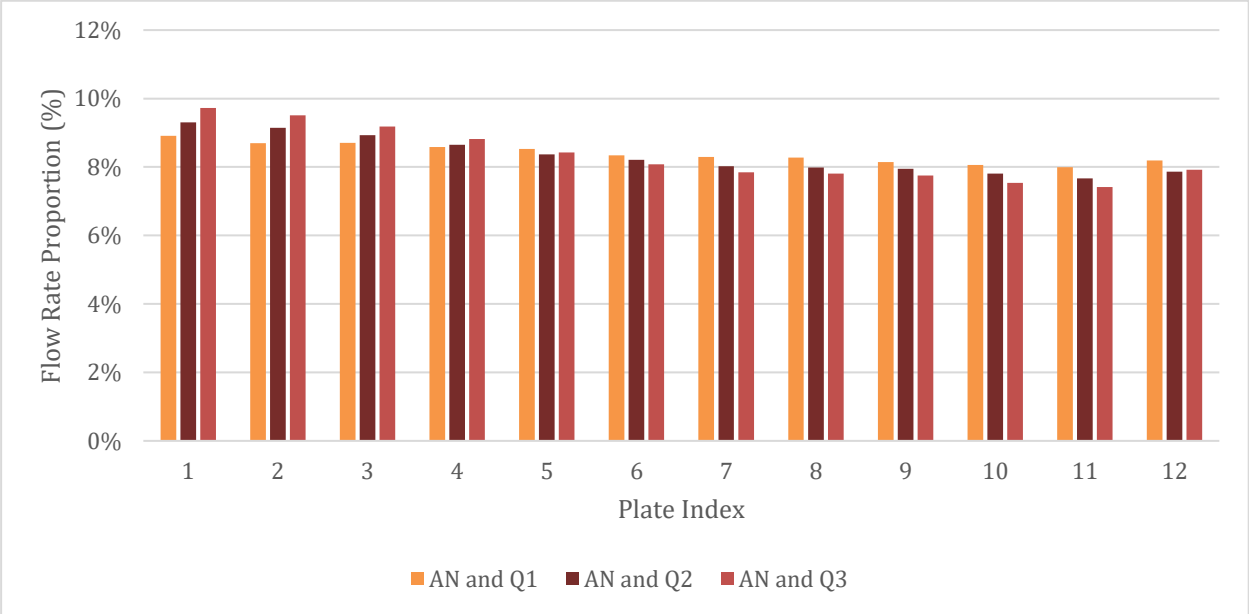


Figure 90 - Flow rate proportion per plate for AN

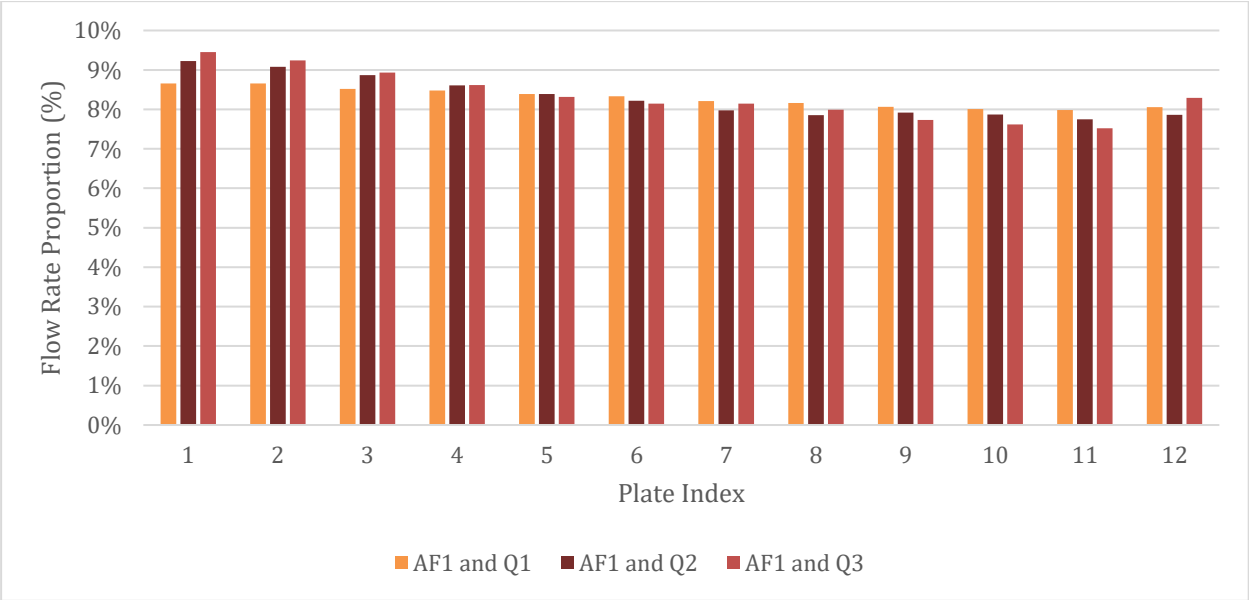


Figure 91 - Flow rate proportion per plate for AF1

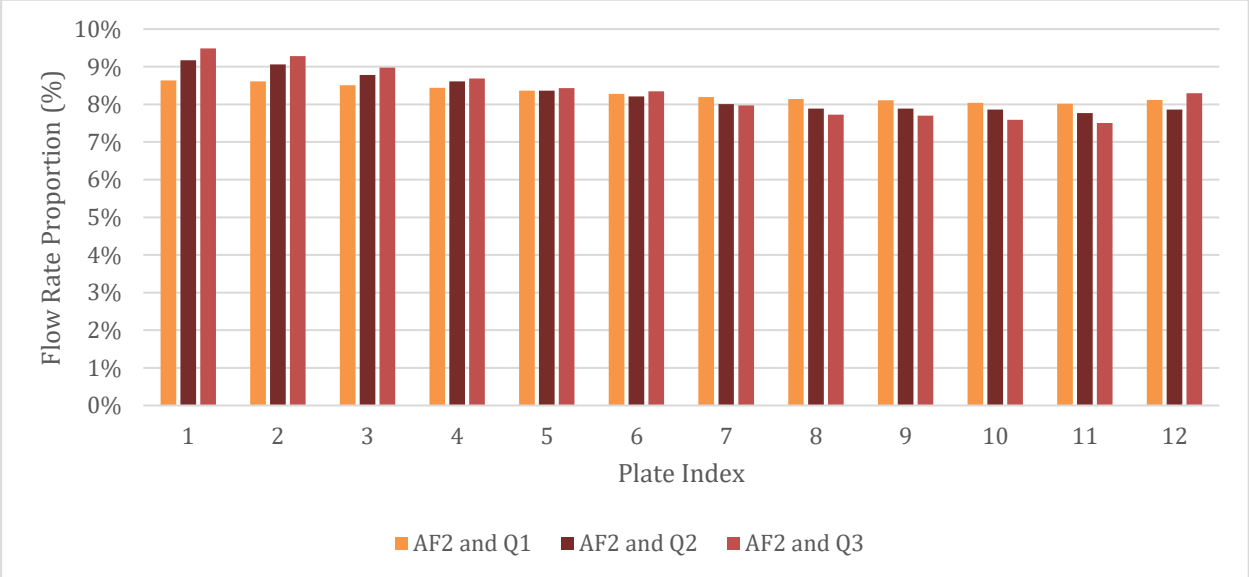


Figure 92 - Flow rate proportion per plate for AF2



Figure 93 - Flow rate proportion per plate for Q1



Figure 94 - Flow rate proportion per plate for Q2



Figure 95 - Flow rate proportion per plate for Q3

A phenomenon that is worth noting is that near the last plates, the flow rate seems to increase, despite being divided by the previous plates This is due to the existence of a recirculation zone near the bottom of the collector tube, as depicted below in Figure 96. As such, the flow rate firstly decreases along the collector tube, but then at the end increases, due to the recirculated oil.

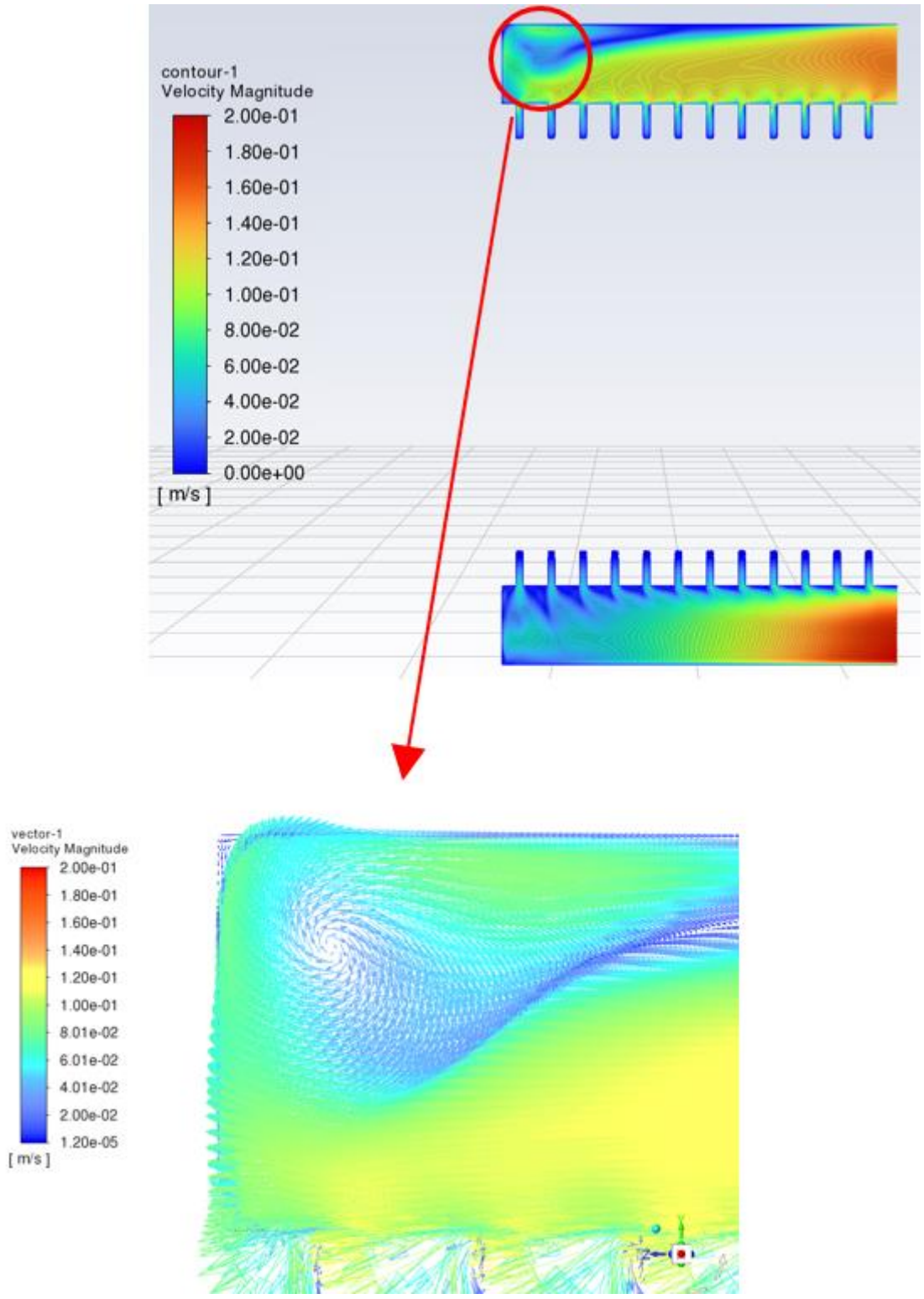


Figure 96 – Recirculation zone taking place at the bottom of the collector tube. (Radiator of 12 plates, height of 0.8 m and $Q1$)

As it can be seen in Figure 96, a recirculation zone forms at the end of the collector tube. This phenomenon results in slightly higher flow rates near the last plates.